TAMPEREEN TEKNILLINEN YLIOPISTO
TAMPERE UNIVERSITY OF TECHNOLOGY
Julkaisu 830 • Publication 830

Janne Pakarinen

Studies of III-V Semiconductors

From Surface Reconstructions to Quantum Nanostructures

Tampere 2009

Tampereen teknillinen yliopisto. Julkaisu 830
Tampere University of Technology. Publication 830

Janne Pakarinen

Studies of III-V Semiconductors

From Surface Reconstructions to Quantum Nanostructures

Thesis for the degree of Doctor of Technology to be presented with due permission for public examination and criticism in Sähkötalo Building, Auditorium S2, at Tampere University of Technology, on the 25th of September 2009, at 12 noon.

Tampereen teknillinen yliopisto - Tampere University of Technology
Tampere 2009

ISBN 978-952-15-2219-2 (printed)
ISBN 978-952-15-2264-2 (PDF)
ISSN 1459-2045

Abstract

In this Thesis, technologically important III-V semiconductors are studied. Structural and electronic properties of bismuth (Bi) stabilized InP(100) and GaAsN(100) are explored. Atomic models for the Bi-stabilized surfaces are proposed and differences in electronic properties are explained by the size effects. A similar “surface scientific view point” is adapted to molecular beam epitaxy growth of GaAs/AlAs quantum well structures, where the optimum growth parameters were found to depend on GaAs(100) and AlAs(100) surface reconstructions. The effect of beryllium doping on optical and structural properties of GaInAsN/GaAs quantum wells, GaInAs/GaAs quantum wells, and InAs/GaAs quantum dots are studied. It was found that Be had a tendency to passivate crystal defects and slightly lower threshold current densities of 980-nm diode lasers prepared in this work.

Acknowledgments

The main part of research in this Ph.D. thesis was carried out in the Optoelectronics Research Centre at Tampere University of Technology. In particular, I want to thank my supervisor, Professor Markus Pessa, for the given opportunity. The Graduate School of Tampere University of Technology is acknowledged for financing this research.

Most of all, science is not an individual sport. Without the support and guidance from the below listed state-of-the-art scientists and friends, I would not have been able to make this Thesis.

Professor Juhani Väyrynen from the University of Turku is acknowledged as being my first contact to III-V semiconductors. He also introduced me to Dr. Pekka Laukkanen, whose superb effort must be highlighted. Pekkas' constructive encouragement, nearly speed-of-light comments to manuscripts and always positive attitude towards science was indispensable during writing this Thesis. I'm deeply indebted to my colleagues at the ORC. The brilliant ideas and innovations of Dr. Changsi Peng conducted nearly half of the included papers. High-quality results just do not exist, they need to be measured. I want to thank M. Sc Ville Polojärvi for his huge effort in assisting the experimental research as well as for all the semi-scientific ideas at the window table of "Pranzo". Being part of the characterization group has really learnt me a lot. Big thanks to the characterizators: Dr. Andreas Schramm, Dr. Antti Tukiainen, and Risto Ahorinta. Furthermore, I would like to acknowledge valuable contributions from the Nitride team Ville-Markus Korpijärvi and Janne Puustinen, Arto Aho, and many others working at the ORC. Dr. Hannu-Pekka Komsa and Professor Tapio Rantala from computational semiconductor physics laboratory are thanked for theoretical and sometimes even philosophic discussions. Too often we noticed that our problems are too big for the 64-atom supercell. My room mate, always positive theoretical physicist, Dr. Eero Arola, is acknowledged for valuable discussions about science and life. Eero always had time to help, whether the problem was related to summer cottage renovation or formation of pseudogaps in superconductors.

Finally, I would like to thank my beloved wife Saara for her support and ability to remind me when the working hours (should) end. The bright-blue eyes of my nearly 2-year old son, Aaron, could not be a better proof for that there definitely exist more important things in life than science. My parents, Harri and Leena, and my sister, Johanna, are thanked for their never-ending support.

Janne Pakarinen

Hämeenlinna, August 2009

Contents

Abstract i
Acknowledgments iii
Contents v
List of Publications vi
Authors Contribution vii
Publications related but not included in the Thesis viii
1. Introduction 1
1.1 The aim of this study 3
2. Characterization methods and sample preparation 4
2.2. Scanning tunneling microscopy (STM) and spectroscopy (STS) 4
2.3 Methods based on diffraction (LEED, RHEED, and XRD) 5
2.4 Photoluminescence (PL) 7
2.5 X-ray photoelectron spectroscopy (XPS) 8
2.6 Molecular beam epitaxy (MBE) 9
2.6.1 Post-growth annealing of MBE-grown materials (Paper 1) 11
3. Studies of the semiconductor surfaces and interfaces 14
3.1 Bi-GaAsN and Bi-InP(100)(Paper 2) 14
3.2 AlAs/GaAs (Paper 3) 19
3.3. Summary 24
4. Studies of the Be-doped III-V's 24
4.1 Be-doped GaInAsN QW (Paper 4) 24
4.2 Be-doped InAs QDs (Paper 5) 27
4.3 Be-doped GaInAs QW 31
4.3 Summary 37
5. Conclusions and final remarks 37
References 40

Appendices

List of Publications

[Paper1] **J. Pakarinen**, C.S. Peng, J. Puustinen, P. Laukkanen, V.-M. Korpijärvi, A. Tukiainen, and M. Pessa, Postgrowth annealing of GaInAs/GaAs and GaInAsN/GaAs quantum well samples placed in a proximity GaAs box: A simple method to improve the crystalline quality, Applied Physics Letters **92**, 232105 (2008).

[Paper2] P. Laukkanen, **J. Pakarinen**, M. Ahola-Tuomi, M. Kuzmin, R.E. Perälä, I.J. Väyrynen, A. Tukiainen, J. Konttinen, P. Tuomisto, and M. Pessa, Structural and electronic properties of Bi-adsorbate-stabilized reconstructions on the InP(100) and GaAsN(100) surface, Physical Review B **74**, 155302 (2006).

[Paper3] **J. Pakarinen**, V. Polojärvi, P. Laukkanen, A. Tukiainen, A. Laakso, C.S. Peng, P. Tuomisto, V-M. Korpijärvi, J. Puustinen, and M. Pessa, An effect of As flux on GaAs/AlAs quantum wells: A combined photoluminescence and reflection high-energy electron diffraction study, Applied Surface Science **255**, 2985 (2008).

[Paper4] **J. Pakarinen**, C.S. Peng, V. Polojärvi, A. Tukiainen, V.-M. Korpijärvi, J. Puustinen, M. Pessa, P. Laukkanen, J. Likonen, and E. Arola, Suppression of annealing-induced In diffusion in Be-doped GaInAsN/GaAs quantum well, Applied Physics Letters **93**, 052102 (2008).

[Paper5] **J. Pakarinen**, V. Polojärvi, A. Aho, P. Laukkanen, C.S. Peng, A. Schramm, A. Tukiainen, and M. Pessa, Annealing of self-assembled InAs/GaAs quantum dots: A stabilizing effect of beryllium doping, Applied Physics Letters **94**, 072105 (2009).

Authors Contribution

This Thesis includes five peer-reviewed articles. The author has been responsible for the manuscript preparation and the experimental group work (including research planning, sample processing, measurements, and analysis) according to the table shown below.

Paper #	Writing	Experiments
1	Main author	75 %
2	Co-author (30 %)	50 %
3	Main author	60 %
4	Main author	50 %
5	Main author	75 %

Publications related but not included in the Thesis

[1] M. P. J. Punkkinen, P. Laukkanen, M. Ahola-Tuomi, J. Pakarinen, M. Kuzmin, A. Tukiainen, R.E. Perälä, J. Lång, M. Ropo, K. Kokko, L. Vitos, B. Johansson, M. Pessa, and I. J.Väyrynen, Core-level shifts of InP(100)(2×4) surface: Theory and experiment, Surface Science **603**, 2664 (2009).

[2] H.-P. Komsa, E. Arola, J. Pakarinen, C. S. Peng, T. T. Rantala, Beryllium doping of GaAs and GaAsN from first principles, Physical Review B **79**, 115208 (2009).

[3] C. Tan, C. S. Peng, J. Pakarinen, M. Pessa, V. N. Petryakov, Y. K. Verevkin, J. Zhang, Z. Wang, S. M. Olaizola, T. Berthou, S. Tisserand, Ordered nanostructures directly written by laser interference, Nanotechnology **20**, 125303 (2009).

[4] C. S. Peng, J. Pakarinen, M. Pessa, New dilute nitride materials, 15th Int. Conference on Molecular Beam Epitaxy, Vancouver, Canada (2008).

[5] J. M. Mäki, F. Tuomisto, A. Tukiainen, P. Tuomisto, J. Pakarinen, M. Guina, M. Pessa, Effect of growth interruptions and N-plasma treatment to the vacancy concentration of GaAsN-layers, E-MRS 2008 Spring Meeting, Strasbourg, France (2008).

[6] J. Pakarinen, C.S. Peng, V. Polojärvi, P. Laukkanen, A. Tukiainen, V.-M. Korpijärvi, J. Puustinen, M. Pessa, The effect of annealing on highly Be-doped InGaAsN/GaAs single quantum wells, Physics Days 2008, Turku, Finland (2008).

[7] E. Arola, H.-P. Komsa, T. T. Rantala, C. S. Peng, R. Ahorinta, J. Pakarinen, V. Polojärvi, M. Pessa, Application of the scissors-correction scheme to the calculation of the complex dielectric function for GaAs1-xNx Alloys with and without Be-Related defects, Physics Days 2008, Turku, Finland (2008).

[8] V. Polojärvi, A. Schramm, A. Tukiainen, J. Pakarinen, A. Aho, R. Ahorinta, M. Pessa, Defect studies and characterization of self-assembled quantum dots grown by molecular beam epitaxy, Physics Days 2008, Turku, Finland (2008).

[9] P. Laukkanen, M. Ahola-Tuomi, J. Adell, M. Adell, K. Schulte, M. Kuzmin, J. Pakarinen, A. Tukiainen, R. Perälä, J. Väyrynen, and M. Pessa, A comparative study of clean and Bi-stabilized InP (100) (2x4) surfaces by the core-level photoelectron spectroscopy, Surface Science **601,** 3395 (2007).

[10] P. Laukkanen, M. Ahola-Tuomi, M. Kuzmin, R.E. Perälä, I.J. Väyrynen, A. Tukiainen, J. Pakarinen, M. Saarinen, M. Pessa, Structural properties of Bi-stabilized reconstructions of GaInAs(100) surface, Applied Physics Letters **90**, 082101 (2007).

[11] P. Laukkanen, M. Ahola-Tuomi, J. Adell, M. Adell, K. Schulte, M. Kuzmin, J. Pakarinen, A. Tukiainen, R. Perälä, J. Väyrynen, M. Pessa, Structural and electronic properties of Bi-stabilized (2x1) reconstruction on the InP(100) surface, 17th Int. Vacuum Congress, Stockholm, Sweden (2007).

[12] J. M. Mäki, F. Tuomisto, A. Tukiainen, P. Tuomisto, J. Pakarinen, M. Guina, M. Pessa, Effect of growth interruptions and N-plasma treatment to the vacancy concentration of GaAsN-layers, 41st Annual Meeting of Finnish Physical Society, Tallinn, Estonia (2007).

[13] P. Laukkanen, J. Pakarinen, M. Ahola-Tuomi, M. Kuzmin, R.E. Perälä, I.J. Väyrynen, A. Tukiainen, V. Rimpiläinen, M. Pessa, M. Adell, and J. Sadowski, Electronic and structural properties of the InP(100)(2x4) surface studied by core-level photoemission and scanning tunneling microscopy, Surface Science **600**, 3022 (2006).

[14] M. Ahola-Tuomi, P.Laukkanen, R.E.Perälä, M.Kuzmin, J.Pakarinen, I.J.Väyrynen, and M.Adell, Structural properties of Bi-terminated GaAs(001) surface, Surface Science **600**, 2349 (2006).

[15] P. Laukkanen, J. Pakarinen, M. Ahola-Tuomi, R.E. Perälä, M. Kuzmin, I.J.Väyrynen, A. Tukiainen, V. Rimpiläinen, M. Pessa, M. Adell, J. Sadowski, Electronic and atomic properties of the InP(100)(2x4) surface, 40th Annual Meeting of Finnish Physical Society, Tampere, Finland (2006).

1. Introduction

The peculiar property of semiconductors emitting light upon electric or optical excitation has wakened an exceptional theoretical, experimental, and commercial interest towards them during the last decades. The first GaAs-based semiconductor laser was realized in 1962 by Hall *et al.* [Hal62] It was based on a forward-biased *p*-*n* junction and operated at liquid N_2 temperature. The idea of double-heterostructure (DH) semiconductor laser, in the early 60s', revolutionized the whole research area. The first DH laser, which operated continuously at room temperature, was made in 1970. The inventor and the executor, Kroemer and Alferov, respectively, were awarded the Nobel Prize in Physics in 2000.

The following chapters of the Thesis describe some breakthroughs that emerged from the wide field of semiconductor optoelectronics and summarize current trends in III-V compound semiconductor technologies.

To achieve population inversion, the occupation probability of the lowest states in the conduction band has to be higher than the population of the highest states in the valence band. By increasing the *p* and *n*-doping of, for example, a GaAs *p*-*n*-junction, these conditions cannot be easily fulfilled, because electron and hole concentrations always tend to be smaller in the active region than in the *n* and *p*-doped regions. Work on compound semiconductors solved this problem; the quasi-electric fields of bang-gap-engineered heterostructures increase the amount of charge carriers in active region above that of the doped regions, thus making room-temperature operation of a semiconductor laser possible. A band-diagram *versus* lattice constant map for numerous III-V compound semiconductors is shown in Fig. 1. [Kro00]

The first semiconductor lasers were grown by liquid-phase epitaxy (LPE), but large-scale scientific and commercial breakthroughs had to wait until the most accurate crystal growth method, molecular beam epitaxy (MBE), was developed. [Art02] Using MBE, growth of heterostructures could be, for the first time, monitored within an atomic layer-by-layer accuracy.

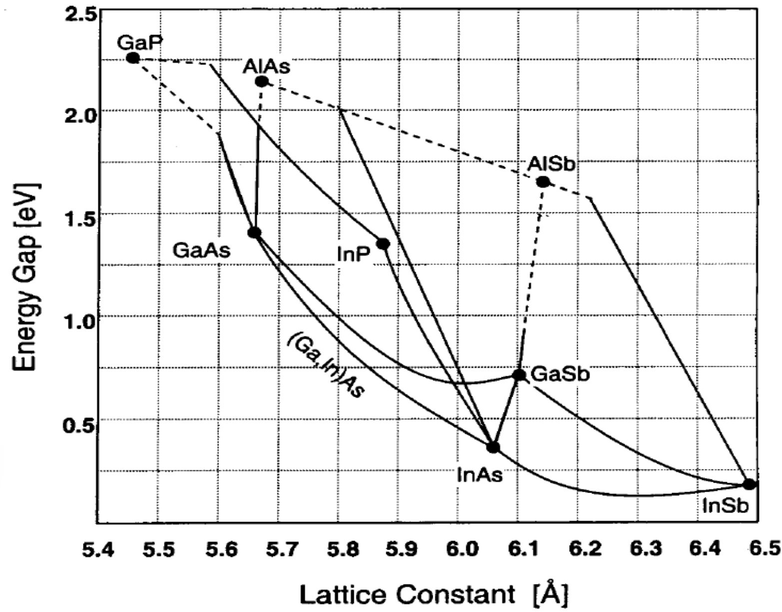

Fig. 1 *Band gaps of III-V compound semiconductors (excluding nitrides) as functions of lattice constant.[Kro00]*

GaAs-based III-V semiconductors, grown by MBE [or by metal-organic chemical vapor deposition (MOCVD)], are building blocks for state-of-the-art optoelectronic devices.[Gar09, Ger08, Har02] The main reasons for using GaAs as a substrate include: low-cost wafers, advantages of closely lattice-matched GaAs/AlAs distributed Bragg reflectors (optical and electrical confinement), and good thermal properties. Wavelengths above 1.2 μm have, in general, been out of reach of the GaAs technology. However, this interesting range can today be covered by using different approaches. In this Thesis, light emission around and above 1.2 μm is demonstrated by incorporating nitrogen into GaInAs/GaAs quantum wells (QWs) or by using self-assembled InAs quantum dot (QDs) on GaAs.

The practical maximum wavelength launched from GaInAs QWs on GaAs is below 1.2 μm, due to unbearable crystal stress as indium composition is increased. Incorporation of nitrogen into GaInAs QW (proposed in 1996 by Kondow *et al.* [Kon96]) reduces the lattice strain because of a small size of the N atom. Simultaneously, N induces a large non-linear bang-gap bowing to the Ga(In)As conduction band, which shifts the emission wavelength well beyond 1.2 μm (up to λ = 1.6 μm is demonstrated).[Ish06] Unfortunately, quaternary $Ga_xIn_{1-x}As_yN_{1-y}$ is metastable in nature, being very difficult to grow and control by any technique. Especially, the bonding environment of N has

remarkable effects on the optical, electronic and structural properties, [Kim01, Lor03, Mus05, Yu02] as will be shown in this Thesis.

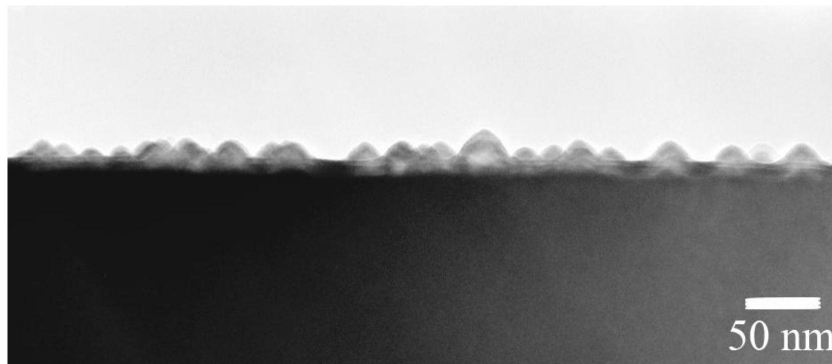

Fig. 2 *Self-assembled InAs QDs on a GaAs(100) surface. (Unpublished results)*

Fig. 2 shows a transmission electron microscopy (TEM) image of self-assembled InAs QDs on a GaAs(100) surface. QDs self assemble to minimize the surface energy, which is due to the large lattice mismatch between the deposited monolayers of InAs and GaAs substrate (Fig. 1). Carriers are confined in all the three directions of QDs, as opposite to QWs where the charge carriers can freely move at the QW plane. The emission wavelength of QDs originates, i. e., from their size, composition and strain,[Bim99] which make QDs perfect candidates for optoelectronic applications. Even though the QDs have been studied over a couple of decades, there is still room for new ideas. For example, a *p*-type modulation doping of QD heterostructures is known to increase thermal stability of QDs being beneficial for laser operation. [Bad07, Jin08]

1.1 The aim of this study

In this Thesis, light emission and surfaces of epitaxially grown III-V compound semiconductors are studied in an attempt to improve the present-day understanding of the physics of these materials. Broadly speaking, the Thesis is divided into two sections. The first goal is to investigate surface reconstructions of III-V(100) surfaces and link them to MBE layer-growth and structural defects. The second goal is to study and explain the effects of post-growth thermal annealing, in particular, on the optical and structural properties of undoped and beryllium-doped GaInAs(N) / GaAs quantum wells and InAs / GaAs quantum dots. These materials allow for an extension of the GaAs technology to the wavelengths beyond 1.2 μm for optical fiber telecommunications.

2. Characterization methods and sample preparation

2.2. Scanning tunneling microscopy (STM) and spectroscopy (STS)

Scanning tunneling microscopy (STM) was developed in the early 1980's by Binning and Rohrer (Nobel Prize in 1986). The method is based on a quantum mechanical tunneling phenomenon when an atomically sharp metal tip is brought in a close proximity of the surface. By measuring the tunneling current from the tip to the sample (constant height mode) or by keeping the tunneling current constant and monitoring the tip height (constant current mode), contours of the surface are obtained by scanning the tip along the surface. A schematic presentation of the STM operation is given in Fig. 3 (a). Fig. 3 (b) shows one of the first contour graphs for a Si(111)(7×7) surface.[Bin83]

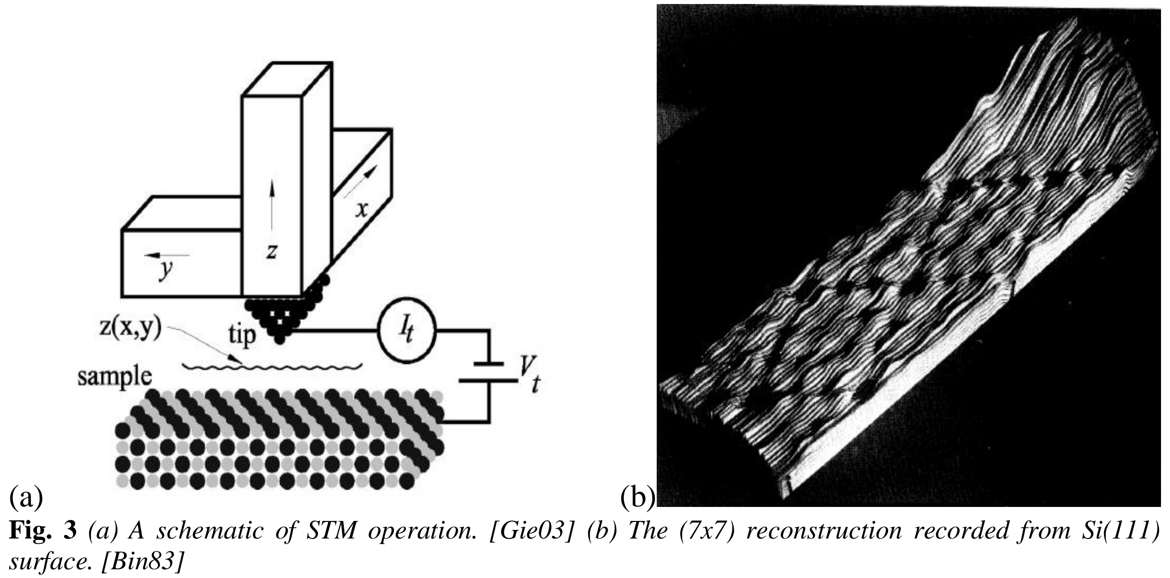

Fig. 3 *(a) A schematic of STM operation. [Gie03] (b) The (7x7) reconstruction recorded from Si(111) surface. [Bin83]*

According to Tersoff and Haman [Ter85] the tunneling current from the metal tip to the sample surface is (1):

$$I = \frac{2\pi e}{\hbar} \sum_{\mu,\upsilon} f(E_\mu)\left[1 - f(E_\upsilon + eV)\right] \left|M_{\mu\upsilon}\right|^2 \delta(E_\mu - E_\upsilon), \qquad (1)$$

where *f(E)* is the Fermi function, *V* is the voltage between the tip and the sample, $M_{\mu\nu}$ is the matrix element between electron wave functions at the tip (Ψ_μ) and at the surface (Ψ_ν), while E_μ and E_ν are the corresponding energy states. The tunneling current, *I*, cannot be

numerically solved without approximations, because the electron wavefunctions in $M_{\mu\nu}$ (at the tip) are unknown. The reason for STM being one of the most accurate surface research methods (vertical resolution is about 0.1 Å) originates from the exponential dependence between the tunneling current and the tip-to-surface separation ($I \propto e^{-d}$). In lateral direction, the resolution is a few ångströms, mainly determined by the scanning unit controls. [Ter85]

Scanning tunneling spectroscopy (STS) has been used in this work to determine, whether the studied surface phases are semiconducting or metallic. By fixing the tip position and scanning the bias voltage, the derivative of the tunneling current (dI/dV) is proportional to the electronic density of states of the surface.[Fee94]

2.3 Methods based on diffraction (LEED, RHEED, and XRD)

Low-energy and reflection high-energy electron diffraction (LEED and RHEED) are techniques that are used for studying structure and symmetry of the surfaces. In LEED an electron beam with low kinetic energy (< 100 eV) is focused to the sample surface with an angle of incidence about 90 degrees and the diffracted beams are monitored on a fluorescent screen. RHEED employs the same idea but the electron beam has higher kinetic energy (> 10 keV) and the angle of incidence is only few degrees. X-ray diffraction (XRD) was applied to solve “bulk” properties (composition, layer thickness, etc.) of crystalline materials. In XRD measurements, the x-rays were generated by using x-ray tube (Cu anode), and then directed to the sample. By adjusting the angle of incidence and the detector angle, the diffracted reflection of interest was chosen [usually GaAs (004)]. A rocking curve (which showed the (004) diffraction from the epilayers) was then recorded in ω-2θ geometry around the GaAs(004) peak.

The main principle of the diffractive methods, used in this Thesis, can be demonstrated by using a concept of Ewald sphere (kinematic theory considered).[Cul87, Hov86] The Ewald sphere is constructed by drawing a sphere in the momentum space, which has a radius corresponding to the momentum of the incoming beam. To obtain a constructive interference in the momentum space, the change in momentum between the incoming beam ($\mathbf{k_0}$) and the diffracted beam ($\mathbf{k_d}$) has to be exactly an integer times the reciprocal

vector **G** (which corresponds to Bragg's law in real space). In the Ewald sphere construction this means that the constructive interference is obtained when the reciprocal lattice intersects with the sphere:

$$\Delta k = G \, . \tag{2}$$

The momentum of the incoming beam (electrons or x-rays) is always known. Understanding diffraction is the question of determining the reciprocal lattice from the point of view of the incoming beam.

(i) X-rays penetrate into semiconductor crystals. Thus, the reciprocal lattice is a three-dimensional grid of reciprocal points.
(ii) Electrons do not penetrate deep into semiconductor crystal. Consequently, the reciprocal lattice is a net of two-dimensional reciprocal lines.
Figs. 4 (a) – (c) illustrate the Ewald sphere schema for XRD, LEED, and RHEED.

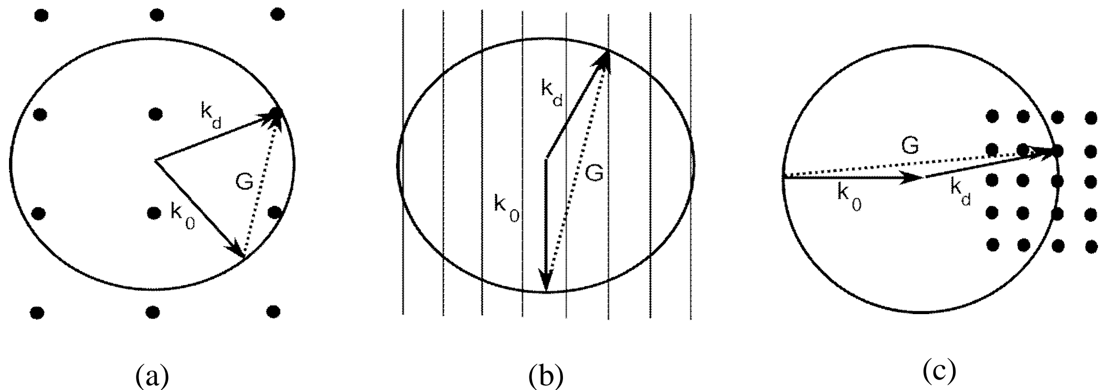

Fig. 4 *Ewald spheres for (a) x-ray diffraction, (b) low-energy electron diffraction, and (c) reflection high-energy electron diffraction. Notice that in (a) the reciprocal lattice consists of a net of points, while in (b) a side view and in (c) a top view of the reciprocal rods are drawn.*

In this Thesis, LEED patterns were used as a complementary method with STM to identify the surface phases of InP(100) and GaAsN(100). Based on the literature and *in-situ* RHEED patterns, the GaAs(100) and AlAs(100) surface phases were studied as functions of As/group-III flux ratios. XRD was used to determine the compositions and layer thicknesses of MBE-grown semiconductors. The XRD rocking curves, in ω-2θ geometry, were recorded using Cu K_{α} radiation. The rocking curves were also simulated. We used a commercial simulation program (Rads Mercury from Bede Scientific), which is based on a dynamical diffraction theory.

2.4 Photoluminescence (PL)

Photoluminescence (PL) is a non-destructive method used to study optical properties of materials.[Her91] A schematic setup of our temperature-dependent PL measurements is shown in Fig. 5. Laser light (λ = 488 nm) is filtered and directed to the sample. The chopper is connected to the lock-in amplifier to reduce noise. The laser beam excites electron-hole pairs of the sample. When the pairs decay, PL is emitted (red light in the figure). Part of this PL is collected by lenses and analyzed by a monocromator. Notice, that in our setup the sample is placed inside a closed-cycle helium cryostat, which allows the temperature-dependent measurements from room temperature (RT, 300 K) to 10 K.

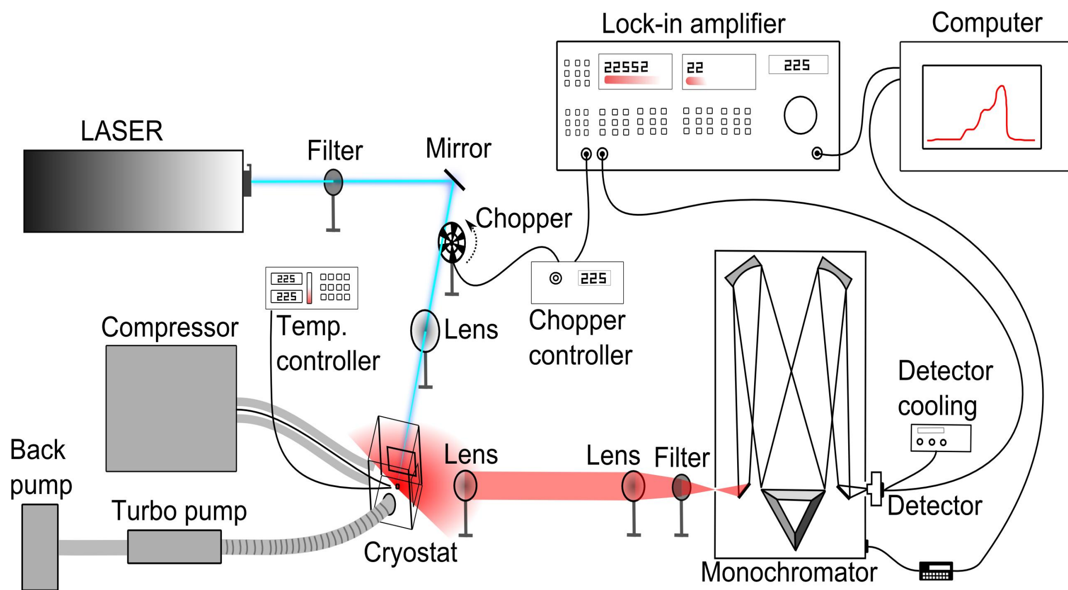

Fig. 5 *A PL setup for temperature-dependent measurements.[POL09]*

Room-temperature PL intensity can be used to examine the optical quality of the sample. The emission gives an indication of the QW composition and thickness. The PL measurement is rather simple and is often automated. The PL intensity and the semiconductor laser threshold are inversely proportional to each other, but care must be exercised when applying this principle, for example, to highly doped materials.

While PL measurements at RT are fast to perform and give enough information of optical quality of materials, PL at low temperature (LT) is more time consuming but the results contain more details.[Gfr00] Using the setup of Fig. 5, LT and temperature-dependent PL measurements for a one sample takes at least a day.

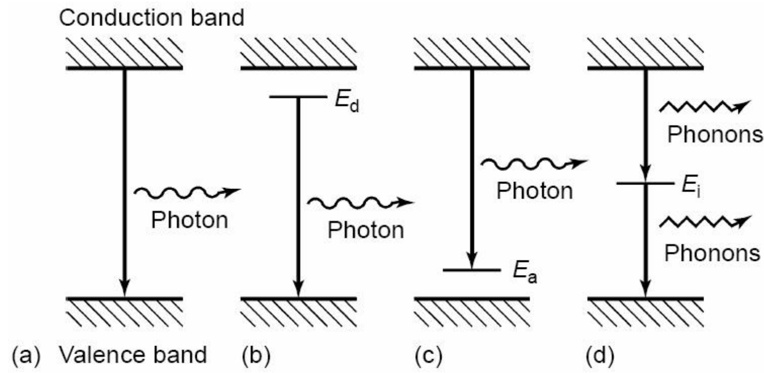

Fig. 6 *(a) – (c) radiative and (d) nonradiative recombination paths. [Gfr00]*

The analysis of LT-PL spectra is demanding. It usually needs complementary measurements, for example, photoluminescence excitation spectroscopy (PLE). Fig. 6 (a) shows an ideal PL measurement; the PL wavelength obtained is characteristic of the material. However, when comparing the unresolved wavelengths of Figs. 6 (b) and (c), the origins of radiative recombinations are clearly different; in (b) from a donor deep level to the valence band, and in (c) from the conduction band to an acceptor deep level. Non-radiative transitions [Fig. 6 (d)] can only be studied indirectly. As the chip temperature is increased, thermal escape of carriers from trap states quenches the defect-related PL features. [Gfr00]

Versatile and non-destructive PL technique was used frequently in this Thesis. Often automated RT-PL measurements were utilized to detect effects of growth parameters or post-growth thermal treatments on the QW and QD samples. We used temperature-dependent PL as a complementary method to identify transitions in QWs of GaAs/AlAs heterostructures.

2.5 X-ray photoelectron spectroscopy (XPS)

X-ray photoelectron spectroscopy (XPS) was pioneered by the Nobel-awarded Siegbahn (Nobel Prize in 1981) in the late 50s'. XPS is a versatile technique for studies of elemental compositions of solid samples, bonding environments of individual atoms, and surface reconstructions *via* surface core-level shifts (SCLSs).[Pun09]

The XPS measurement resorts to an interaction between electromagnetic radiation and matter. The energy of an x-ray quantum is absorbed *via* dipole interaction by an electron of the sample. The excited electron moves toward the surface and escapes to vacuum. By measuring the kinetic energy (E_K) of the escaped (photo)electron, the bonding energy (E_B) can be deduced. Because E_B is specific to each atom, an elemental analysis is feasible. With respect to the Fermi level, E_B of the photoelectron can be written as:

$$E_B = E_X - E_W - E_K , \qquad (3)$$

where E_X is the energy of the incoming x-ray beam and E_W is the work function of the electron spectrometer. It is worth noting that E_W of the sample itself plays no role in the analysis. [Car75]

We used XPS to monitor the amount of deposited bismuth on InP(100) and GaAsN(100) surfaces. The analysis was done recording the Bi *4f* peak intensity after each annealing (at UHV) and comparing the peak value to that of non-annealed sample.

2.6 Molecular beam epitaxy (MBE)

The samples were grown by solid-source MBE. The MBE reactor consists of three chambers, which were separated by valves: (i) a load lock chamber, (ii) a sample preparation chamber for cleaning and other pre-growth treatments, and (iii) a growth chamber. The side view of a commercial MBE reactor, similar to MBE of ORC, is presented in Fig. 7.

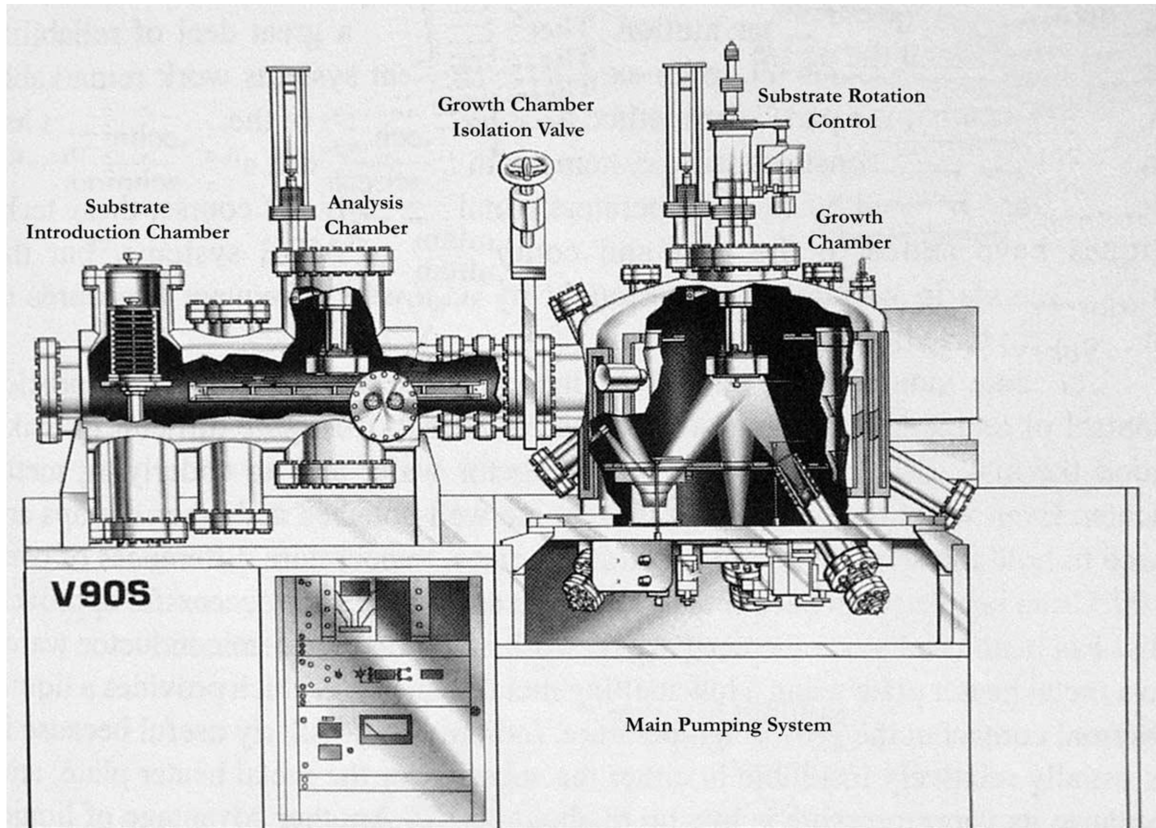

Fig. 7 *A cut-away view from a commercial MBE system which consists of three different UHV chambers: the small load lock chamber for substrate import and export, the preparation (analysis) chamber, and the actual growth chamber (Courtesy of Vacuum Generators, Ltd). [Art02] A similar MBE reactor was used in the present work.*

"Epi-ready" substrate wafers were used. First the wafer was thermal annealed to clean the surface from native oxides, etc. After the wafer was cleaned it was transferred to the growth chamber and faced towards the molecular sources. Molecular beams were generated by effusion cells or valved crackers (including gas and plasma sources). The substrate was kept at elevated temperature (usually over 450 °C), which provided enough thermal energy for the atoms to migrate to their correct lattice sites. During growth, the wafer was rotated to ensure homogenous quality. Mechanical shutters were placed in front of each source oven. Controlling the material fluxes by adjusting, for example the effusion oven temperature or the mechanical shutters, MBE growth could be controlled within an atomic layer accuracy. For growth of the GaInAsN / GaAs QW samples, an rf nitrogen plasma source was used.

The author has not been directly assigned to grow the epi-wafers, but has been involved in planning the heterostructures.

2.6.1 Post-growth annealing of MBE-grown materials (Paper 1)

Post-growth annealing usually improves the material quality. In particular, MBE-grown dilute nitrides benefit from annealing, because they must be grown at lower temperature (~ 470 °C) than GaAs (~ 580 °C). The low growth temperature prevents the surface segregation of nitrogen [Pan00] and induces crystal defects, such as interstitials and vacancies.[Jan03, Slo06, Wis05]

To protect the sample surface during annealing, several methods have been applied. Most commonly, the sample is coated with SiO_2 or SiN_x or proximity-capped with a GaAs wafer.[Liu04, Zha07] However, problems arise from the different thermal expansion coefficients of the dielectric films and GaAs. SiO_2 coating, with nearly 10 times bigger thermal expansion coefficient than that of GaAs, induces Ga-vacancies in underlying GaAs upon annealing.[Ooi97] These vacancies enhance diffusion of In from GaInAs(N) QWs.[Liu04] Because the thermal expansion coefficient of SiN_x is close to GaAs, SiN_x is thought to be a better coating to protect the sample surface.[Li00]

In this work, a set of $Ga_{0.62}In_{0.38}As$ and $Ga_{0.62}In_{0.38}As_{0.0985}N_{0.015}$ triple-quantum wells (TQWs) were studied to explore effects of different surface protections during annealing. The studied scenarios were: (i) samples capped with 200-nm layers of SiO_2, (ii) samples placed inside a GaAs proximity box, and (iii) samples left uncapped. A proximity GaAs box is presented in Fig. 8.

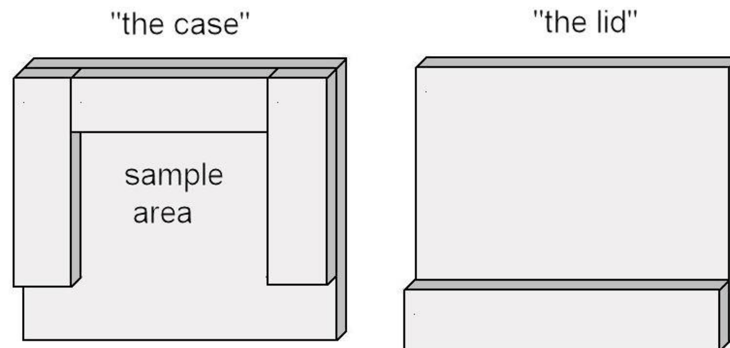

Fig. 8 *A GaAs box used in this work. It provided "proximity conditions" in all directions. The samples were placed face down to the "sample area". The box dimensions were roughly 25 mm × 30 mm and the GaAs wafer thickness was 350 µm.*

The results for annealing GaInAs and GaInAsN TQWs at 700 and 800 °C are displayed in Fig. 9. From PL peak intensity (which was compared to as-grown peak intensity), We concluded that the GaAs-box approach gave the best optical quality for GaInAs and GaInAsN TQWs. If the SiO_2 cap was used, PL was always reduced by annealing, while the uncapped samples showed slight improvements in PL.

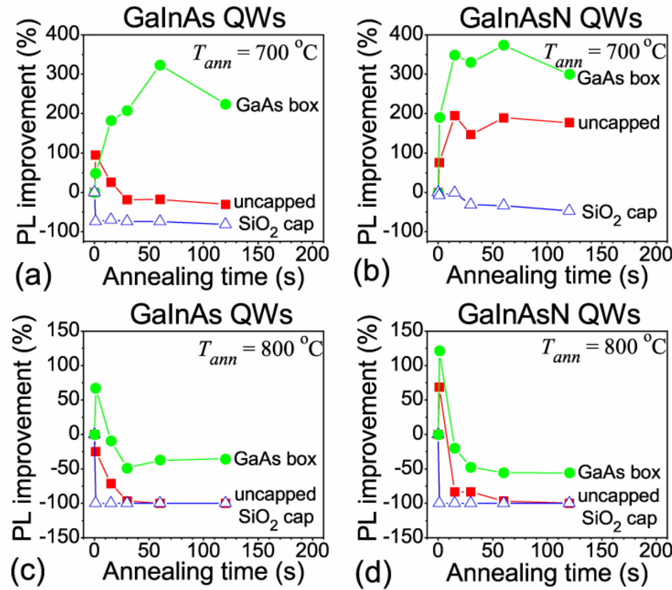

Fig. 9 *PL peak intensities for GaInAs and GaInAsN TQWs upon annealing at 700 [(a) and (b)] and 800 °C [(c) and (d)]. [Paper1]*

The blue-shifts of the photoluminescence (BS of PL) emission wavelength as functions of annealing time (Fig. 10) and the XRD measurements from as-grown and annealed GaInAs and GaInAsN (Fig. 12) confirmed the results of previous studies published in the literature. The conclusions are as follows.

(i) SiO_2 capping enhanced BS with respect to the uncapped and proximity-capped GaAs box samples. Most likely, the reason for this was the introduction of Ga-vacancies into the capped samples. The vacancies enhanced diffusion of In over the QW-barrier interface. [Ooi97] Interestingly, the BS of PL was larger for the SiO_2 capped GaInAs than for GaInAsN upon prolonged annealing [curve 1 in Figs. 10 (a) and (b)]. This was interpreted as due to the formation of stable In-N bonds which suppressed In diffusion.

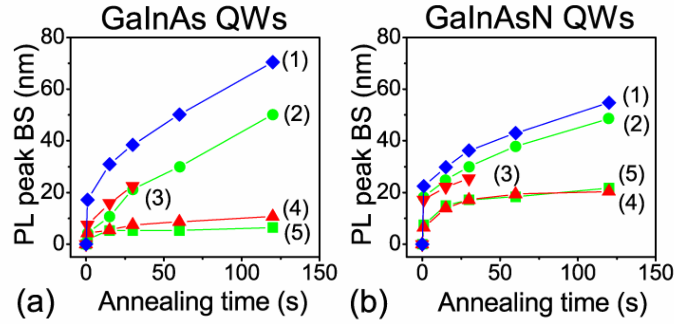

Fig. 10 *BS of PL after annealing at T_{ann} = 700 and 800 °C for GaInAs (a), and for GaInAsN (b) TQWs. Curve (1): T_{ann} = 700 °C for a SiO_2 cap layer, curve (2): T_{ann} = 800 °C for the samples kept inside the "GaAs box", curve (3): T_{ann} = 800 °C for the samples without caps, curve (4) T_{ann} = 700 °C for samples without caps, and curve (5): T_{ann} = 700 °C for the sample placed inside the GaAs box.[Paper1]*

(ii) A larger BS was observed for uncapped GaInAsN than for the uncapped GaInAs samples upon annealing at 700 °C [curves 4 and 5 in Figs. 10 (a) and (b)]. As-grown GaInAsN possesses a random arrangement bonds, e.g., In atom can be bonded to As or N. Upon annealing, however, the In-N bonding is favored,[Lor03] because cohesive energy of In-N bond is higher (1.93 eV) than that of In-As (1.55 eV).[Kim01] When these In-N bonds are formed, the PL wavelength is decreased (BS occurs). Figs. 11 (a) and (b) display atoms in the lattice before and after the formation of a (annealing-induced) In-N bond.[Kur01]

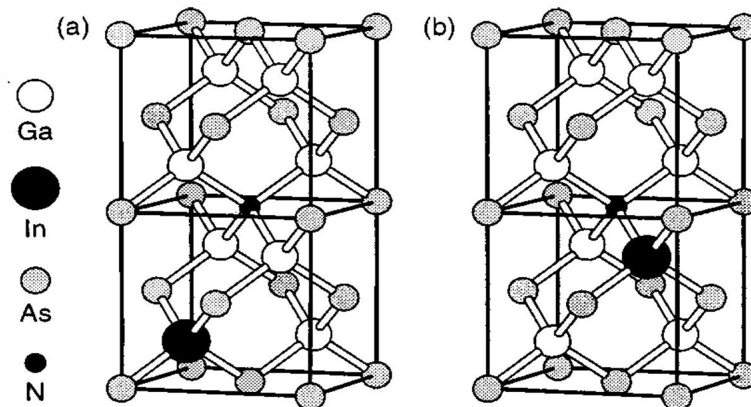

Fig. 11 *GaAs lattice with (a) isolated In and N atoms and (b) N and In next to each other.[Kur01]*

(iii) Judging from (i) and (ii) BS for GaInAsN QWs can be attributed to short-range ordering of N inside the QW and to outdiffusion of In from the QWs. [Pen05]

(iv) XRDs further confirmed N-induced stabilization; e.g., the annealing-induced changes were less dramatic for GaInAsN TQWs [Figs. 12 (a) and (c)] than for GaInAs TQWs [Figs. 12 (b) and (d)]. [Mus05]

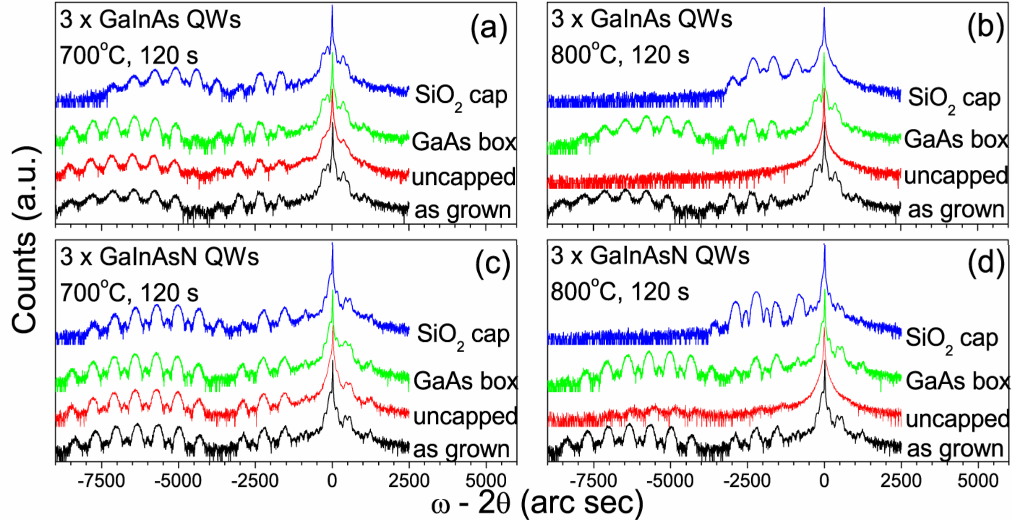

Fig. 12 *XRD(004) rocking curves for the GaInAs and GaInAsN quantum wells before and after annealing 120 s at T_{ann} = 700 °C [(a) and (c)] and at T_{ann} = 800 °C [(b) and (d)] for the samples with the SiO_2 caps (set 1) or for the samples placed inside GaAs box (set 2), or for those left uncapped (set 3). The spectra are shifted vertically for clarity.[Paper1]*

Due to its simplicity (no etching of dielectrics etc.) and proven positive effects on the optical quality, the GaAs-box approach was used for all post-growth annealings performed in this Thesis.

3. Studies of the semiconductor surfaces and interfaces

3.1 Bi-GaAsN and Bi-InP(100)(Paper 2)

In an infinite semiconductor crystal, the positions of atoms are unambiguously determined by the forces acting between them. The surface atoms do not experience the same inter-atomic forces. The surface atoms (~5 atom layers) find new lattice positions; i.e., surface reconstruction occurs, which minimizes the surface energy. A direct consequence is that the surface geometry is usually more complex than the (1×1) bulk geometry. Most of the

stable III-V(100) semiconductor surface reconstructions follow a few basic principles [Sch03]:

(i) Surface atoms dimerize to reduce the amount of unsaturated dangling bonds.

(ii) Electron counting model (ECM) predicts that all of the group-V dangling bonds are doubly occupied, while those of the group-III are unoccupied. This is because the group-V atoms exhibit a larger electronegativity.[Pas89]

(iii) Surface energy is minimized by the spatial arrangement of the dimers.

According to ECM, the smallest surface unit cell for the III-V surface is (2×4).[Pas89] If the cell were smaller than that, not all of the group-V dangling bonds would be saturated (doubly occupied) or there would be “extra” electron(s) after the group-V dangling bonds are filled. Surface phases that do not follow ECM exist. [Whi97] The reason for their existence is suggested to be lowered structural energy, which overcomes the electronic-energy cost of occupying midgap or conduction-band states.

Surfactant-terminated III-V(100) surfaces have gained remarkable commercial and scientific interest, due to their important role in device growth.[Nos99] It has been shown, for example, that using Sb as a surfactant during growth of GaInAsN / GaAs QW significantly improved the optical properties.[Che07] Sb was also reported to remove a CuPt-like crystal order from GaInP.[Fet00] Positive effects of using Bi as a surfactant has been suggested and demonstrated, as well. [Gok07 and Liu07]

Paper 2 explored what kinds of surface reconstructions appeared, when bismuth (the largest group-V element) was evaporated onto clean GaAsN(100) and InP(100) surfaces. GaAsN(100) and InP(100) were chosen because they had a smaller and larger lattice constant than GaAs (100) in which the existence of unusual Bi-stabilized (2×1) was previously reported.[Aho06] The surface phases were monitored by LEED and STM. XPS intensity of Bi *4f* was used to estimate the amount of Bi on the surface. Electronic properties of the surface phases were inspected by STS.

Figs. 13 (a)-(c) and (d)-(f) show LEED patterns of Bi-InP(100) and Bi-GaAsN(100). While increasing the chip temperature, the InP(100) surface showed clear (2×1), (2×4)/(2×8), and, finally (2×4) reconstructions. For GaAsN(100), We found the (2×1) phase to appeared for the highest amount of Bi. Upon annealing, the (2×4) and (4×2) phases were detected.

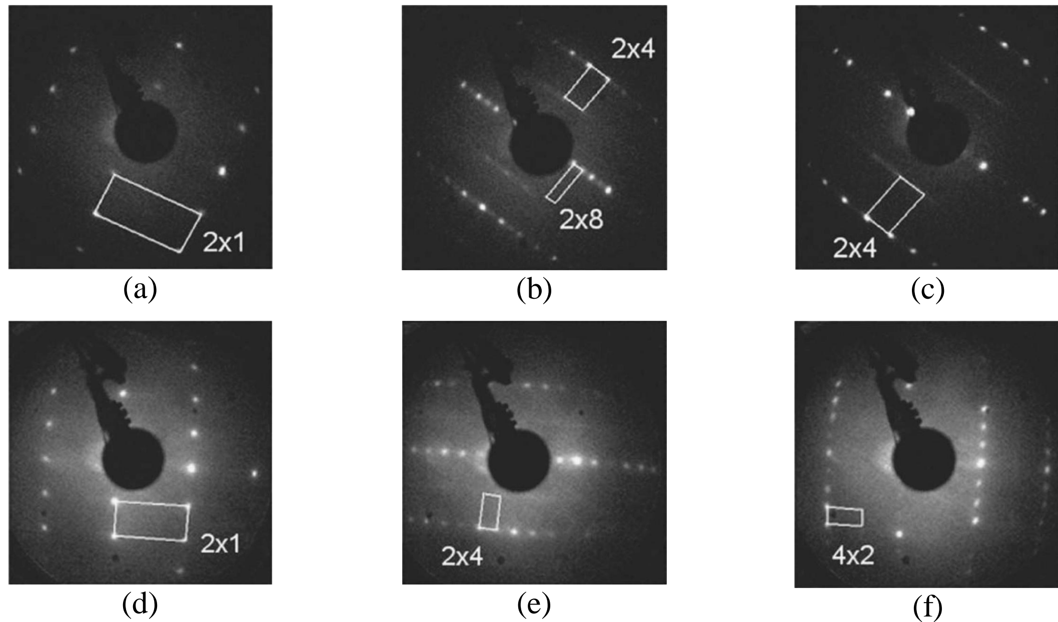

Fig. 13 *LEED for Bi-InP(100) (a)-(c) and for Bi-GaAsN(100) (d)-(f).[Paper2]*

Figs. 14 (a) and (b) show the relative coverage of bismuth (as determined from Bi 4*f* XPS intensities) as a function of annealing temperature. A difference was observed between the InP(100) and GaAsN(100) surfaces; the upper temperature limits for the Bi-stabilized reconstructions were higher for InP(100) than for Bi-GaAsN(100). Similarly, the ratio between the coverage of Bi on InP(100)(2×1) and InP(100)(2×4) was about 3.5, whereas the corresponding ratio between Bi-GaAsN(100)(2×1) and (2×4) was 2.4. These observations indicate that the Bi-stabilized reconstructions were more stable on the InP(100) surface than on the GaAsN(100) surface.

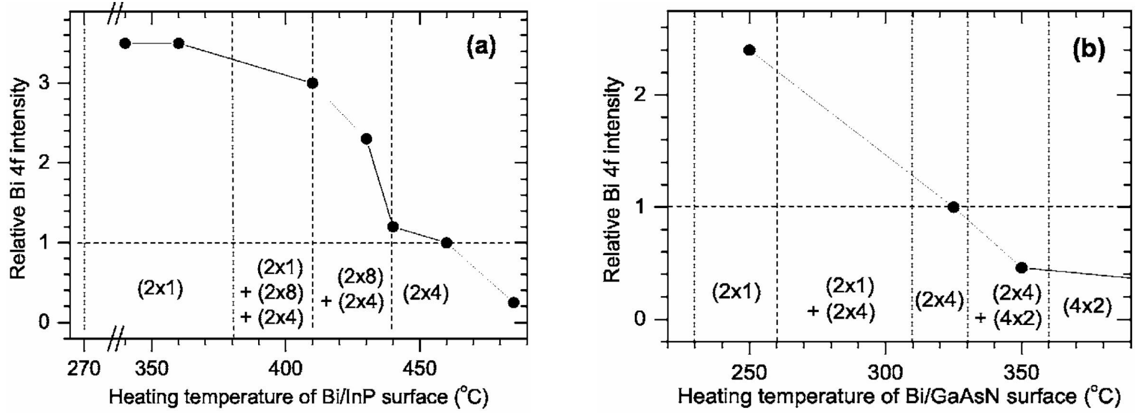

Fig. 14 R*elative Bi 4f intensities from (a) Bi-InP(100) and (b) Bi-GaAsN(100) surfaces. The vertical lines represent the phase transitions, which were observed by LEED and STM.[Paper2]*

Atomic models for the Bi-stabilized (2×4) reconstructions on GaAsN(100) and InP(100) were proposed based on the basis of STM observations and previous results in the literature. STM images for Bi-InP(100) (2×4)/(2×8) and (2×4) are shown in Figs. 15 (a) and (b), respectively. The GaAsN(100) also surface showed a (2×4) reconstruction. A ball-and-stick model, showing an α2(2×4) model with a Bi-dimer on the topmost atomic layer and another Bi-dimer at the third atomic layer, is displayed in Fig. 15 (c). We proposed that InP(100)(2×4) and GaAsN(100)(2×4) were slightly modified from this basic model. For InP(100), in accordance with the previous findings from Bi-InAs(100),[Lau05] it was assumed that half of the third layer Bi-atoms were replaced by P atoms. For the GaAsN(2×4)(100) surface, it was assumed that the Bi was not present at the third atomic layer.[Aho06] With these modifications to the α2(2×4) model, the Bi coverage for InP(100)(2×4) was 0.375 and 0.25 for GaAsN(100)(2×4). When comparing large-scale STM images for InP(100) and GaAsN(100) (2×4) with each other, it was found that the InP surface had better long-range ordering. The reason for the better organized Bi-InP(100) surface was related to the larger lattice constant of InP(100) as compared to GaAsN(100), which allowed more space for the Bi-Bi dimers.

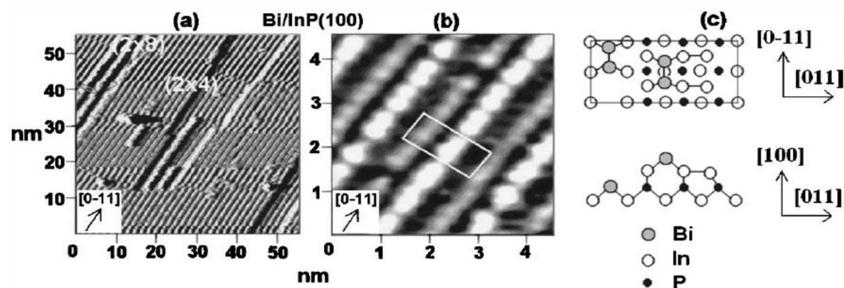

Fig. 15 *(a) Bi-InP(100)(2×4)/(2×8) surface in large scale. (b) Bi-InP(100)(2×4) in atomic scale. The ball-and-stick model of (c) is proposed to explain the observed STM features for (2×4) reconstructions.[Paper2]*

Judging from STM observations, We proposed models for (2×1) reconstructions, see Fig. 16 (a). In addition to the conventional unit cell consisting of only group-V dimers (left panel), the possibility of a mixed-dimer surface phase was considered [right panel in Fig. 16 (a)], because it is shown to exist on the clean InP(100)(2×4) surface as well.[Lau06] Bi coverage of the suggested (2×1) reconstruction models were 0.5 (mixed-dimer) and 1 (Bi-Bi dimmer), which implied (see Fig. 14) that the former was more likely to appear on Bi-GaAsN(100)(2×1) and the latter on Bi-InP(100)(2×1). The electronic properties of the surface phases were examined using STS. The findings are presented in Fig. 16 (b). The well-behaving Bi-GaAsN(2×4) reconstruction (obeys ECM) was found to be semiconducting in good agreement with the theory.[Pas89] Interestingly, electronic properties of the Bi-stabilized (2×1) reconstructions on InP(100) and GaAsN(100) appeared to be different. The (2×1) unit cell is too small to obey ECM and should therefore have a metallic character.[Pas89] However, the InP(2×1) surface was semiconducting, while GaAsN(2×1) surfaces were more metallic.

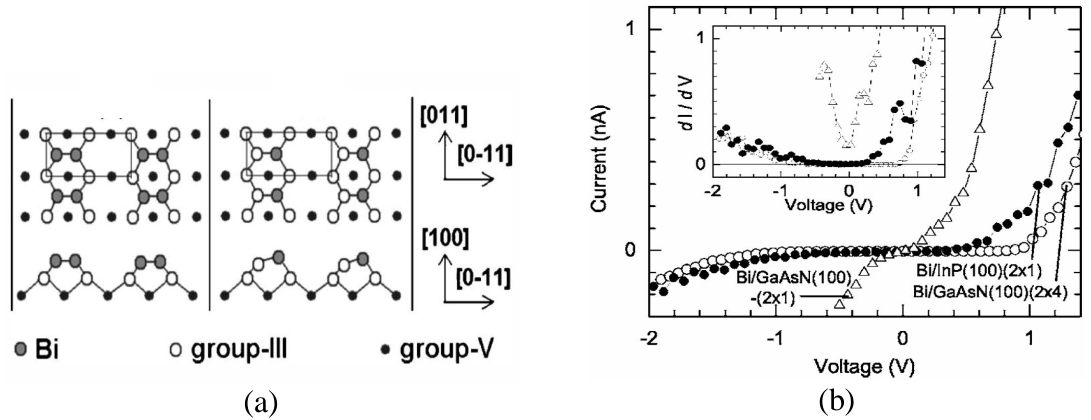

Fig. 16 *(a) Proposed models for Bi-stabilized (100)(2×1) reconstructions. (b) STS [I(V)] measured from Bi-GaAsN(100)(2×4) (open circles), Bi-GaAsN(100)(2×1) (open triangles) and Bi-InP(100)(2×1) (solid circles). The inset displays the corresponding differential curves dI/dV(V) that reflect the surface density of states.[Paper2].*

Reasons for the differences in electronic properties of Bi-stabilized (2×1) reconstructions were tentatively addressed to surface stress. It was suggested that the Bi-Bi dimer (≈ 3 Å in length) could more easily accommodate on the InP(100) surface (with a larger lattice constant) than on the GaAsN(100) surface (with a smaller lattice constant).

A further theoretical and experimental research by Laukkanen *et al.* confirmed that relief of surface stress is one of the main reasons for the stable (2×1) reconstruction on GaAs(100) and InP(100).[Lau08] With *ab initio* calculations, it was shown that the dimerization of Bi atoms reduced surface stress. It was also suggested, that the metallic character of Bi-GaAs(2×1) was due to the size effects: due to the long Bi-Ga back bond, the sp_3 hybridization changes towards p_3 hybridization, which opens a pseudogap at the Fermi energy (e.g., there exist states inside the band gap, explaining the metallic character).

3.2 AlAs/GaAs (Paper 3)

GaAs/AlAs multilayers are used as Bragg reflectors [see Figs. 17 (a) and (b)] because of their large refractive index difference (Δn). AlAs can be deposited with a nearly perfect lattice-match onto GaAs (Fig. 1). MBE growth of AlAs/GaAs multi quantum well (MQW) structures, however, is not problem-free. The structural and electronic properties of GaAs-on-AlAs and AlAs-on-GaAs interfaces are different.[Kri95] In addition, the optimal growth parameters for growth of high-quality GaAs and AlAs differ. [Kim90]

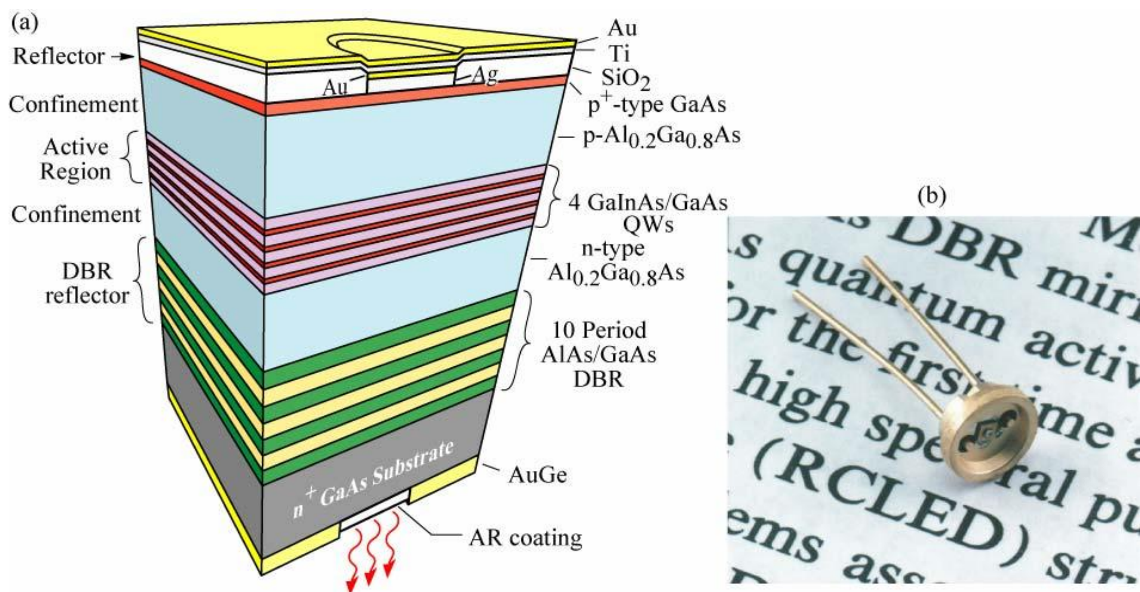

Fig. 17 *(a) A schematic and (b) real image of a GaInAs/GaAs substrate-emitting resonant-cavity light emitting diode (RCLED). Notice the GaAs/AlAs DBR. [Sch94]*

Paper 3 discusses optimization of RT-PL for AlAs/GaAs MQW (nine 10-nm thick GaAs QWs separated by 50-nm AlAs barriers) as a function of constant As/group-III flux ratio.

The constant As/group-III ratio during MBE growth was chosen because it is a reasonable choice for practical device growth. RT-PL intensity was optimized due to it often correlates with the semiconductor laser threshold. Temperature-dependent PL was used as a complementary technique to identify the QW-related optical transitions. Reflection high-energy electron diffraction (RHEED) was used during growth to study surface reconstructions. By increasing the As flux (with constant Ga flux) during growth at 580 °C, GaAs(100) (4×2)-(2×4) phase transition was determined. A similar test with constant Al flux was performed for AlAs(100). AlAs(100) showed (3×1) with low As flux and typically (2×4) reconstruction with higher As flux. Fig. 18 (a) displays the observed phase diagram for the GaAs(100) and AlAs(100) surfaces. Typical RHEED observations for GaAs(100) growth just before the occurrence of (2×4)-(4×2) and (4×2)-(2×4) phase transitions are presented in Figs. 18 (b) and (c).

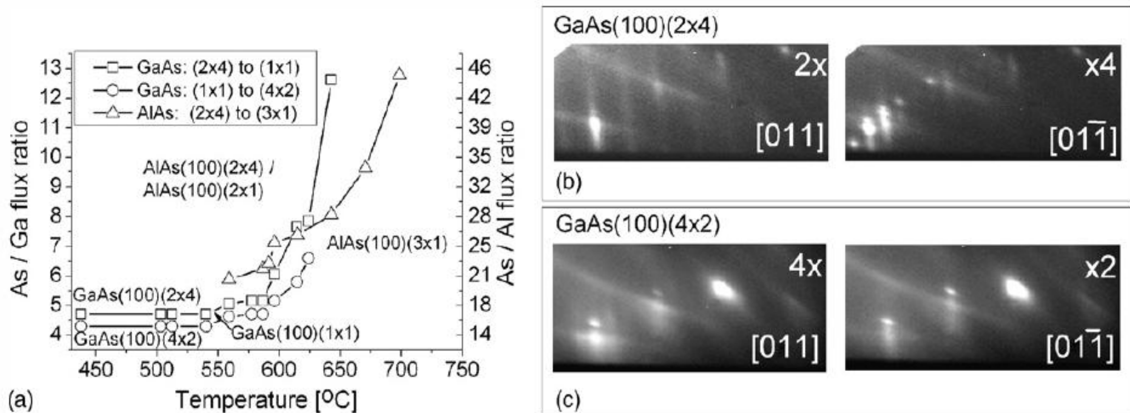

Fig. 18 *(a) As/group-III flux ratio dependent surface phases of GaAs(100) and AlAs(100). RHEED patterns for (b) GaAs(100)(2×4) and (c) GaAs(100)(4×2). [Paper3]*

Numerical values for the As/group-III ratios were determined form Bayard-Albert ionization gauge readings. Five samples were grown with As/Ga flux-ratio ranging from 7 to 24 (As/Al flux-ratio ranged from 28 to 86). The Ga and Al fluxes were same during all growths, while each sample was grown with different constant As flux. Notice that surface reconstructions displayed in Fig. 18 (a) are conveniently related to the As/group-III flux ratio and comparable for different types of MBE reactors.

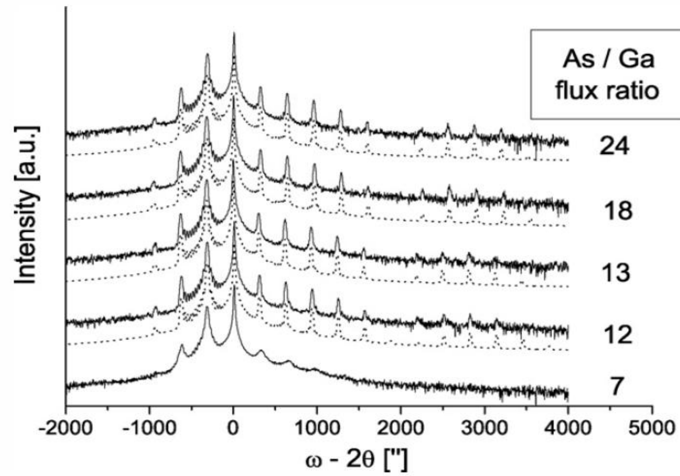

Fig. 19 *XRD (004) rocking curves. Simulated spectra are shown with dashed lines.[Paper3]*

Fig. 19 shows XRD rocking curves. The layer thicknesses were determined from the measured spectra by Rads Mercury simulations. The simulation software uses a dynamical diffraction theory. From the simulations, thicknesses of GaAs QWs and AlAs barriers were 9.8 and 50.6 nm, respectively. The rocking curve for the sample having the lowest As/Ga flux ratio (7) clearly differed from the samples grown with higher As/Ga flux ratio. In addition to the broadened XRD features, the sample surface was gray as compared to the other samples. These observations were addressed to poor crystal quality, which was most likely due to the unsuitable (3×1) growth mode of AlAs.

Fig. 20 summarizes PL observations for the AlAs/GaAs MQW structures. As depicted in Figs. 20 (a) and (b), the best RT-PL was obtained from the sample grown at As/Ga flux ratio of 12, while the lowest PL corresponded to the sample grown with the smallest As/Ga flux ratio of 7. RT-PL intensity also decreased, when As/Ga flux ratio was increased over 12. Hence, the optimum value for MQW growth was determined to be around 12.

To identify the RT-PL features of Fig. 20 (a), the temperature dependency of the two resolved peaks was determined from RT to 10 K. Fig. 20 (c) shows the spectra from the sample with the best RT-PL peak intensity (grown with the As/Ga flux ratio of 12). By comparing the intensity-to-temperature behavior of these two PL peaks [Fig. 20 (d)] to the previous work of Kumar et al.,[Kum97] one can interpret the peaks to originate from e1-hh1 and e1-lh1 transitions in the QWs.

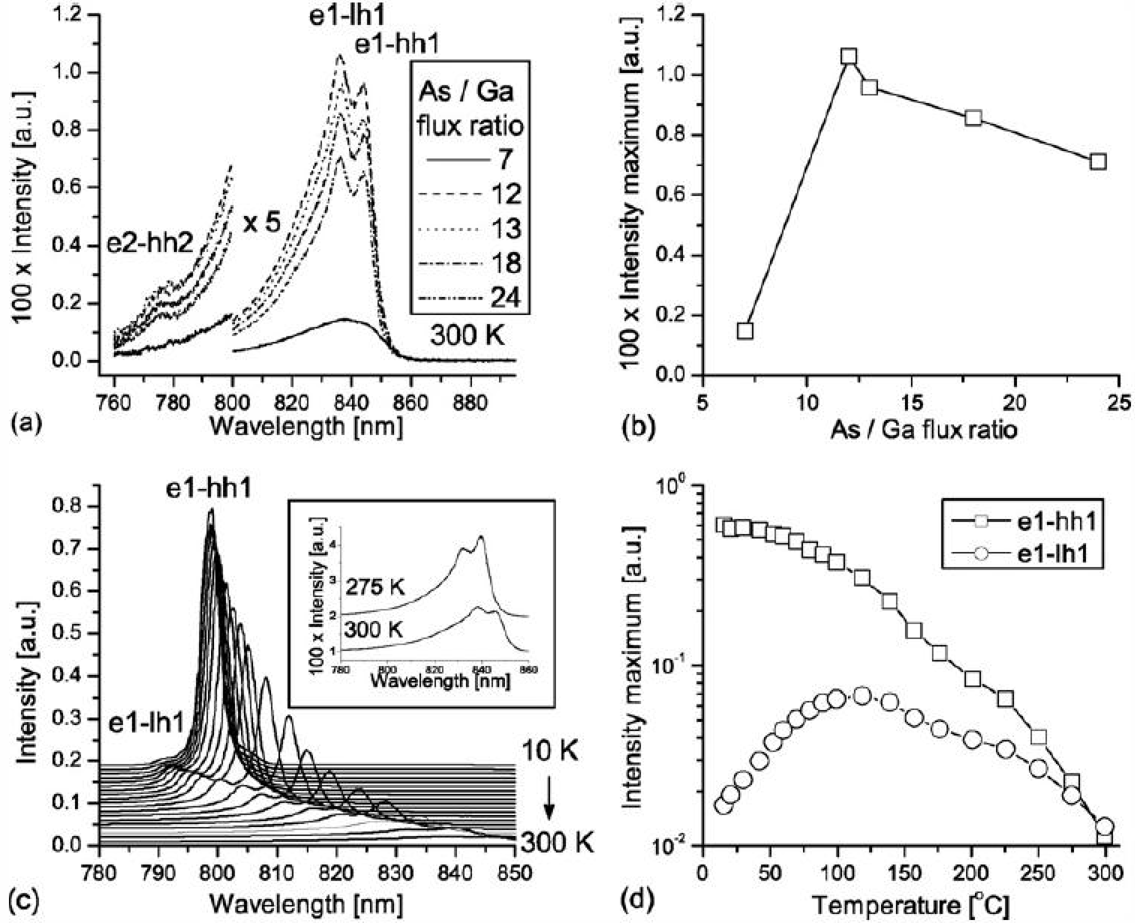

Fig. 20 *(a) RT-PL spectra from the samples grown with different As/Ga flux ratios. Optical transitions e1-hh1, e1-lh1, and e2-hh2 are labeled. (b) Peak-intensity vs applied As/Ga flux ratio for the studied samples. (c) Temperature dependency of PL for the sample with As/Ga flux ratio 12. (d) The temperature behavior of peak intensities of the labeled e1-hh1 and e1-lh1 transitions.[Paper3]*

The suggested peak identification was confirmed using LASTIP simulations. In the simulations, valence and conduction bands were assumed parabolic, and the potential energy profile was assumed to be flat-band and step-wise. Parameters for the simulations were taken from [Vur01]. The material gain for different electron concentrations in the QW (Fig. 21) was calculated based on a parameterized quantum mechanical model. Because the simulation model neglects surface roughness and Γ-X intermixing, peaks at the material gain correspond to an ideal defect-free PL spectrum. By comparing Fig. 20 (a) with Fig. 21, We concluded that all the observed features were due to optical transitions in the QWs.

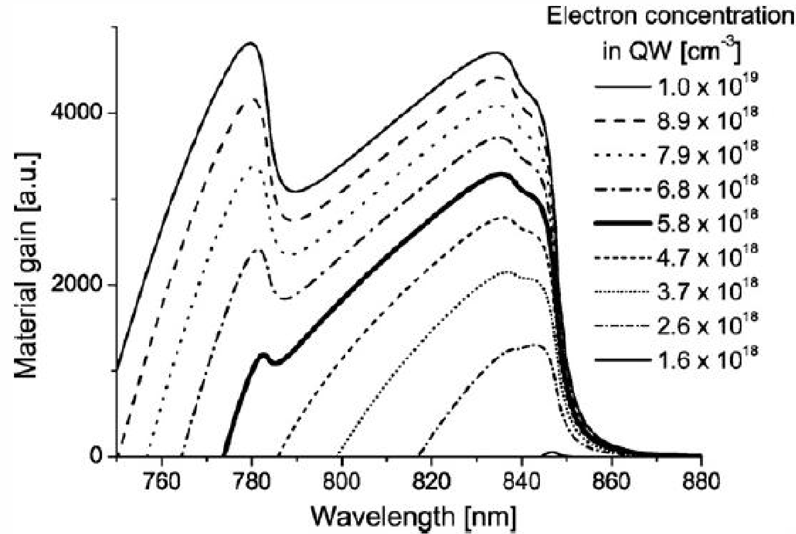

Fig. 21 *Calculated material gain at 300 K for different electron concentrations at the GaAs/AlAs MQW.[Paper3]*

Improved AlAs/GaAs MQW quality was related to the diffusivity of Ga and Al atoms on the growing surface. In the observed optimum range (As/Ga around 12), the GaAs surface has just changed from (4×2) to (2×4) phase. Under such conditions, GaAs(100)(2×4) consists of *α2* and *β2* phases, which are shown in Figs. 22 (a) and (b).

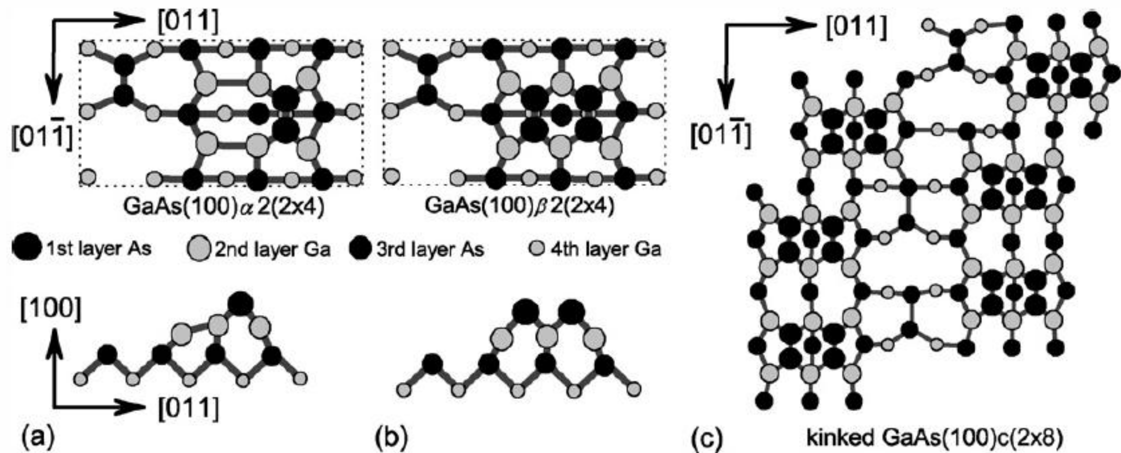

Fig. 22 *Ball-and-stick models for (a) α2 and (b) β2, [Pun07] and (c) kinked c(2×8) GaAs(100) surface.[Has95]*

The group-III atoms migrate among the "ditches" between the As dimes on GaAs(100)(2×4), as demonstrated by the first-principles calculations of Shiraishi.[Shi92] The amount of kink sites [Fig. 22. (c)] increases, as the amount of As dimers is increased. GaAs(100)*β2*(2×4) has twice the number of As-As dimers compared to dimers on GaAs(100)*α2*(2×4). The length of ditches is then reduced, as the amount of As is

increased, which leads to reduction in migration length of Ga on the surface. We proposed that this was the main reason for the optimal As/Ga ratio being close to the phase transition from GaAs(4×2) to GaAs(2×4).

3.3. Summary

In the two previous chapters, surface reconstructions, and their influence on MBE growth were studied. In [Paper 2], an interesting stable (2×1) reconstruction was found for the Bi-stabilized GaAsN(100) and InP(100) surfaces. Due to the presence of large Bi-Bi dimers, the GaAsN(100) surface was found metallic, in agreement with ECM. In contrast, the stable (2×1) reconstruction on InP(100) with a larger lattice constant was semiconducting. In [Paper3] the effects of different GaAs(100) and AlAs(100) surface phases on MBE growth were outlined. By studying PL, the optimal As/Ga flux ratio (~12) was shown to correspond a situation where the GaAs(100) surface has changed from (4×2) to (2×4). The reason for the optimal As/Ga ratio being close to the (4×2)-(2×4) phase transition was attributed to group-III migration properties on the growing front.

4. Studies of the Be-doped III-V's

4.1 Be-doped GaInAsN QW (Paper 4)

GaAs-based dilute nitrides have been hot topics of the scientific community, due to their desired properties, which may be suitable for telecommunication links. However, doping dilute nitrides has been less explored than doping GaN or Al(Ga)As.[Que98] Interesting physical phenomena take place in doped GaAsN, due to the small size of dopants and the electronic character of N atoms. For example, when Si-doped GaAsN was annealed the effect of N on the band-gap and the effect of Si-doping (*n*-type dopant) on the electron concentration were found to diminish.[Li01,Yu02] This "mutual passivation" was recently shown (by the first principles calculations) to originate from the formation of Si-N split interstitial defects.[Jan08]

Density functional theory (DFT) calculations have only recently tackled the *p*-type doping of GaAsN.[Kom09] In a nutshell, it was found that the small Be and N atoms interact with each other and are likely to form defect clusters around substitutional Be (at the Ga-site) and N (at the As-site). Experimentally, when a high *p*-type doping was incorporated into GaInAsN QWs, PL intensity dramatically increased upon prolonged annealing and the threshold current of the laser was decreased.[Pen05b] Paper 4 discusses reasons for the annealing-enhanced optical properties on the basis of XRD and secondary mass ion spectrometry (SIMS) results.

In our experiments, a 100-nm GaAs buffer was grown at T_{growth}=580 °C on a Si-doped GaAs substrate. Then, $Ga_{0.65}In_{0.35}As_{0.99}N_{0.01}$ QWs (6.50 nm) were deposited at T_{growth}= 460 °C and capped with a 100-nm GaAs layer, while T_{growth} was ramped back to 580 °C. In one sample, the QW was undoped; in another, the QW was doped with Be to 6×10^{19} cm^{-3} (calibrated with separate *p*-GaAs Hall-effect samples). Post-growth annealing the samples was done at 800 °C in a closed GaAs box.[Paper1] PL was measured upon each annealing. XRD and SIMS were measured for the as-grown and annealed samples.

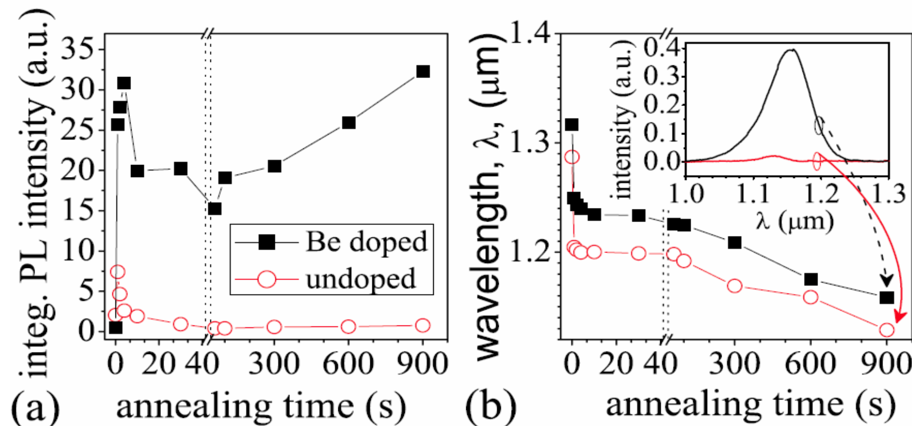

Fig. 23 *(a) Integrated PL intensity and (b) wavelength for the Be-doped and undoped GaInAsN samples.[Paper4]*

Fig. 23 (a) shows integrated PL intensities of the GaInAsN QWs upon annealing. A typical increase (see [Paper 1]) in integrated intensity first appears for both samples. When annealing was continued, integrated PL of the Be-doped QW showed an increasing trend – in sharp contrast to the undoped sample. As depicted in Fig. 23 (b), the wavelengths of the undoped and Be-doped QW samples behaved in much the same way;

i.e., the blueshift took place. However, the blueshift of Be-GaInAsN was 40 nm smaller than that of undoped GaInAsN for all annealing times.

SIMS and XRD results for the as-grown and annealed (900 s at 800 °C) samples are shown in Fig. 24. The widening of the In profile upon annealing for the undoped sample indicated that In diffused out of the QW. XRD (004) rocking curves exhibited a similar indication; the broad QW-related peak (around -6000 arc sec) showed that lattice relaxation was suppressed for the Be-doped sample. Due to the high strain of the QW ([In] ≈ 35 %), we could not exclude the possibility that crystal defects existed, reducing strain. [Gra01] Beryllium doping increased thermal stability of the GaInAsN QW, as judged from the XRD and SIMS.

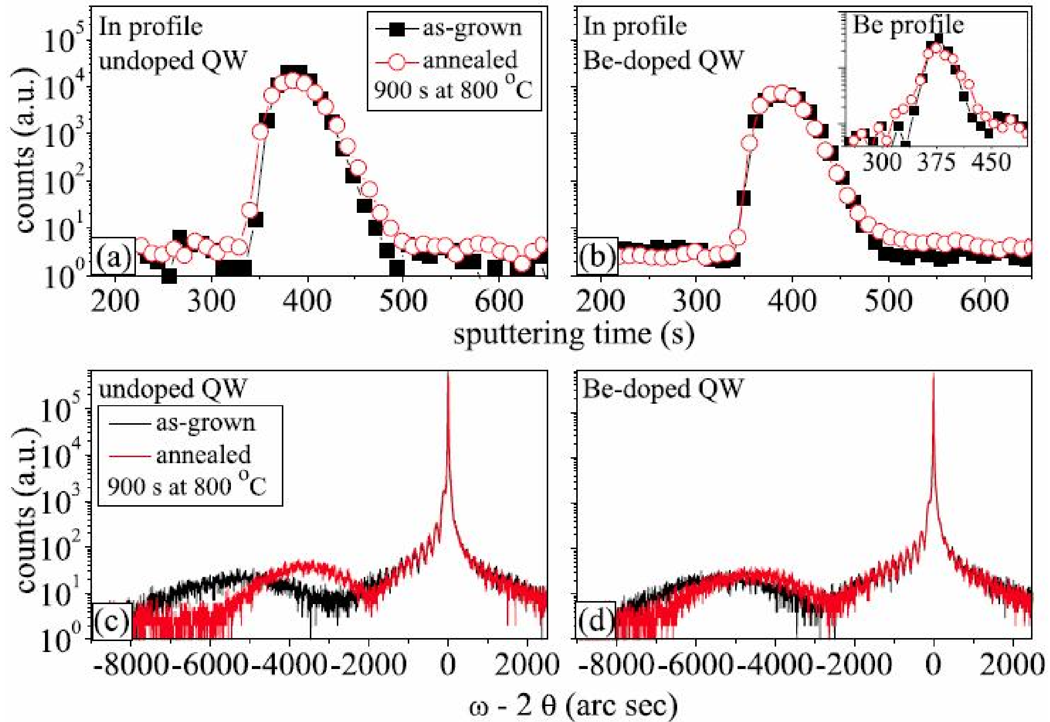

Fig. 24 *SIMS profiles for undoped sample (a) and Be-doped sample (b) before (black) and after (red) the annealing. Corresponding XRD (004) rocking curves are shown in (c) and (d), respectively.[Paper4]*

The mechanism for Be-induced suppression of indium diffusion was discussed. Ga-vacancies have a promoting effect on diffusion of indium. [Paper1 and references therein] Especially, these vacancies are present in dilute nitride materials, due to presence of N and relatively low growth temperature. It was suggested that beryllium and indium diffuse *via* the same defect-assisted path. However, since the small Be atoms diffuse more easily [inset of Fig. 24 (b)], they could block the diffusion path for indium. The recent first-

principle calculations agree with the interpretation; Be was found to incorporate Ga sites whenever possible in GaAs and GaAsN.[Kom09]

PL intensity of the undoped sample quenched upon prolonged annealing. Extended crystal defects, which may be created during the annealing of highly strained QWs,[Gra01] act as non-radiative centers and decrease PL. An interaction between Be and these extended defects has been reported.[Iha02] We proposed that in addition to the suppressed diffusion of In, superior optical properties of the Be doped sample were likely to be related to the Be-induced relaxation of local stress without the formation of crystal defects.

An additional aspect, not considered in [Paper4], is the Be-induced change in electronic properties. In the literature, quenching of PL for dilute nitride QWs has been attributed to the escape of holes from the QWs.[Hug07, Tan03] While N induces a large bandgap bowing for the GaInAs conduction band, effects on the valence band are minor. The ratio of the conduction band offset to the valence band offset is roughly 80:20 for GaInAsN/GaAs QWs.[Hen04] The improved PL for the Be-doped sample could, in part, be accounted for by an increased amount of holes in the QW.

4.2 Be-doped InAs QDs (Paper 5)

Self assembled InAs quantum dots on GaAs are promising building blocks for semiconductor devices. MBE growth of QDs resembles the growth of dilute nitrides, because growth temperature of QDs is ~100 °C less than the optimal one for GaAs. Therefore, the GaAs barriers play a significant role. High growth-temperature procedure for the barriers improves the structural and optical quality of QD heterostructures and also improves QD laser charasteristics. [Liu04b] In addition to ramping the growth temperature up and down before and after the QD deposition, the uppermost barrier also suffers from crystal defects, because it is deposited onto the dotted surface. [Men07]

Modulation doping of the QD lasers with beryllium has been shown to improve the temperature stability,[Bad07] but at the same time it increases the lasing threshold. PL studies have also indicated [Cao08] that *p*-doping the GaAs barriers improve the thermal

stability of QD heterostructures. In Paper 5, We systematically studied effects of *p*-doping on InAs/GaAs QD structures.

By modifying the same MBE recipe ([Paper 5] includes MBE details), six samples (Samples 1-6) with different dopings were grown, as shown in Fig. 25. Sample 1 was left undoped. Sample 2 was undoped, except for the QDs which were doped with Be to about 1×10^{20} cm^{-3}. Sample 3 consisted of a 3-nm thick layer of doped GaAs, which was placed 15 nm away (below and above) the undoped QDs. Sample 4 contained similar 3-nm thick GaAs:Be layers but 40 nm away the undoped QDs. Sample 5 had the doped layer only 15 nm above the QDs, while Sample 6 had the doped layer placed 15 nm below the QDs.

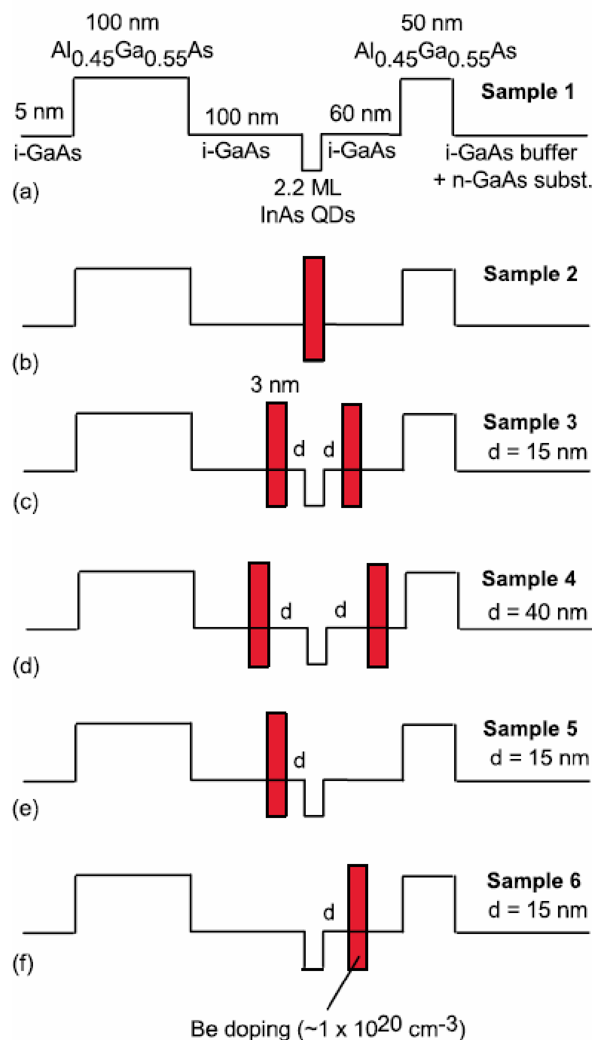

Fig. 25 The *grown QD structures: (a) Sample 1 without Be doping; (b) Sample 2 with Be-doped QDs; (c) Sample 3 with 3-nm thick Be-doped GaAs layers placed 15 nm away from the QDs; (d) Sample 4 with 3 nm Be-doped layers placed 40 nm away from the QDs; (e) Sample 5 with a 3-nm Be-doped GaAs layer placed 15 nm above the QDs; (f) Sample 6 with a 3-nm Be-doped GaAs layer placed 15 nm below the QDs. Doping concentration was about* 1×10^{20} *cm*$^{-3}$*.[Paper5]*

Fig. 26 summarizes the PL results for Samples 1-6 upon annealing at 800 °C. The PL spectra were least-square fitted to three Gaussian peaks (as shown in the insets of Fig. 26): the ground state (E_0), the first excited state (E_1), and the second excited state (E_2). A clear trend in E_0 intensities appeared for Samples 3 and 5, where the Be-doped layer was 15 nm above the undoped QDs. PL first decreased, but then stayed at a higher level than that of undoped Sample 1. If the doping was placed far away (Sample 4) or below the QDs (Sample 6), the effect of doping was not so remarkable. For Sample 2 with QDs highly doped with Be, PL increased upon annealing, but the effect was less remarkable than that in the case of Be-doped GaInAsN QW. [Paper 4] An interesting observation was that Samples 3 and 5, with Be doped GaAs layers placed 15-nm above the QDs, showed a combination of the PL behaviors of undoped Sample 1 (rapid decrease immediately) and Sample 2 with doped QDs (i.e., an increasing trend after 1 s annealing).

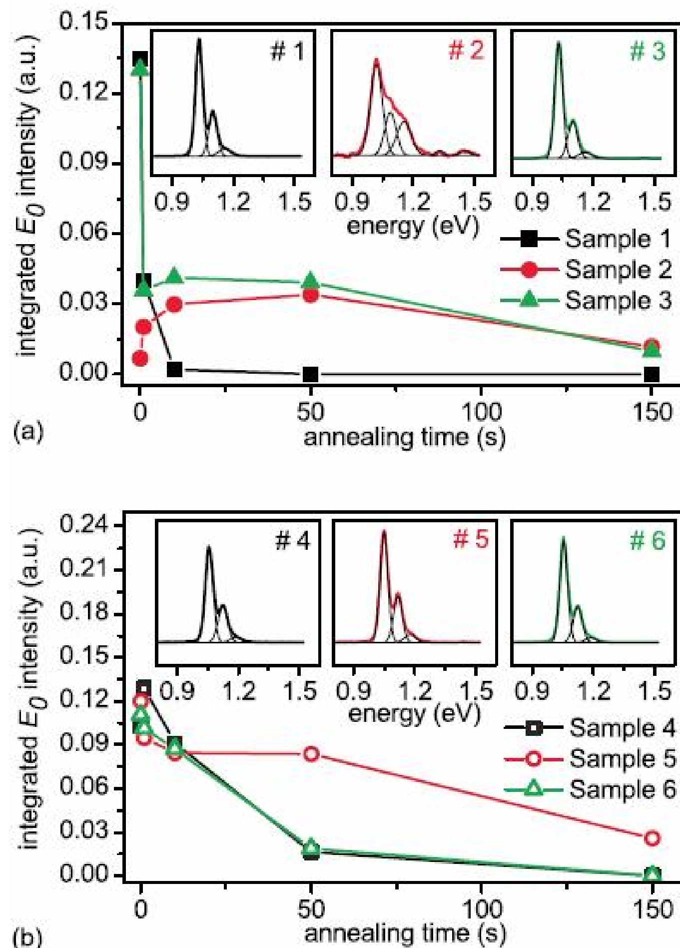

Fig. 26 *Integrated PL intensities for the E_0 transitions as functions of annealing time at 800 °C for (a) Samples 1-3 and (b) Samples 4-6.The insets display the measured and fitted spectra for the as-grown samples.[Paper5]*

The ground state wavelength, its separation from the first excited state (*ΔE*) and full-width-at-half maximum (FWHM) and are displayed in Figs. 27 (a) – (c). While emission blue-shifted, *ΔE* for all of the samples decreased nearly linearly. At the same time, the FWHM values for Samples 2-6 showed an interesting trend, namely, the peaks first became wider, then sharpened. According to previous results in the literature, both of the observed features can be related to deformation of the confinement potential due to outdiffusion of indium from the QDs. The decrease in *ΔE* upon increase in E_0 is schematically shown in Fig. 27 (d). [Leo98] Fig. 27 (e) depicts simulated results for the FWHM behavior upon interdiffusion in the growth direction. [Ras04] Clearly, the outdiffusion of indium from the QDs was suppressed for Samples 2, 3, and 5, which had the doped QDs or which had the Be-doped layers placed 15-nm away the undoped QDs, respectively. However, the FWHM values for Sample 1 with doped QDs only showed a decreasing trend. To fully understand the effects of Be-doping on the QDs, further theoretical research on the electronic properties of the QDs must be conducted.

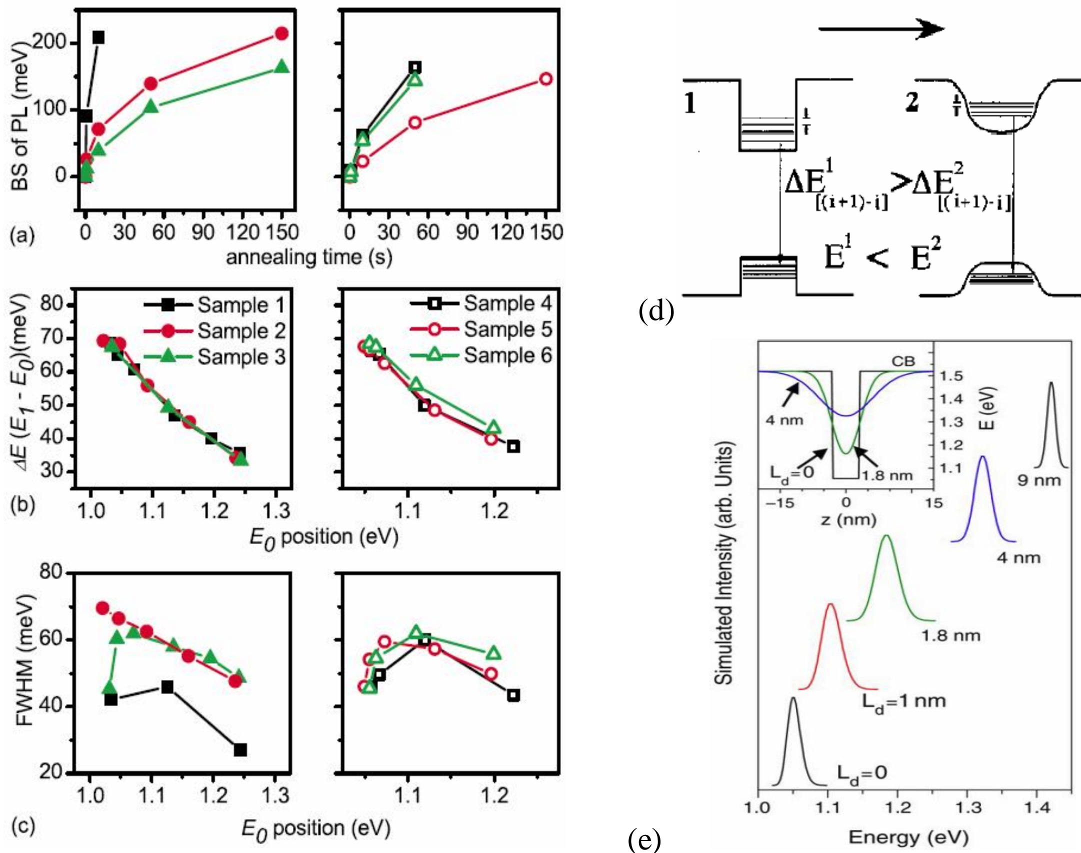

Fig. 27 *(a) PL emission blue-shift as a function of annealing time (b) separation of the first excited state and the ground state as a function of the ground state energy (c) FWHM values for the ground state transitions.[Paper5](d) The QD energy bands behavior before (1) and after (2) annealing. [Leo98] (e) Simulated PL spectra for a narrow QW as a function of diffusion length (L_d).[Ras04]*

According to earlier reports, doping a semiconductor heavily with beryllium improves PL intensity, shifts the PL peaks to longer wavelength, and broadens the peaks.[Ile77] Comparing these results with those of Fig. 27, it is clear that the high doping was responsible for the widened PL peaks (the undoped sample had the sharpest E_0) and the doping also redshifted the wavelength. A question then arose whether the differences in BS could originate from a kind of activation of the dopants by annealing, rather than from suppressed diffusion of indium. This possibility was, however, ruled out, because the effect of doping (less than 50 meV) was much less than the suppressed BS (over 100 meV).

In agreement with previous results for GaInAsN QWs,[Paper4] suppression of indium diffusion was shown to be due to the presence of beryllium. By varying the Be doping location, it was pointed out that the most detrimental defects became passivated in the GaAs layer, which was deposited onto the dotted surface during the growth temperature ramp-up.

4.3 Be-doped GaInAs QW

Beryllium doping of GaInAs / InP has been investigated because of its use in heterojunction bipolar transistors (HBTs). The interest has been in controlling the diffusion of the Be during thermal processing of the HBTs. For GaInAs / GaAs, diffusion of In has been of main interest because it has been addressed to the degradation of 980-nm GaInAs QW lasers.[Chu04] Due to the stability problems of the GaInAs lasers, and motivated by the results obtained from the Be-doped GaInAsN QWs and InAs QDs, beryllium was incorporated into GaInAs/GaAs QWs, which can be deemed a simple model system for monitoring the atomic diffusion.[Bol05]

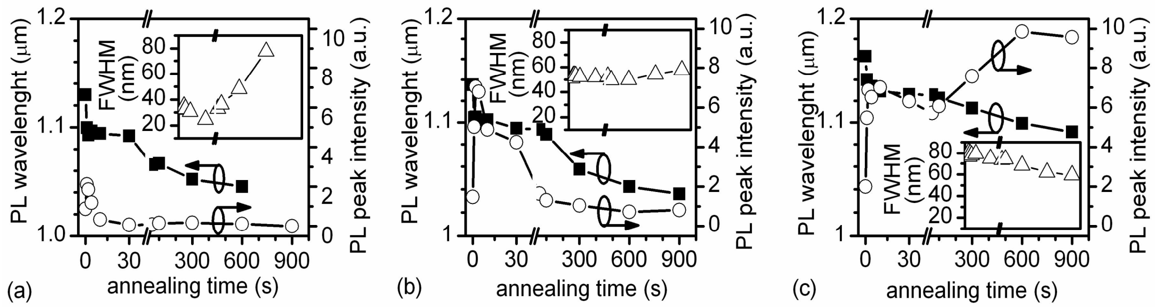

Fig. 28 *PL peak intensities and wavelengths for (a) the undoped sample, (b) the sample with QW doped to 5×10^{18} cm^{-3}, and (c) QW doped to 6×10^{19} cm^{-3} as a function of annealing time. The insets display the FWHM values upon annealing.*

An annealing test (inside the GaAs box [Paper1] at 800 °C) was performed for the GaInAs samples similar to what was done for the GaInAsN samples in [Paper4]. Figs. 28 (a) – (c) summarize our PL observations as a function of annealing time. For the undoped sample, PL was first slightly improved but then it quenched. A sample with a QW Be-doped to 5×10^{18} cm^{-3} showed a similar trend, but it took longer (~ 30 s) for PL to quench. A drastic difference was noticed when the sample with a QW doped to 6×10^{19} cm^{-3} was annealed; PL kept increasing, resembling the behavior of GaInAsN QW sample studied in [Paper4]. Again, Be-doping increased the FWHM values of PL peaks and redshifted the emission wavelength.

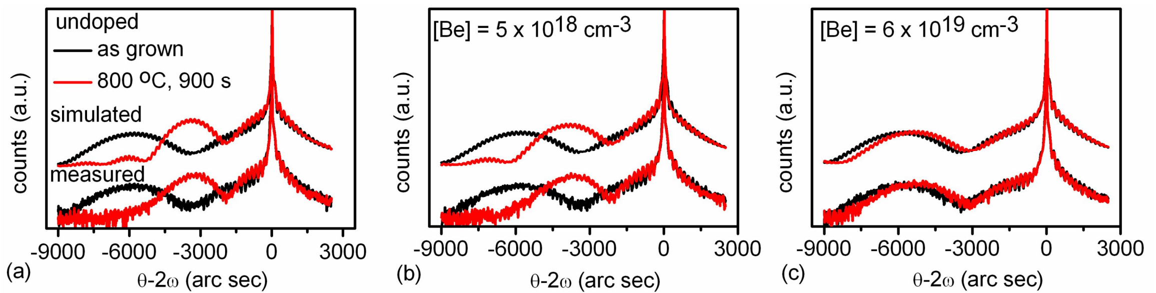

Fig. 29 *XRD spectra and simulations (shifted in the vertical direction for clarity) for as-grown (black) and annealed (red) (a) an undoped sample, (b)* a *sample with QW doped to 6×10^{18} cm^{-3}, and (c) a sample with QW doped to 5×10^{19} cm^{-3}.*

XRD rocking curves were measured for the as-grown and 900 s at 800 °C annealed samples. The spectra were simulated by using Rads Mercury simulation software. In the simulations, the composition of indium ([In]) and the QW width (*d*) were left as open parameters. Fig. 29 (a) – (c) shows the measured and simulated spectra. The XRD measurements and simulations were in good agreement with the PL measurements, thus showing the smallest annealing-induced changes for the sample with QW doped to 5×10^{19} cm^{-3}. The undoped sample suffered from the most pronounced effects: the biggest

reduction in [In] and the biggest increase in *d*. Simulated values are collected to Part A of Table I.

Table I. *Properties of GaInAs/GaAs QWs before and after annealing at 800 ºC. The indium compositions of the samples [In] and the QW widths (d) were determined from the simulations.*

Part A	as-grown				annealed	
Sample		[Be] (cm^{-3})	*d*(nm)	[In]	*d*(nm)	[In]
1		undoped	6.4	33.8	10.9	18.9
2		5×10^{18}	6.4	33.8	9.8	21.4
3		6×10^{19}	6.4	33.8	6.8	31.1
Part B	as-grown				annealed	
Sample	coating	[Be] (cm^{-3})	*d*(nm)	[In]	*d*(nm)	[In]
4	SiO_2	undoped	6.4	33.8	26.2	7.2
5	uncapped	undoped	6.4	33.8	17.5	11.7
6	SiO_2	6×10^{19}	6.4	33.8	10.8	19.0
7	uncapped	6×10^{19}	6.4	33.8	9.7	22.2

To elucidate the mechanisms that led to improved thermal stability of the Be-doped GaInAs/GaAs QWs, another set of annealing was carried out. The samples were either capped with 200-nm thick SiO_2 (which produces Ga vacancies) or left uncapped. Fig. 30 shows the measured PL spectra for (a) the undoped and uncapped sample, (b) the undoped and SiO_2 capped sample, (c) the $6\times10^{19}cm^{-3}$ doped and uncapped sample, and (d) the $6\times10^{19}cm^{-3}$ doped and SiO_2 capped sample. The PL intensity behavior of the uncapped samples [Figs. 30 (a) and (c)] closely resembled the behavior shown in Figs. 28 (a) and (c); PL for the undoped sample quenched, while it increased upon prolonged annealing for the Be-doped sample. For the SiO_2 capped samples [Figs. 30 (b) and (d)], PL of the undoped sample quenched much faster than in the uncapped case. PL for the capped and doped sample [Fig. 30 (d)] was clearly observable upon the longest annealing, albeit at small intensity.

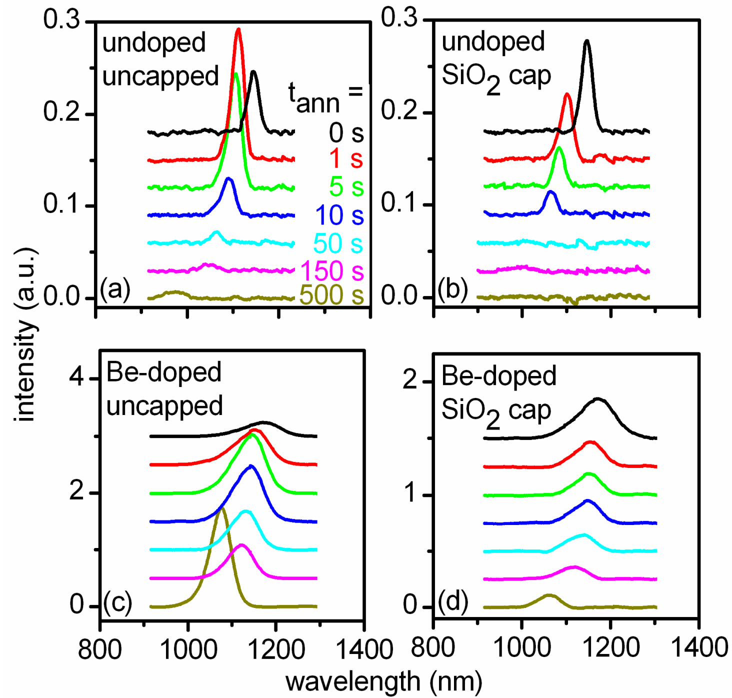

Fig. 30 M*easured PL spectra upon different annealing times for (a) the undoped and uncapped sample, (b) the undoped and SiO_2 capped sample, (c) the Be-doped and uncapped sample, and (d) the Be-doped and SiO_2 capped sample.*

The BS of PL, as determined from the PL spectra, is shown in Fig. 31. A clear difference was observed between the doped and undoped samples; SiO_2 capping induced a rapid BS for the undoped sample but the effect was strongly suppressed for the Be-doped samples. This behavior further gave justification for the suggestions given in [Paper4] and [Paper5]; Be-doping has a tendency to stabilize the structure likely *by* passivation of Ga vacancies. XRD rocking curves, in good agreement with PL observations, are shown in Fig. 32 and the simulated values for [In] and *d* are collected to Part B of Table I.

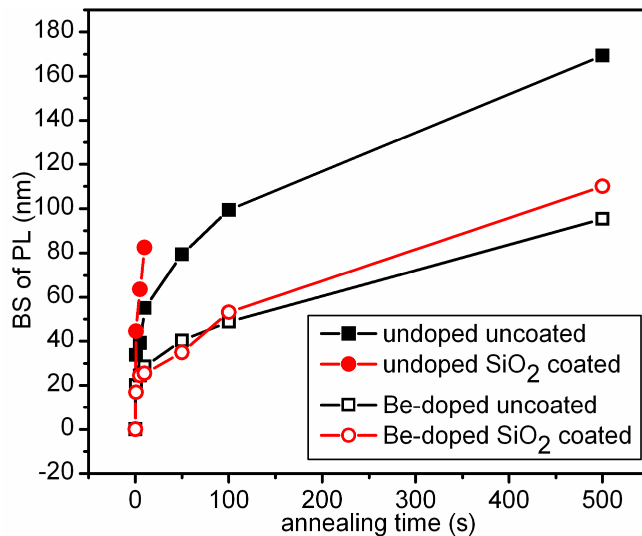

Fig. 31 *BS of PL for the uncapped and SiO2 capped samples with or without Be doping.*

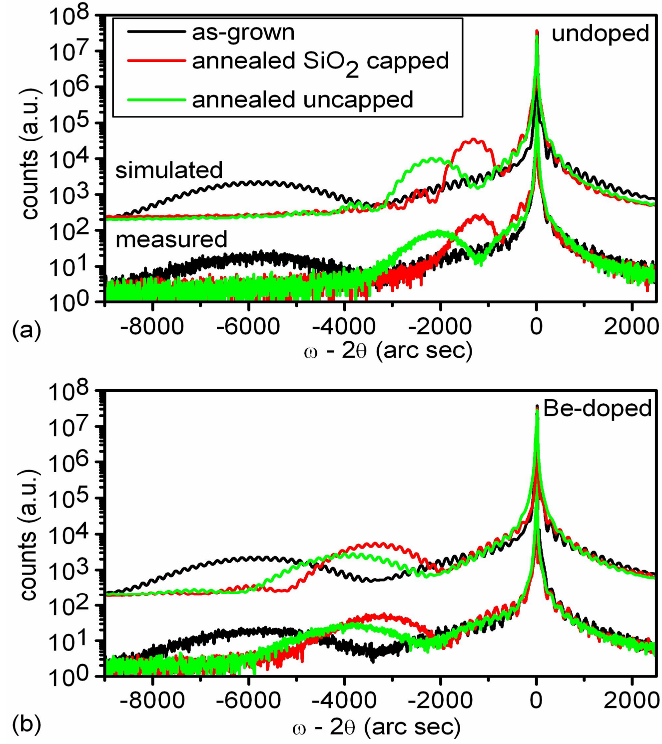

Fig. 32 *XRDs before and after the annealing for (a) an undoped and (b) Be-doped sample coated with SiO_2 or left uncapped. Simulated spectra are shifted in the vertical direction for clarity.*

A box-shape function was used to describe the shape of the In profile. To maintain the box shape, In atoms diffuse depending on its concentration, e.g., In atoms on the center of the QW must have larger diffusion coefficient than those close to the interfaces. For all our uncapped samples, the model worked fine, deviations between the simulated total In (In composition times the QW width) for the as-grown and annealed samples were below 5 %. However, when the undoped sample was coated with SiO_2, deviation between the simulated total In values showed a clear increase (more than 10 %). A similar effect was not seen for the Be doped sample having the SiO_2 cap upon annealing. Most likely, the diffusion mechanism was changed from its concentration-dependent model for the capped and undoped sample, due to the presence of Ga vancies, which have a tendency to promote diffusion of In over the GaInAs / GaAs QW/barrier interface.

The previous observation on deformation of the In profile upon annealing for the undoped SiO_2 capped sample in contrast to the Be-doped SiO_2 capped sample, which maintained its shape, lends further support to the idea of passivated Ga vacancies of the Be-doped sample.

Gain guided broad-area lasers with the oxide stripe width (W) of 40 μm were fabricated to test the ability of Be-doped 980-nm laser diodes. A comparison was made between two lasers. One consisted of undoped GaInAs triple-QWs. The second had an otherwise similar structure but the QWs were doped with Be up to 6×10^{18} cm^{-3}. Altogether, six devices were processed; cavity lengths (L) were 600, 1000 and 1600 μm, and two devices of each were fabricated.

Threshold current densities (J_{th}) of the laser diodes with different cavity lenghts were determined from the measured light output versus injection current (L-I) curves (Fig. 33). Table II summarizes the results. The J_{th} values for the laser with Be-doped QWs were systematically smaller and the L-I slopes were slightly higher.

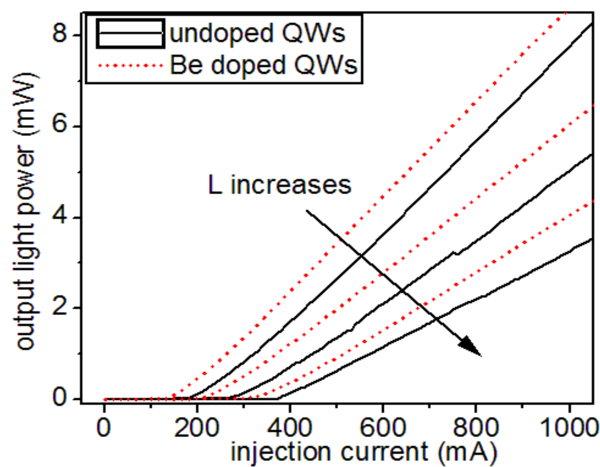

Fig. 33 *Light output versus injection current curves for Be-doped (dotted red line) and undoped (solid black line) QW laser diodes.*

Table II. *J_{th}s for the undoped and Be-doped GaInAs QW lasers with different cavity lengths.*

cavity length (μm)	600	1000	1600
J_{th} for Be doped device (A/cm^2)	562.5	550.0	492.2
J_{th} for undoped device (A/cm^2)	687.5	587.5	562.5

Even a higher Be-doping was tested for the 980-nm lasers, but it degraded the laser performance, probably due to scattering of carriers from the large amount of ionized dopant atoms. An interesting question arises whether there would be applications for

highly Be-doped (over 10^{19} cm^{-3}) and thermally very stable QWs among optically pumped devices.

Further research on thermal stablility of Be-doped GaInAs QW lasers will be performed. According to PL results of Fig. 28, there should be some improvement in the even when the doping level is only 5×10^{18} cm^{-3}.

4.3 Summary

It was found that when GaAs-based GaInAsN and GaInAs QWs were doped with beryllium, annealing-induced strain relaxation was significantly suppressed. SIMS measurements for GaInAsN QWs provided evidence that diffusion of In was suppressed. This observation was further confirmed by XRD. Similar trends were observed for GaInAs/GaAs QWs. By coating the GaInAs samples with SiO_2, Be showed a tendency to passivate annealing-induced Ga vacancies. Another strain relaxation mechanism, the formation of dislocations, which act as non-radiative centers was likely responsible for quenching of PL for the undoped GaInAs(N) samples upon annealing. A moderate Be-doping (5×10^{18} cm^{-3}) increased PL peak intensity for the as-grown GaInAs samples and enhanced their temperature stability. The moderate level of Be-doping decreased the threshold current density of a GaInAs triple-QW laser operating at λ= 980 nm. A higher level of doping (5×10^{19} cm^{-3}) increased the threshold.

The stabilizing effect by Be-doping was found in self-assembled InAs QDs on GaAs. By introducing a 3-nm Be-doped region (~ 1×10^{20} cm^{-3}) close to the undoped QDs, diffusion of In was suppressed, as deduced from PL spectra. It was proposed that Be had a tendency to passivate point defects that were due to low growth temperature and deposition of GaAs onto the dotted surface.

5. Conclusions and final remarks

In this Thesis, III-V semiconductors and devices were prepared and studied in many different ways. Along the "journey", five articles were published in peer-reviewed journals.

A lot of interesting (surface) physics can be found from clean and surfactant stabilized III-V(100) surfaces. It was found that bismuth (with a substantially larger atomic size than that of arsenic) stabilizes (2×1), (2×4)/2×8), and (2×4) reconstructions on InP(100) and (2×1), (2×4), and (4×2) reconstructions on GaAsN. Interestingly (2×1) reconstructions of InP(100) and GaAsN(100) were semiconducting and metallic, respectively, probably due to large size of a Bi-Bi dimer. By monitoring the early stages of nucleation of GaAs(100) and AlAs(100) formation using RHEED, an optimum As/Ga(Al) ratio (~ 12) for growth of a multiple-QW structure was found near the conditions where GaAs(100) surface underwent a phase transition from (2×4) to (4×2). This phenomenon was related to diffusion length of the group-III atoms on the growing surface.

The optical and structural properties of GaInAs and GaInAsN triple-QWs were studied upon different post-growth thermal treatments. In was found that a box made of GaAs was the best method for improving the optical quality by annealing, while SiO_2 capping, as well as uncapping, led to lower PL and larger BS. Several previous results could be confirmed: (i) N-induces thermal stability, (ii) BS of PL is a sum of two factors, namely, In-N bonding and In/Ga intermixing over the QW/barrier interface, and (iii) SiO_2 capping increased In/Ga intermixing, probably linked to the formation of Ga vacancies at the SiO_2 /GaAs interface.

Incorporating beryllium into a GaInAsN/GaAs QW, a GaInAs/GaAs QW, or InAs/GaAs QDs increased thermal stability of these heterostructures. It was found that the strain relaxation of Be-doped GaInAsN QWs was reduced when compared to an undoped sample. From SIMS, XRD, and PL measurements, the mechanism behind the phenomenon was suggested to be suppressed diffusion of In and the Be-induced relaxation of local stress without formation of crystal defects. Similar effects were observed for the GaInAs QWs, as well. However, the stabilizing effect of Be was even more pronounced for GaInAs QWs because of larger lattice stress (GaInAs and GaInAsN samples had the same amount of In). By SiO_2 capping the GaInAs samples and taking RT-PL measurements We concluded that Be had a tendency to passivate annealing-induced Ga vacancies. Furthermore, a Be-doping of 5×10^{18} cm^{-3} decreased lasing threshold for 980-nm GaInAs QW lasers. For self-assembled InAs QDs, the effects of location of Be in the crystal were studied. We found, that the most detrimental defects were formed at the topmost GaAs barrier layer. Temperature stability of the InAs/GaAs

QD heterostructure was improved by placing 3-nm thick Be-doped GaAs layer close to the QDs.

A few open questions and topics remained unresolved for further research.

(i) GaAsBi and related alloys, in addition to Bi surfactant effects, need more studies.

(ii) There is no theoretical explanation for the Be-induced suppression of diffusion of indium for any of the studied cases at the writing of this Thesis.

(iii) Applications for the heavily Be-doped III-V's should be examined. From the PL, XRD, and SIMS results obtained in this work, it is expected that thermal stability of devices could be improved. Modulation doping schema (similar to InAs QDs) for GaInAs and GaInAsN QW could give new insight into defect formation in these heterostructures.

References

[Aho06] M. Ahola-Tuomi, P. Laukkanen, R. E. Perälä, M. Kuzmin, J. Pakarinen, I. J. Väyrynen, and M. Adell, Structural properties of Bi-terminated GaAs(100), Surf. Sci. **600**, 2349 (2006).

[Art02] J. R. Arthur, Molecular beam epitaxy, Surf. Sci. **500**, 189 (2002).

[Bad07] T. J. Badcock, R. J. Royce, D. J. Mowbray, M. S. Skolnick, H. Y. Liu, M. Hopkinson, K. M. Groom, and Q. Jiang, Low threshold current density and negative characteristic temperature 1.3 μm InAs self-assembled quantum dot lasers, Appl. Phys. Lett. **90**, 111102 (2007).

[Bim99] D. Bimberg, M. Grundmann, N.N. Ledentsov, *Quantum Dot Heterostructures*, Wiley, Chichester (1999).

[Bin83] G. Binning, H. Rohrer, Ch. Gerber, and E. Weibel, 7×7 reconstruction on Si(111) resolved in real space, Phys. Rev. Lett. **50**, 120 (1983).

[Cao08] Q. Cao, S. F. Yoon, C. Y. Liu, and C. Z. Tong, Effects of rapid thermal annealing on optical properties of *p*-doped and undoped InAs/InGaAs dots-in-a-well structures, J. Appl. Phys. **104**, 033522 (2008).

[Car75] T. A. Calson, *Photoelectron and Auger Spectroscopy*, Plenum Press, New York, United States of America (1975).

[Che07] W.C. Chen, Y.K. Su, R.W. Chuang, M.C. Tsai, K.Y. Cheng, Y.S. Wang, Optical investigations on the surfactant effects of Sb on InGaAsN multiple quantum wells grown by MOVPE, J. Crystal Growth **298**, 145 (2007).

[Chu07] S. N. Chu, N. Chand, W. B. Joyce, P. Parayanthal, and D. P. Wilt, Generic degradation mechanism for 980 nm $In_xGa_{1-x}As$/GaAs strained quantum-well lasers, Appl. Phys. Lett. **78**, 3166 (2004).

[Cul78] B. D. Cullity, *Elements of X-ray diffraction*, 2nd edition, Addison-Wesley Publishing Company Inc, United States of America (1978).

[Fee94] R. M. Feenstra, Tunneling spectroscopy of the (110) surface of direct-gap III-V semiconductors, Phys. Rev. B **50**, 4561 (1994).

[Fet00] C. M. Fetzer, R. T. Lee, J. K. Shurtleff, G. B. Stringfellow, S. M. Lee, and T. Y. Seong, The use of a surfactant (Sb) to induce triple periodic ordering in GaInP, Appl. Phys. Lett. **76**, 1440 (2000).

[Gar09] I. García, I. Rey-Stolle, and C. Algore, A 32.6% efficient lattice-matched dual-junction solar cell working at 1000 suns**,** Appl. Phys. Lett. **94**, 053509 (2008).

[Ger08] T. D. Germann, A. Strittmatter, J. Pohl, U. W. Pohl, D. Bimberg, J. Rautiainen, M. Guina, and O. G. Okhotnikov, High-power semiconductor disk laser based on InAs/GaAs submonolayer quantum dots, Appl. Phys. Lett. **92**, 101123 (2008).

[Gfr00] T. H. Gfroerer, *Enclypedia of Analytical Chemistry:* Photoluminescence in Analysis of Surfaces and Interfaces, pp. 9209, Wiley, Chichester (2000).

[Gie03] F. J. Giessibl, Advances in atomic force microscopy, Rev. Mod. Phys. **75**, 949 (2003).

[Gok07] A. A. Gokhale, T. F. Kuech, and M. Mavrikakis, A theoretical comparative study of the surfactant effect of Sb and Bi on GaN growth, J. Crystal Growth **303**, 493 (2007).

[Gra01] A. L. Gray, A. Stintz, K. J. Malloy, T. C. Newell, and L. F. Lester, Morphology and relaxation in $In_yGa_{1-y}As$/GaAs multi-layer structures, J. Cryst. Growth **222**, 726 (2001).

[Hal62] R. N. Hall, G. E. Fenner, J. D. Kingsley, T. J. Soltys, and R. O. Carlson, Coherent light emission from GaAs junctions, Phys. Rev. Lett. **9**, 366 (1962).

[Har02] J. S. Harris, GaInNAs long-wavelength lasers: progress and challenges, Semicond. Sci. Technol. **17**, 808 (2002).

[Has95] T. Hashizume, Q. K. Xue, A. Ichimiya, and T. Sakurai, Determination of the surfaces structures of the GaAs(001)-(2×4) As-rich phase, Phys. Rev. B **51**, 4200 (1995).

[Hen04] M. Henini, *Dilute Nitride Semiconductors: Physics and Technology*, Elsevier Science, Oxford, United Kingdom (2004).

[Her91] M. A. Herman, D. Bimberg, and J. Christen, Heterointerfaces in quantum wells and epitaxial growth processes: Evaluation by luminescence techniques, J. Appl. Phys. **70**, R1 (1991).

[Hov86] M. A. Van Hove, W.H. Weinberg, and C.-M. Chan, *Low-Energy Electron Diffraction, Experiment, Theory and Surface Structure Determination*, Springer, Berlin, Germany (1986).

[Hug07] M. Hugues, B. Damilano, J.-Y. Duboz, and J. Massies, Exciton dissociation and hole escape in the thermal photoluminescence quenching of (Ga,In)(N,As) quantum wells, Phys. Rev. B **75**, 115337 (2007).

[Iha02] M. Ihaddadene, J. Marcon, M. Idrissi-Benzohra, K. Ketata, S. Demichel, J. Flicstein , J.L. Pelouard, and M. Ketata, Anomalous thermal redistribution of beryllium implanted in InGaAs: a possible interaction with extended defects, Comp. Mat. Sci. **24**, 257 (2002).

[Ile77] M. Ilegems, Beryllium doping and diffusion in molecular-beam epitaxy of GaAs and $Al_xGa_{1-x}As$, J. Appl. Phys. **48**, 1278 (1977).

[Ish06] F. Ishikawa, M. Höricke, U. Jahn, A. Trampert, and K. H. Ploog, Molecular beam epitaxial growth window for high-quality (Ga,In)(N,As) quantum wells for long wavelength emission, Appl. Phys. Lett. **88**, 191115 (2006).

[Jan03] A. Janotti, S.-H. Wei, S. B. Zhang, and S. Kurtz, Interactions between nitrogen, hydrogen, and gallium vacancies in $GaAs_{1-x}N_x$ alloys, Phys. Rev. B **67**, 161201 (2003).

[Jan08] A. Janotti, P. Reunchan, S. Limpijumnong, and C. G. V. de Walle, Mutual Passivation of Electrically Active and Isovalent Impurities in Dilute Nitrides, Phys. Rev. Lett. **100**, 045505 (2008).

[Jin08] C. Y. Jin, H. Y. Liu, Q. Jiang, M. Hopkinson, and O. Wada, Simple theoretical model for the temperature stability of InAs/GaAs self-assembled quantum dot lasers with different *p*-type modulation doping levels, Appl. Phys. Lett. **93**, 161103 (2008).

[Ket98] M. Ketata, K. Ketata, S. Koumetz, P. Martin, J. Marcon, and C. Dubois, Be diffusion in InGaAs layers grown by gas source molecular beam epitaxy, J. Cryst. Growth **194**, 161103 (1998).

[Kim01] K. Kim and A. Zunger, Spatial Correlations in GaInAsN Alloys and their Effects on Band-Gap Enhancement and Electron Localization, Phys. Rev. Lett. **86**, 2609 (2001).

[Kim90] J. Y. Kim, D. Bassi, and L. Jostad, Reflection high-energy electron diffraction dynamics study of GaAs, AlAs, and $Al_{0.5}Ga_{0.5}As$ layer growth under As_4 and/or As_2 molecular beam species, Appl. Phys. Lett. **57**, 2197 (1990).

[Kom09] H.-P. Komsa, E. Arola, J. Pakarinen, C. S. Peng, T. T. Rantala, Beryllium doping of GaAs and GaAsN from first principles, Phys. Rev. B **79**, 115208 (2009).

[Kon96] M. Kondow, K. Uomi, A. Niwa, T. Kitani, S. Watahiki, and Y. Yazava, GaInAsN – A novel material for long wavelength laser diodes with excellent high temperature performance, Jpn. J. Appl. Phys. **35**, 1273 (1996).

[Kum97] R. Kumar, S.S. Prabhu, and A.S. Vengurlekar, Temperature Dependence of Luminescence Spectra Related to Free Carrier and Exciton Recombination in GaAs Quantum Wells, Phys. Scripta **56**, 308 (1997).

[Kur01] S. Kurtz, J. Webb, L. Gedvilas, D. Friedman, J. Geisz, J. Olson, R. King, D. Joslin, and N. Karam, Structural changes during annealing of GaInAsN, Appl. Phys. Lett. **78**, 748 (2001).

[Kri95] P. Krispin, R. Hey, and H. Kostial, Intrinsic origin and composition dependence of deep-level defects at the inverted GaAs/$As_xGa_{1-x}As$ interface grown by molecular-beam epitaxy, J. Appl. Phys. **77**, 5773 (1995).

[Kro00] H. Kroemer, *Quasi-electric fields and band offsets: Teaching electrons new tricks*, Nobel lecture (2000).

[Lau05] P. Laukkanen, M. Ahola, M. Kuzmin, R. E. Perälä, I. J. Väyrynen, and J. Sadowski, Bi-induced (2×6), (2×8), and (2×4) reconstructions on the InAs(100) surface, Surf. Sci. **598**, L361 (2005).

[Lau06] P. Laukkanen, J. Pakarinen, M. Ahola-Tuomi, M. Kuzmin, R. E. Perälä, I. J. Väyrynen, A. Tukiainen, V. Rimpiläinen, M. Pessa, M. Adell, J. Sadowski, Electronic and structural properties of the InP(100)(2x4) surface studied by core-level photoemission and scanning tunneling microscopy, Surf. Sci **600**, 3022 (2006).

[Lau08] P. Laukkanen, M. P. Punkkinen, H.-P. Komsa, M. Ahola-Tuomi, K. Kokko, M. Kuzmin, J. Adell, J. Sadowski, R. E. Perälä, M. Ropo, T. T. Rantala, I. J. Väyrynen, M. Pessa, L. Vitos, J. Kollár, S. Mirbt, and B. Johansson, Anomalous bismuth-stabilized (2×1) reconstructions on GaAs(100) and InP(100) surfaces, Phys. Rev. Lett. **100**, 086101 (2008).

[Leo98] R. Leon, S. Fafard, P. G. Piva, S. Ruvimov, adn Z. Liliental-Weber, Tunable intersublevel transitions in self-forming semiconductor quantum dots, Phys. Rev. B **58**, R4262 (1998).

[Li00] E. H. Li and J. T. Lie, *Semiconductor quantum wells intermixing: material properties and optoelectronic applications*, CRC Press, Amsterdam, Netherlands (2000).

[Li01] W. Li, M. Pessa, J. Toivonen, and H. Lipsanen, Doping and carrier transport in $Ga_{1-3x}In_{3x}N_xAs_{1-x}$ alloys, Phys. Rev. B **64**, 113308 (2001)

[Liu04] H. F. Liu, C.S. Peng, E.-M. Pavelescu, T. Jouhti, S. Karirinne, J. Konttinen, M. Pessa, Annealing effects on optical and structural properties of 1.3-um GaInNAs/GaAs quantum-well samples capped with dielectric layers, Appl. Phys. Lett. **84**, 478 (2004).

[Liu04b] H. Y. Liu, R. Sellers, T. J. Badcock, D. J. Mowbray, S. Skolnick, K. M. Groom, M. Gutiérrez, M. Hopkinson, J. S. Ng, J. P. R. David, and R. Beanland, Improved performance of 1.3 μm multilayer InAs quantum-dot lasers using a high-growth temperature GaAs spacer layer, Appl. Phys. Lett. **85**, 704 (2004).

[Liu07] T. Liu, S. Chandril, A. J. Ptak, D. Korakakis, and T. H. Myers, Bismuth surfactant effects for GaAsN and beryllium doping of GaAsN and GaInAsN grown by molecular beam epitaxy, J. Crystal Growth **304**, 402 (2007).

[Lor03] V. Lordi, V. Gambin, S. Friedrich, T. Funk, T. Takizawa, K. Uno, amd J. S. Harris, Nearest-Neighbor Configuration in (GaIn)(NAs) Probed by X-Ray Absorption Spectroscopy, Phys. Rev, Lett. **90**, 145505 (2003).

[Men07] X. Q. Meng, Z. Q. Chen, P. Jin, Z. G. Wang, and L. Wei, Defects around self-organized InAs quantum dots measured by slow positron beam, Appl. Phys. Lett. **91**, 093510 (2007).

[Mus05] G. Mussler, L. Däweritz, and K.H. Ploog, Nitrogen-induced suppression of an indium-gallium interdiffusion in $In_xGa_{1-x}As_{1-y}N_y$/GaAs multiple-quantum wells, Appl. Phys. Lett. **87**, 081903 (2005).

[Nos99] B. Z. Nosho, W. H. Weinberg, W. Barvosa-Carter, B. R. Bennet, B. V. Shanabrook, and L. J. Whitman, Effects of surface reconstruction on III-V surface formation: The role of III/V composition, Appl. Phys. Lett. **74**, 1704 (1999)

[Ooi97] B. S. Ooi, K. McIlvaney, M. W. Street, A. S. Helmy, S. G. Ayling, A. C. Bryce, J. H. Marsh, and J. S. Roberts, Selective quantum-well intermixing in GaAs-AlGaAs structures using impurity-free vacancy diffusion**,** IEEE J. Quantum Electron. **33**, 1784 (1997).

[Pan00] Z. Pan, L. H. Li, W. Zhang, Y. W. Lin, and R. H. Wu, Kinetic modeling of N incorporation in GaInNAs growth by plasma-assisted molecular-beam epitaxy, Appl. Phys. Lett. **77**, 214 (2000).

[Pas89] M. D. Pashley, Electron counting model and its application to island structures on molecular-beam epitaxy grown GaAs(001) and ZnSe(001), Phys. Rev. B **40**, 10481 (1989).

[Pen05] C.S. Peng_, H.F. Liu, J. Konttinen, and M. Pessa, Mechanism of photoluminescence blue shift in InGaAsN/GaAs quantum wells during annealing, J. Crystal Growth **278**, 259 (2005).

[Pen05b] C. S. Peng, J. Konttinen, T. Jouhti, and M. Pessa, High-gain GaInAsN materials, Proc. SPIE **6020**, 60200H (2005).

[Pol09] V. Polojärvi, *InAs/GaAs quantum dot nanostructures: deep levels and optical properties*, M.Sc. Thesis, Tampere University of Technology (2009).

[Pun07] M. P. J. Punkkinen, P. Laukkanen, K. Kokko, M. Ropo, M. Ahola-Tuomi, I. J. Väyrynen, H.-P. Komsa, T. T. Rantala, M. Pessa, M. Kuzmin, L. Vitos, J. Kollár, and B. Johansson, Surface core-level shifts of GaAs(100)(2×4) from first principles, Phys. Rev. B **76**, 115334 (2007).

[Pun09] M. P. J. Punkkinen, P. Laukkanen, M. Ahola-Tuomi, J. Pakarinen, M. Kuzmin, A. Tukiainen, R.E. Perälä, J. Lång, M. Ropo, K. Kokko, L. Vitos, B. Johansson, M. Pessa, and I. J.Väyrynen, Core-level shifts of InP(100)(2×4) surface: Theory and experiment, Surface Science **603**, 2664 (2009).

[Que98] H. J. Queisser and E. E. Haller, Defects in Semiconductors: Some Fatal, Some Vital, Science **281**, 945 (1998).

[Ras04] A. Rastelli, S. M. Ulrich, E.-M. Pavelescu, T. Leinonen, M. Pessa, P. Michler and O. G. Schmidt, Self-assembled quantum dots for single-dot optical investigations, Superlattices Microstruct. **36**, 181 (2004).

[Sch94] E. F. Schubert, *Light Emitting Diodes*, University Press, Cambridge, United Kingdom.

[Sch03] W. G. Schmidt, P. H. Hahn, F. Bechstedt, N. Esser, P. Vogt, A. Wange, and W. Richter, InP(001)-(2×1) Surface: A Hydrogen Stabilized Structure, Phys. Rev. Lett. **90**, 126101.

[Shi92] K. Shiraishi, Ga adatom diffusion on an As-stabilized GaAs(001) surface via missing As dimer rows: First-principles calculation, Appl. Phys. Lett. **60**, 1363 (1992).

[Slo06] J. Slotte, K. Saarinen, E.-M. Pavelescu, T. Hakkarainen, and M. Pessa, Nitrogen related vacancies in GaAs based quantum well structures, Appl. Phys. Lett. **89**, 061903 (2006).

[Tan03] N. Tansu, J.-Y. Yeh, and L. J. Mawst, Experimental evidence of carrier leakage in InGaAsN quantum-well lasers, Appl. Phys. Lett. **83**, 2112 (2003)

[Ter85] J. Tersoff and D. R. Hamann, Theory of scanning tunneling microscope, Phys. Rev. B **31**, 805 (1985).

[Vur01] I. Vurgaftman, J.R. Meyer, L.R. Ram-Mohan, Band parameters for III–V compound semiconductors and their alloys, J. Appl. Phys. **89**, 5815 (2001).

[Whi97] L. J. Whitman, P. M. Thibado, S. C. Erwin, B. R. Bennett, and B. V. Shanabrook, Metallic III-V(001) surfaces: Violations of the electron counting model, Phys. Rev. Lett. **79**, 639 (1997).

[Wis05] M. A. Wistey, S. R. Bank, H. B. Yuen, H. Bae, and J. S. Harris Jr., Nitrogen plasma optimization for high-quality dilute nitrides, J. Cryst. Growth **278**, 229 (2005).

[Yu02] K.M. Yu, W. Walukiewicz, J. Wu, D. E. Mars, D. R. Chamberlin, M. A. Scarpulla, O. D. Dubon, and J. F. Geisz, Mutual passivation of electrically active and isovalent impurities, Nat. Mat. **1**, 185 (2002).

[Zha07] H. Zhao. Y. Q. Xu. H. Ni. S. Zhang. Q. Han. Y. Du. X. Yang. R. Wu. and Z. Niu. Application of rapid thermal annealing on 1.3 – 1.55 μm GaInNAs(Sb) lasers grown by molecular beam epitaxy, J. Cryst. Growth **301-302**, 979 (2007).

Appendices

Paper 1

J. Pakarinen, C.S. Peng, J. Puustinen, P. Laukkanen, V.-M. Korpijärvi, A. Tukiainen, and M. Pessa, Postgrowth annealing of GaInAs/GaAs and GaInAsN/GaAs quantum well samples placed in a proximity GaAs box: A simple method to improve the crystalline quality, Applied Physics Letters **92**, 232105 (2008).

Reprinted with permission from the publisher. Copyright 2008, American Institute of Physics.

Postgrowth annealing of GaInAs/GaAs and GaInAsN/GaAs quantum well samples placed in a proximity GaAs box: A simple method to improve the crystalline quality

J. Pakarinen,[a] C. S. Peng, J. Puustinen, P. Laukkanen, V.-M. Korpijärvi, A. Tukiainen, and M. Pessa
Optoelectronics Research Centre, Tampere University of Technology, FIN-33101 Tampere, Finland

(Received 7 May 2008; accepted 16 May 2008; published online 11 June 2008)

The effects of thermal annealing on GaInAs/GaAs and GaInAsN/GaAs quantum wells, grown by molecular beam epitaxy, were investigated. Optical and structural properties were examined upon annealing when the samples had a 200 nm thick SiO_2 cap layer, or were placed in a so-called GaAs box or were left uncapped. The GaAs box gave rise to the strongest photoluminescence without significant blueshift or structural changes at moderate annealing temperature. Capping with SiO_2 impaired the samples and caused a more pronounced blueshift for the GaInAs quantum wells than for the GaInAsN ones. These results consolidate our understanding of the blueshift mechanisms. © *2008 American Institute of Physics*. [DOI: 10.1063/1.2943157]

It is difficult to prepare device-quality quantum well (QW) heterostructures of dilute nitrides, $Ga_{1-x}In_xAs_{1-y}N_y$ ($y<0.03$), on GaAs substrates.[1] Because growth temperature (T_{sub}) of these heterostructures is low in the molecular-beam-epitaxy (MBE) method, postgrowth annealing is often required.[2] To reduce the formation of annealing-induced defects, protective layers have usually been employed.[3,4]

SiO_2 coating is found to introduce Ga vacancies into underlying GaAs upon annealing, likely due to the generation of tensile stress at the interface of $GaAs/SiO_2$ with the different thermal-expansion coefficients.[5] These Ga vacancies enhance diffusion of indium and increase the blueshift (BS) of photoluminescence (PL) from the GaInAsN/GaAs QWs.[3] If SiO_2 is replaced by SiN_3 the BS is reduced and significant improvement in PL is obtained.[3]

We show in this letter that the postgrowth annealing (under N_2 flow) of the QW samples in a "GaAs box," which provides GaAs proximity conditions, is a simple and the most efficient method to improve PL from dilute nitride QWs, resulting in a small unwanted BS upon annealing.

The samples were grown by a solid-source MBE system equipped with a radio-frequency nitrogen plasma source. After depositing a 150 nm GaAs buffer layer onto an *n*-type (Si-doped) GaAs(100) substrate at $T_{sub}\approx 580\ °C$, the temperature was decreased to 480 °C. Then triple QW (TQW) structures of the nominal alloy compositions of $Ga_{0.62}In_{0.38}As_{0.0985}(N_{0.015})$, each QW being 6.5 nm thick and separated by 20 nm GaAs barriers, were grown and capped with a 75 nm GaAs layer. T_{sub} was raised back to 580 °C during the deposition of the top GaAs layer. The GaInAs QWs were grown in the same way. The GaInAs TQW and the GaInAsN TQW emitted PL at $\lambda\approx 1170$ and 1270 nm, respectively. The as-grown samples were cut into $5\times 5\ mm^2$ pieces. For annealing, three different procedures were done. For the sample "set 1," the cap layer of SiO_2 (200 nm in thickness) was prepared by plasma-enhanced chemical vapor deposition in another chamber. During annealing, pieces of set 1 were put face up on a Si wafer. The samples "set 2" and "set 3" were left uncoated. During annealing, the sample set 2 was placed inside a box, which was made of GaAs wafers, and the sample set 3 was put face up on a Si wafer, similarly to the SiO_2 capped samples. Annealing of all the samples was simultaneously done in the same chamber. The annealing temperature (T_{ann}) was controlled by an optical pyrometer.

Room-temperature PL was immediately measured after each annealing with an Nd:YAG (neodymium-doped yttrium aluminum garnet) laser ($\lambda=532$ nm) and a GaInAs detector array. X-ray diffraction (XRD) (004) rocking curves were recorded in $\omega-2\theta$ geometry by a double-crystal x-ray diffractometer (using Cu $K\alpha$ radiation).

Figures 1(a) and 1(b) illustrate PL from the GaInAs TQW and the GaInAsN TQW upon annealing at T_{ann}

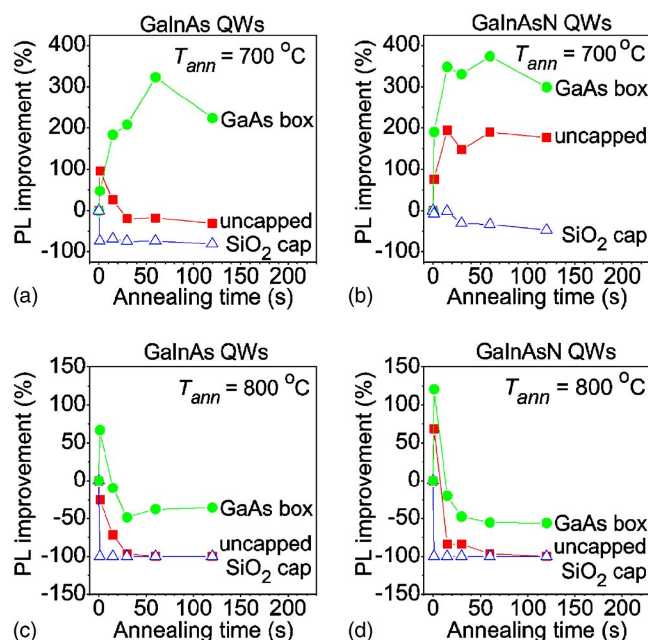

FIG. 1. (Color online) Improvement in peak intensities of PL from GaInAs and GaInAsN triple TQWs measured after different postannealing procedures at $T_{ann}=700\ °C$ [(a) and (b)] and at $T_{ann}=800\ °C$ [(c) and (d)].

[a]Electronic mail: janne.pakarinen@tut.fi.

Author complimentary copy. Redistribution subject to AIP license or copyright, see http://apl.aip.org/apl/copyright.jsp

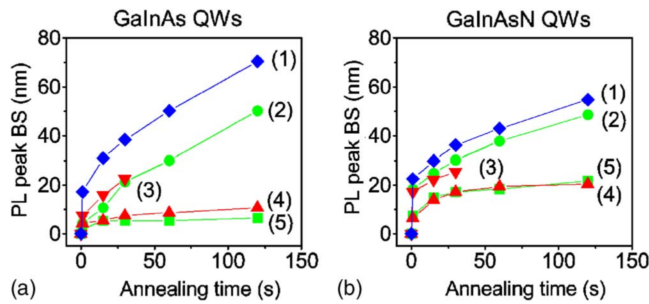

FIG. 2. (Color online) Annealing-induced BS after annealing at T_{ann}=700 and 800 °C for GaInAs [panel (a)], and for GaInAsN [panel (b)] triple TQW structures. Curve (1): T_{ann}=700 °C for the samples with a SiO_2 cap layer (set 1), curve (2): T_{ann}=800 °C for the samples placed inside the GaAs box (set 2), curve (3): T_{ann}=800 °C for the samples without caps (set 3), curve (4): T_{ann}=700 °C for samples without caps (set 3), and curve (5): T_{ann}=700 °C for the sample placed inside the GaAs box (set 2).

=700 °C. The effects of annealing were dramatic. By annealing the uncapped samples in the GaAs box (set 2), PL from both the GaInAs and GaInAsN TQWs were increased by 300%. Capping the samples with SiO_2 (set 1) reduced PL upon annealing; this effect was more pronounced for the GaInAs TQW than for the GaInAsN TQW. The samples without any cap (set 3) exhibited PL that quickly saturated at intensity levels that were about 20% lower and 200% higher than the as-grown PL for the GaInAs TQW and the GaInAsN TQW, respectively. When annealed at higher temperatures (T_{ann}=800 °C), PL completely disappeared for all the capped and uncapped samples [Figs. 1(c) and 1(d)] except for the GaAs box samples which remained optically active (albeit at small intensity).

The BSs of PL are given in Figs. 2(a) and 2(b). When T_{ann} was 700 °C, the GaAs box samples and those without SiO_2 caps [curves (4) and (5) in Fig. 2] exhibited BS that saturated to approximately 10 and 20 nm for the GaInAs TQW and the GaInAsN TQW, respectively. When SiO_2 capping was applied (T_{ann}=700 °C) or T_{ann} was raised to 800 °C [curves (1),(2), and (3) in Fig. 2], all samples showed large BSs. Interestingly, the BS for the GaInAs TQW was larger than that for the GaInAsN TQW. We could not observe PL from the the uncoated GaInAs and GaInAsN TQWs (set 3) after 60 and 120 s, respectively, if T_{ann} was 800 °C.

The XRD (004) rocking curves for the GaInAs TQW and the GaInAsN TQW after 120 s at T_{ann}=700 and 800 °C are displayed in Fig. 3. Several effects are seen. (i) Annealing the samples at T_{ann}=700 °C in the closed GaAs box (set 2) improved the crystalline quality of the GaInAs TQW, as deduced from the sharpening of the XRD fringes [Fig. 3(a)], but no improvement was found for the GaInAsN TQW [Fig. 3(c)]. (ii) For the SiO_2 capped samples (set 1), indium diffused out of the QWs into the GaAs barriers (at T_{ann} =700 °C and T_{ann}=800 °C), which is directly seen in XRD by the movement of the envelope curves of the TQW fringes closer to the substrate peak.[6] (iii) The Incorporation of nitrogen into the GaInAs TQW improved thermal stability. This effect was concluded from the QW fringes that were observable for the uncapped GaInAsN TQW (set 3) after 120 s at T_{ann}=800 °C [Fig. 3(c)], whereas the XRD rocking curve for the uncapped GaInAs TQW was totally flat [Fig. 3(b)]. Apparently, the presence of nitrogen reduced annealing-induced relaxation.

There are at least two reasons for the BS of PL from the GaInAsN/GaAs QWs upon thermal annealing. One of them is reorganization of the N neighborhood, a so-called short range ordering effect (SRO).[7] The main reason for the SRO-induced BS is the fact that the originally random GaInAsN alloy has an increased number of In–N bonds after annealing.[8] Another reason is the out diffusion of indium atoms through the QW/barrier interfaces.[9] The SRO effect is dominant at low T_{ann}.[10] Recently, an important observation was made, according to which the nitrogen mole fraction is locally enhanced at the MBE-grown GaInAsN/GaAs QW interfaces.[11] It is this enhancement in nitrogen, we believe, that reduces In out diffusion because the cohesive energy of the In–N bonds (1.93 eV) is larger than the In–As ones (1.55 eV).[7] In other words, the N atoms at the QW interfaces catch the out diffusing In atoms, preventing diffusion. When studying the PL and XRD results, we can see that the BS of PL for the uncoated and GaAs box samples (sets 2 and 3) upon T_{ann}=700 °C was larger for the GaInAsN TQW than for the GaInAs TQW (Fig. 2), but the XRD $\omega-2\theta$ angles of the GaInAsN TQW remained completely unchanged [Fig. 3(c)], pointing out an occurrence of SRO (which does not change XRD). However, as T_{ann} was raised to 800 °C, large changes in XRD took place for all the samples, most remarkably for the GaInAs TQW. This observation provides clear-cut evidence for the presence of atomic diffusion. Taken to-

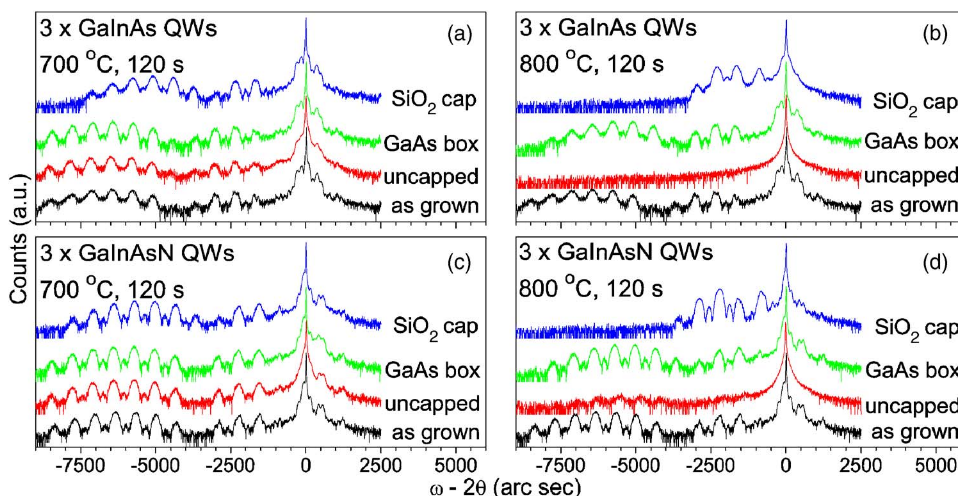

FIG. 3. (Color online) XRD(004) rocking curves for the GaInAs and GaInAsN QWs before and after annealing 120 s at T_{ann}=700 °C [(a) and (c)] and at T_{ann}=800 °C [(b) and (d)] for the samples with the SiO_2 caps (set 1) or for the samples placed inside GaAs box (set 2), or for those left uncapped (set 3). The spectra are vertically shifted for clarity.

Author complimentary copy. Redistribution subject to AIP license or copyright, see http://apl.aip.org/apl/copyright.jsp

gether, we conclude that the uncapped and GaAs box GaInAsN samples (sets 2 and 3) only suffered from SRO effect at $T_{ann}=700\ ^{\circ}C$,[10] but at $T_{ann}=800\ ^{\circ}C$ the BS was mainly caused by In out diffusion.[9]

The PL intensity from the uncapped GaInAsN TQW was improved by annealing at 700 °C (Fig. 1), due to the annihilation of point defects, in accordance with the study of Li *et al.*.[12] Larger changes in the XRD rocking curves upon annealing took place for the GaInAs TQW than for the GaInAsN TQW. This observation agrees with the study of Mussler *et al.*,[6] in which the alloying nitrogen with GaInAs/GaAs QWs suppressed the In/Ga interdiffusion. There are also huge differences in both PL and XRD data for the uncapped (sets 2 and 3) and SiO_2 capped samples (set 1). It is known that capping GaAs with SiO_2 creates a large number of Ga vacancies upon annealing.[5] These vacancies lower the activation energy for indium diffusion[13] and cause significant changes in crystal structure of the GaInAs TQW [Figs. 3(a) and 3(b)], but does so to a lesser extent in the GaInAsN TQW [Figs. 3(c) and 3(d)] where nitrogen reduces out diffusion of indium.

In summary, we have shown that the postgrowth annealing of uncapped GaInAsN heterostructures in a GaAs box significantly improves the PL and reduces the BS. The GaAs box annealing may be the simplest method to treat dilute nitride heterostructures upon MBE growth. We also conclude that nitrogen, enriched at the QW/barrier interfaces, suppresses out diffusion of indium from the QW. The SRO in GaInAsN is the predominant effect for the BS of PL at low annealing temperatures ($T_{ann}\approx 700\ ^{\circ}C$), but out diffusion of indium becomes the dominant BS mechanism at higher temperatures ($T_{ann}\approx 800\ ^{\circ}C$).

This work was supported, in part, by the Academy of Finland within the NEONATE Project and by the Finnish Funding Agency for Technology and Innovations (TEKES). The author to whom correspondence should be addressed (J.P.) acknowledges financial support from the Graduate School of the Tampere University of Technology.

[1] J. S. Harris, Semicond. Sci. Technol. **17**, 880 (2002).
[2] C. S. Peng, E.-M. Pavelescu, T. Jouhti, J. Konttinen, W. Li, and M. Pessa, Appl. Phys. Lett. **80**, 4720 (2002).
[3] H. F. Liu, C. S. Peng, E.-M. Pavelescu, T. Jouhti, S. Karirinne, J. Konttinen, and M. Pessa, Appl. Phys. Lett. **84**, 478 (2004).
[4] H. Zhao, Y. Q. Xu, H. Ni, S. Zhang, Q. Han, Y. Du, X. Yang, R. Wu, and Z. Niu, J. Cryst. Growth **301-302**, 979 (2007).
[5] B. S. Ooi, K. McIlvaney, M. W. Street, A. S. Helmy, S. G. Ayling, A. C. Bryce, J. H. Marsh, and J. S. Roberts, IEEE J. Quantum Electron. **33**, 1784 (1997).
[6] G. Mussler, L. Däweritz, and K. H. Ploog, Appl. Phys. Lett. **87**, 081903 (2005).
[7] K. Kim and A. Zunger, Phys. Rev. Lett. **86**, 2609 (2001).
[8] V. Lordi, V. Gambin, S. Friedrich, T. Funk, T. Takizawa, K. Uno, and J. S. Harris, Phys. Rev. Lett. **90**, 145505 (2003).
[9] C. S. Peng, H. F. Liu, J. Konttinen, W. Li, and M. Pessa, J. Cryst. Growth **278**, 259 (2005).
[10] M. Hugues, B. Damilano, J.-M. Chauveau, J.-Y. Duboz, and J. Massies, Phys. Rev. B **75**, 045313 (2007).
[11] M. Albrecht, H. Abu-Farsakh, T. Remmele, L. Geelhaar, H. Riechert, and J. Neugebauer, Phys. Rev. Lett. **99**, 206103 (2007).
[12] W. Li, M. Pessa, T. Ahlgren, and J. Decker, Appl. Phys. Lett. **79**, 1094 (2001).
[13] J. S. Tsang, C. P. Lee, S. H. Lee, K. L. Tsai, C. M. Tsai, and J. C. Fan, J. Appl. Phys. **79**, 664 (1996).

Author complimentary copy. Redistribution subject to AIP license or copyright, see http://apl.aip.org/apl/copyright.jsp

Paper 2

P. Laukkanen, J. Pakarinen, M. Ahola-Tuomi, M. Kuzmin, R.E. Perälä, I.J. Väyrynen, A. Tukiainen, J. Konttinen, P. Tuomisto, and M. Pessa, Structural and electronic properties of Bi-adsorbate-stabilized reconstructions on the InP(100) and GaAsN(100) surface, Physical Review B **74**, 155302 (2006).

Reprinted with permission from the publisher. Copyright 2006, American Physical Society.

Structural and electronic properties of Bi-adsorbate-stabilized reconstructions on the InP(100) and $GaAs_xN_{1-x}$(100) surfaces

P. Laukkanen, J. Pakarinen, M. Ahola-Tuomi, M. Kuzmin, R. E. Perälä, and I. J. Väyrynen
Department of Physics, University of Turku, FIN-20014 Turku, Finland

A. Tukiainen, J. Konttinen, P. Tuomisto, and M. Pessa
Optoelectronics Research Centre, Tampere University of Technology, FIN-33101 Tampere, Finland
(Received 12 June 2006; revised manuscript received 21 August 2006; published 4 October 2006)

Bismuth (Bi) adsorbate-stabilized reconstructions on the InP(100) and $GaAs_xN_{1-x}$(100) surfaces have been studied by scanning tunneling microscopy (STM) and spectroscopy (STS), x-ray photoelectron spectroscopy, and low-energy electron diffraction. With decreasing coverage, Bi is found to stabilize the (2×1), (2×8), and (2×4) reconstructions on the InP(100) surface and the (2×1) and (2×4) reconstructions on the $GaAs_xN_{1-x}$(100). STM results show that both the Bi/InP(100)(2×4) and Bi/$GaAs_xN_{1-x}$(100)(2×4) reconstructions can be described with the $\alpha2$-like structural model. The current-voltage curves measured by STS show the Bi/InP(100)(2×1) and Bi/$GaAs_xN_{1-x}$(100)(2×1) structures, which do not obey the electron counting model, to be semiconducting and metallic, respectively. Combining our experimental findings, we propose atomic models for the (2×1) reconstructions. An issue why Bi stabilizes unusual (2×1) structures is discussed.

DOI: 10.1103/PhysRevB.74.155302 PACS number(s): 68.35−p, 68.43.Hn, 73.61.Ey

I. INTRODUCTION

Various reconstructions of clean and adsorbate-stabilized III–V compound-semiconductor surfaces can be interpreted with the following driving mechanisms.[1] (i) Surface atoms dimerize to reduce the number of unsaturated dangling bonds. (ii) As the electron counting model (ECM) predicts,[2] dangling bonds of the electropositive atoms (group III) are empty and those of the electronegative atoms (group V) are doubly occupied, resulting in a semiconducting surface with vacant dimer sites. (iii) Spatial arrangement of dimers minimizes the electrostatic energy. However, some exceptional surfaces exist; for example, GaSb(100)$(n\times5)$ and Sb-stabilized GaAs(111)(1×3) reconstructions do not comply with the principle (ii).[3,4] Structural energies of these surfaces have been shown to be lowered enough to overcome the electronic energy cost associated with occupying the midgap or conduction-band states. Knowledge of the structural and electronic properties of such exceptional III-V surfaces is essential for a thorough understanding of physical mechanisms behind reconstructions.

Group-V adsorbate-stabilized III–V(100) surfaces such as Sb/GaAs(100) and As/InP(100) have attracted a lot of interest because they have an important role in the preparation (growth) of heteroepitaxial device structures (e.g., Refs. 5–10). Among these surface systems, the behavior of bismuth (Bi) on III–V(100) is less known. It has been shown very recently that on the GaAs(100) and InAs(100) surfaces, Bi stabilizes (2×4) reconstructions similar to the clean (i.e., As-stabilized) and Sb-stabilized GaAs(100)(2×4) and InAs(100)(2×4) reconstructions.[11,12] At the higher Bi coverage, the Bi/GaAs(100)(2×4) reconstruction is found to undergo a structural transition to an unusual (2×1) phase,[12] instead of the prototypical $c(4\times4)$ phase induced by As on the GaAs(100).[13] Such a small (2×1) unit cell necessarily violates the ECM concept,[2] and thus the Bi/GaAs(100)(2×1) surface can be expected to be metallic. Currently, it is, however, unclear whether the Bi/GaAs(100)(2×1) is metallic or semiconducting, and no atomic model has been proposed for this reconstruction. Interestingly, the (2×1) symmetry, which is characteristic for the Si(100) and Ge(100) surfaces, has been previously observed also on the P-stabilized InP(100) surface.[14] Furthermore, the P/InP(100)(2×1) surface has been found to be semiconducting, which has been proposed to be due to the electron-correlation effect.[14] Since then, it has been, however, shown that the InP(100)(2×1) reconstruction is not a clean surface but stabilized by hydrogen.[1,15]

Here, we report that Bi stabilizes unusual (2×1) reconstructions on the InP(100) and $GaAs_xN_{1-x}$(100) surfaces, which have larger and smaller lattice constants than the GaAs(100) surface, respectively. The Bi/InP(100) and Bi/$GaAs_xN_{1-x}$(100) surfaces have been studied by scanning tunneling microscopy (STM) and spectroscopy (STS), x-ray photoelectron spectroscopy (XPS), and low-energy electron diffraction (LEED). With decreasing coverage, bismuth is found to stabilize the (2×1), (2×8), and (2×4) reconstructions on the InP(100) surface and the (2×1) and (2×4) reconstructions on the $GaAs_xN_{1-x}$(100) surface. Particularly, the properties of the Bi-stabilized (2×1) and (2×4) reconstructions have been investigated in this work. According to the STS results, the Bi/InP(100)(2×1) surface is semiconducting, and the Bi/$GaAs_xN_{1-x}$(100)(2×1) is metallic. Atomic models that explain the experimental results of the (2×1) and (2×4) reconstructions are proposed.

II. EXPERIMENTS

Measurements were performed in an Omicron ultrahigh-vacuum (UHV) system equipped with LEED, STM, and XPS. STM images were taken in the constant current mode,

 ©2006 The American Physical Society

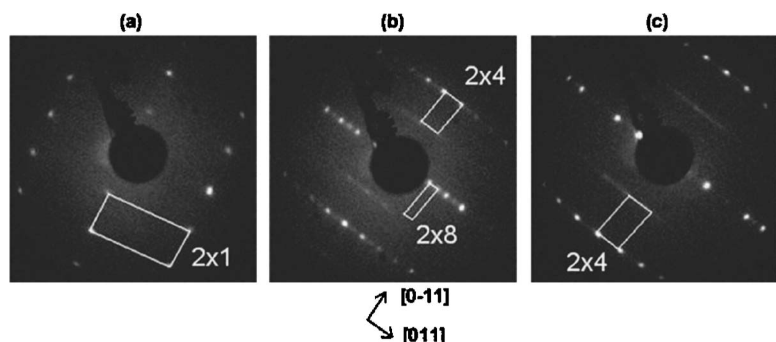

FIG. 1. (a) LEED (66 eV) from the Bi/InP(100)(2×1) surface heated to 340 °C, (b) LEED (79 eV) from the Bi/InP(100)(2×4)+(2×8) surface heated to 430 °C, and (c) LEED (48 eV) from the Bi/InP(100)(2×4) surface heated to 460 °C. The white rectangles represent the reciprocal unit cells.

and the tunneling spectroscopy was performed simultaneously with the topographic measurement. The Mg $K\alpha$ line (1253.6 eV) was used for excitation in XPS. All the measurements were carried out at room temperature (RT) in UHV with the pressure in the 10^{-11} mbar range.

The clean InP(100) substrates with the established mixed-dimer (2×4) surface structure were prepared according to the process described in Ref. 16. That is, the InP substrates were grown by molecular-beam epitaxy (MBE) on epiready *n*-type InP(100) wafers. The thermal desorption of native oxides was carried out at 515 °C for 10 min under a phosphorus flux, upon which the undoped InP layer with a thickness of 100 nm was grown at 490 °C. The substrate temperature was read with an infrared pyrometer. Indium was provided from a standard Knudsen effusion cell and phosphorus (P_2) from a three-zone valved cracker source.

Two different types of the capping layer were used in order to protect the grown InP(100) surfaces against air exposure during sample transfer between separate UHV systems. One cap was a double layer of phosphorus and arsenic: After the MBE growth, the substrate temperature was slowly reduced to near room temperature under the P_2 flux. After closing the P_2 source, the As_2 valve was opened and an amorphous arsenic layer was deposited on the surface for 35 min. Another cap was a pure phosphorus layer, which was deposited by keeping the grown surface at near room temperature under the P_2 flux for 30 min.

Both capping layers were removed by heating the InP(100) substrates to 420–450 °C in UHV. It repeatedly produced a clear 2×4 LEED pattern, which improved after heating the substrate up to 490 °C. According to STM observations, the double layer of phosphorus and arsenic protected the InP(100) surface better than the pure phosphorus layer since the observed clean mixed-dimer-reconstructed areas were larger on the former substrate. Thus, the substrate protected by the double layer of phosphorus and arsenic was used in this work. However, we tested the other substrate: STM observations showed that similar Bi-stabilized structures were obtained with the InP(100) substrate protected by the pure phosphorus cap.

A $GaAs_xN_{1-x}$(100) substrate was grown on the GaAs(100) by MBE with a nitrogen plasma source. The nitrogen composition $1-x$ of the $GaAs_xN_{1-x}$ film was estimated to be 0.04. Upon the growth of 100-nm-thick $GaAs_xN_{1-x}$, the surface was protected against the air exposure by an arsenic capping layer deposited at RT. After the transfer through air, the protective layer was removed by heating the substrate in UHV up to 600 °C, which produced (4×2)-reconstructed $GaAs_xN_{1-x}$(100) surface. A typical LEED pattern of this surface is shown in Fig. 2(c). Due to a limited sharpness of the 4×2 pattern, we cannot distinguish it from a $c(8\times2)$ pattern.

Approximately 1.5-monolayer (ML) thick Bi layers were evaporated from a W-coil source onto the InP(100)(2×4) and $GaAs_xN_{1-x}$(100)(4×2) surfaces held at RT. Then the Bi/InP(100) and Bi/$GaAs_xN_{1-x}$(100) surfaces were heated gradually in UHV, as described below. Temperatures were measured by a pyrometer.

III. RESULTS AND DISCUSSION

Figures 1 and 2 show typical LEED patterns obtained from the Bi/InP(100) and Bi/$GaAs_xN_{1-x}$(100) reconstructions, respectively, after heating the surfaces to different temperatures. The temperature ranges, in which different reconstructions were observed by LEED and STM, are summarized in Fig. 3. Also, the Bi 4f photoelectron intensities measured by XPS from the Bi/InP(100) and Bi/$GaAs_xN_{1-x}$(100) reconstructions as a function of the heat-

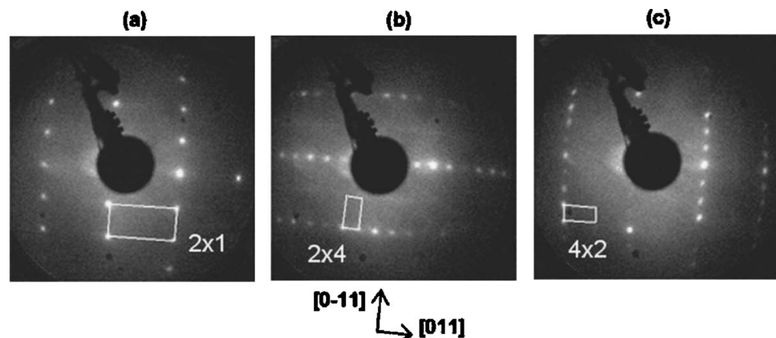

FIG. 2. (a) LEED (128 eV) from the Bi/$GaAs_xN_{1-x}$(100)(2×1) surface heated to 250 °C, (b) LEED (124 eV) from the Bi/$GaAs_xN_{1-x}$(100)(2×4) surface heated to 320 °C, and (c) LEED (123 eV) from the $GaAs_xN_{1-x}$(100)(4×2) surface heated to 580 °C. The white rectangles represent the reciprocal unit cells.

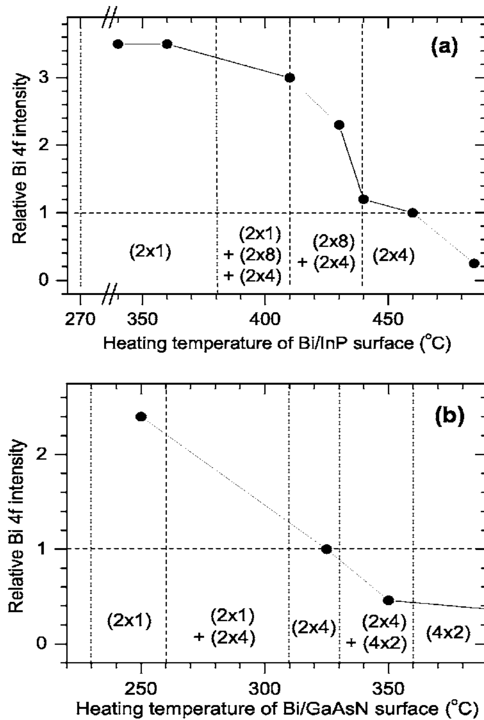

FIG. 3. The relative Bi 4f intensities (black dots represent data points) measured by XPS from the Bi/InP (a) and Bi/GaAs$_x$N$_{1-x}$ (b) surfaces as a function of the heating temperature. The vertical lines separate the temperature ranges where the different reconstructions were observed by LEED and STM.

ing temperature are presented in Fig. 3 in proportion to the intensities of the (2×4) reconstructions. From the Bi 4f measurements, we estimate that the Bi coverage of the Bi/InP(100)(2×1) surface is 3.5 times the coverage of the Bi/InP(100)(2×4) and that the corresponding coverage ratio between the Bi/GaAs$_x$N$_{1-x}$(100)(2×1) and (2×4) is 2.4. Moreover, the upper temperature limits for the Bi/InP(100) reconstructions are clearly higher than the corresponding ones for the Bi/GaAs$_x$N$_{1-x}$(100), as can be seen in Fig. 3, suggesting the Bi-induced reconstructions are thermally more stable on the InP(100) surface than on the GaAs$_x$N$_{1-x}$(100) surface.

Figure 4(a) presents a filled-state STM image of the Bi/InP(100)(2×4) surface that includes (2×8)-reconstructed areas [i.e., Bi/InP(100)$(2\times4)+(2\times8)$]. The Bi/InP(100)(2×8) reconstruction appears in Fig. 4(a) as white rows with a separation of about 33 Å. An atomic-resolution filled-state image of the (2×4)-reconstructed Bi/InP(100) surface is shown in Fig. 4(b). This image can well be explained with the α2-like model having the Bi coverage of 0.5 ML [Fig. 4(c)]. The white paired maxima are related to the first-layer Bi-dimer atoms, and the rows of the gray maxima, located asymmetrically between the rows of the white features, are assigned to the third-layer Bi dimers. In passing, here we do not disentangle the (2×4) reconstruction from the $c(2\times8)$ one. The STM-line profiles (not shown) reveal a typical distance between two maxima of both the white and gray dimers to be about 3 Å, which is close to the double of a covalent radius of Bi atom (1.46 Å). However, based on our previous finding that in the Bi/InAs(100)(2×4)-$\alpha2$ reconstruction only half of the third-layer dimer sites are occupied by Bi atoms,[11] we propose the Bi coverage of the Bi/InP(100)(2×4) also to be 0.375 ML. In other words, half of the third-layer atoms of the Bi/InP(100)(2×4)-$\alpha2$ are proposed to be P ones. This is consistent with the fact that the starting mixed-dimer InP(100)(2×4) surface consists of 0.125 ML of P atoms, which can appear on the Bi/InP(100)(2×4) surface. Thus, we estimate, by means of the Bi 4f intensity ratio, the Bi coverage of the Bi/InP(100)(2×1) surface to be 1.3 ML.

It is worth noting that, in agreement with previous findings for the Bi/GaAs(100)(2×4) and Bi/InAs(100)(2×4) surfaces,[11,12] only the α2-like structure was found on the Bi/InP(100)(2×4) surfaces heated to the different temperatures, covering the (2×4) and $(2\times4)+(2\times8)$ conditions in Fig. 3. That is, the behavior of the Bi/InP(100)(2×4) surface clearly differs from the clean InP(100)(2×4) reconstruction where the mixed-dimer phase dominates in a wide range of the preparation conditions and where the α2 phase is stable only in a very limited range of the conditions.[16–21] The observation agrees with the theory showing the In-In dimer-related stress of the mixed-dimer structure to increase with a radius of the group-V atom.[19]

A clear difference between the Bi/InP and Bi/GaAs$_x$N$_{1-x}$(100)(2×4) surfaces is that the ordering of the white first-layer dimer rows is better on the former surface than on the latter one, as can be seen in the filled-state images of Figs. 4(b) and 5(a). This may arise from the different surface-lattice constants of GaAs$_x$N$_{1-x}$ (<4.0 Å) and InP (≈4.2 Å), leading to different interactions of the Bi dimers on these surfaces. For the Bi/GaAs$_x$N$_{1-x}$(100)(2×4) surface, the α2-like structure is also proposed to be valid (Fig. 5). The white features of the empty-state STM image in Fig. 5(b) are related to the empty dangling bonds of

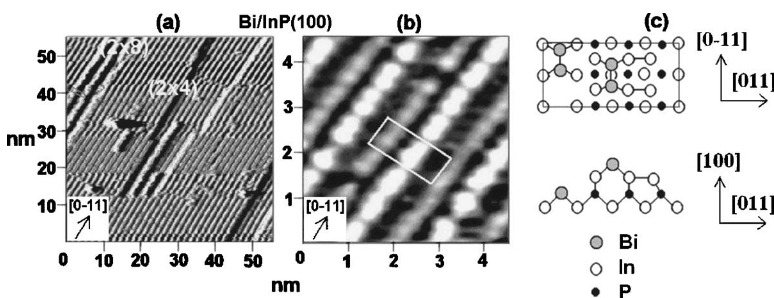

FIG. 4. (a) A filled-state STM image of the Bi/InP(100)(2×4) surface showing a local (2×8)-reconstructed area; the tunneling current is 0.46 nA and the voltage 2.15 V; the gray rectangle in the left top corner represents the (2×8) unit cell. (b) An atomic-resolution filled-state image of the Bi/InP(100)(2×4); the tunneling current is 0.42 nA and the voltage 1.80 V; the white rectangle represents the (2×4) unit cell. (c) The α2-like unit-cell model proposed for the Bi/InP(100)(2×4).

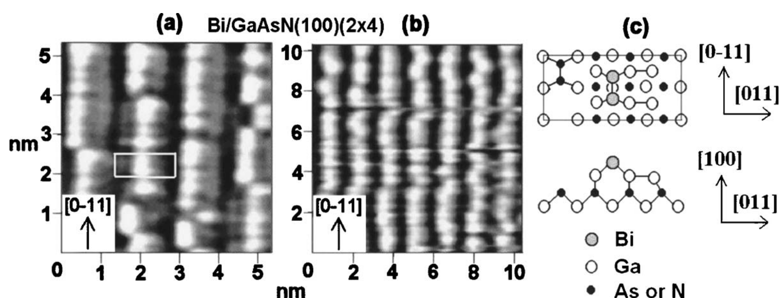

FIG. 5. (a) A filled-state STM image of the $Bi/GaAs_xN_{1-x}(100)(2\times4)$ surface; the tunneling current is 0.35 nA and the voltage 1.70 V; the white rectangle represents the unit cell. (b) An empty-state STM image of the $Bi/GaAs_xN_{1-x}(100)(2\times4)$ surface; the tunneling current is 0.21 nA and the voltage 1.70 V. (c) The $\alpha2$-like unit-cell model proposed for the $Bi/GaAs_xN_{1-x}(100)(2\times4)$.

the threefold-coordinated second-layer Ga atoms and/or of the first-layer mixed (Bi-Ga) dimer atoms[12] (not shown in the model of Fig. 5). Based on our previous observations that the Bi atoms lie only in the topmost atomic layer in the $Bi/GaAs(100)(2\times4)$-$\alpha2$ reconstruction,[12] we propose the Bi coverage of the $Bi/GaAs_xN_{1-x}(100)(2\times4)$ surface similarly to be 0.25 ML. Thus, the coverage of the $Bi/GaAs_xN_{1-x}(100)(2\times1)$ reconstruction is approximately 0.6 ML, according to the Bi 4f intensity ratio.

Well-ordered (2×1)-reconstructed areas were found on both the Bi/InP(100) and $Bi/GaAs_xN_{1-x}(100)$ surfaces, as can be deduced from the LEED images (Figs. 1 and 2) and from the STM images of Figs. 6(a) and 6(d). Atomic resolution filled- and empty-state STM images of the $Bi/InP(100)(2\times1)$ are shown in Figs. 6(b) and 6(c), respectively. The protrusion A in Fig. 6(b) may arise from a filled or half-filled dangling bond of a dimer atom, while the protrusion C in Fig. 6(c) may be related to an empty or half-filled dangling bond. Some of the white filled-state protrusions, like B, are oblong in the [0–11] direction, indicating that the $Bi/InP(100)(2\times1)$ surface consists of two or more different unit cells. Similar interpretations apply to the filled- and empty-state features, D and E, in the STM images of the $Bi/GaAs_xN_{1-x}(100)(2\times1)$ surface in Figs. 6(e) and 6(f), respectively.

The current-voltage curve of the $Bi/GaAs_xN_{1-x}(100)\times(2\times1)$ in Fig. 7 shows this surface to be metallic, as can be expected on the basis of the ECM concept. In contrast, the $Bi/InP(100)(2\times1)$ surface surprisingly appears to be semiconducting. The curve of the $Bi/GaAs_xN_{1-x}(100)(2\times4)$ surface, which obeys the ECM and is semiconducting, is presented in Fig. 7 for comparison. The inset shows the differential curves, which are proportional to the electronic density of states.[22] Figure 7 shows that the surface band gaps are approximately 0.8 and 1.4 eV for the $Bi/InP(100)(2\times1)$ and $Bi/GaAs_xN_{1-x}(100)(2\times4)$, respectively. The band gap of the $Bi/InP(100)(2\times1)$ surface is smaller than 1.2 ± 0.2 eV found previously on the $P/InP(100)(2\times1)$ surface.[14] Nowadays, it is accepted that the $P/InP(100)\times(2\times1)$ surface is terminated by hydrogen,[1,15] as mentioned in Sec. I. Here, such bonding of hydrogen to Bi dimers (i.e., one H atom per dimer) is, however, unlikely due to the surface-preparation conditions.

Combining the observations, we propose in Fig. 8 tentative atomic models for the (2×1) reconstructions. The Bi coverages for the models in Figs. 8(a) and 8(b) are 1 and 0.5 ML, respectively. Since the coverage of the $Bi/GaAs_xN_{1-x}(100)(2\times1)$ surface was estimated to be 0.6 ML, we suggest the structure in Fig. 8(b) dominates on the $Bi/GaAs_xN_{1-x}(100)(2\times1)$ surface and that the structure of Fig. 8(a) appears only locally. Both of the models violate the ECM because not all dangling bonds of the Bi atoms can be doubly occupied, agreeing with the metallic character of the $Bi/GaAs_xN_{1-x}(100)(2\times1)$ surface. Furthermore, the filled-state STM protrusion D of the $Bi/GaAs_xN_{1-x}(100)(2\times1)$ in Fig. 6(e) is related to a half-filled Bi dangling bond of the mixed In-Bi dimer, whereas the empty-state protrusion E in

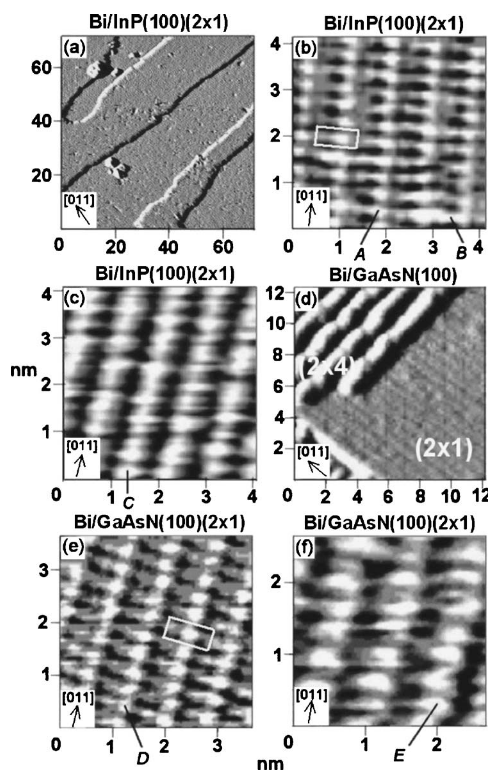

FIG. 6. (a) A large-scale filled-state STM image of the $Bi/InP(100)(2\times1)$ surface; the tunneling current is 3.34 nA and the voltage 2.63 V. (b) An atomic-resolution filled-state image of the $Bi/InP(100)(2\times1)$ surface; the tunneling current is 0.51 nA and the voltage 1.73 V; the white rectangle represents the unit cell. (c) An empty-state image of the $Bi/InP(100)(2\times1)$; the tunneling current is 3.87 nA and the voltage 1.00 V. (d) A filled-state STM image of the $Bi/GaAs_xN_{1-x}(100)(2\times1)+(2\times4)$ surface; the tunneling current is 0.42 nA and the voltage 2.94 V. (e) An atomic-resolution filled-state STM image of the $Bi/GaAs_xN_{1-x}(100)(2\times1)$; the tunneling current is 0.51 nA and the voltage 1.39 V; the white rectangle represents the unit cell. (f) An empty-state STM image of the $Bi/GaAs_xN_{1-x}(100)(2\times1)$; the tunneling current is 0.25 nA and the voltage 1.55 V.

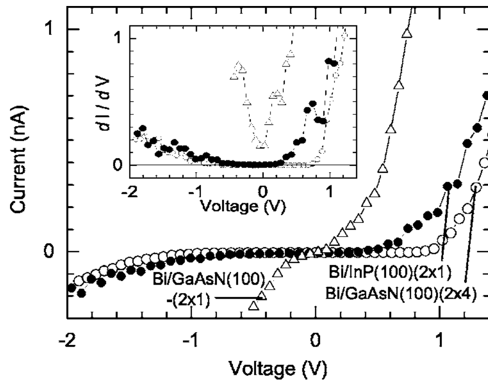

FIG. 7. The current-voltage curves, $I(V)$, measured from the Bi/InP(100)(2×1), Bi/GaAs$_x$N$_{1-x}$(100)(2×1), and Bi/GaAs$_x$N$_{1-x}$(100)(2×4) surfaces using STS. The tunneling spectroscopy was performed simultaneously with the topographic measurement using the filled-state voltage of 3.56 V and the current of 0.97 nA for the Bi/InP surface and the filled-state voltage of 3.04 V and the current of 0.50 nA for the Bi/GaAs$_x$N$_{1-x}$ surfaces. The inset shows the corresponding differential curves, $dI/dV(V)$, which are proportional to the electronic density of states.

Fig. 6(f) is proposed to arise from an empty In dangling bond and/or a half-filled Bi dangling bond of the mixed In-Bi dimer.

Since the Bi coverage of the Bi/InP(100)(2×1) was estimated to be 1.3 ML, the model in Fig. 8(a) is more plausible for this surface than the model of Fig. 8(b). The discrepancy in the coverage can be due to a replacement of the second-layer In atoms by Bi in the actual Bi/InP(100)(2×1) structure, which is not shown in the model of Fig. 8. Such Bi antisites can also make the Bi/InP(100)(2×1) structure more stable than the Bi/GaAs$_x$N$_{1-x}$(100)(2×1) via the formation of strong group-V-group-V bonds,[4] agreeing with the finding that higher temperatures were needed to remove the Bi-stabilized (2×1) reconstruction from the InP(100) than GaAs$_x$N$_{1-x}$(100) surface and that the Bi/InP(100)(2×1) reconstruction was stable in a wide temperature range (Fig. 3). Another reason for this coverage discrepancy can simply be an erroneous determination of the Bi amount of the Bi/InP(100)(2×1). For example, defects like Bi clusters on the Bi/InP(100)(2×1) surface can cause such overestimation of the coverage from the Bi 4f intensity-ratio measurements.

The filled-state STM protrusion A of the Bi/InP(100)(2×1) in Fig. 6(b) is interpreted to arise from a doubly occupied dangling bond of the Bi-Bi dimer, and the empty-state protrusion C in Fig. 6(c) is related to a half-filled Bi dangling bond. Furthermore, the semiconducting character of the Bi/InP(100)(2×1) surface is suggested to be due to the electron-correlation effect or inequivalent dimers,[14,23] however future investigations are required to clarify the observed energy gap of the Bi/InP(100)(2×1) surface.

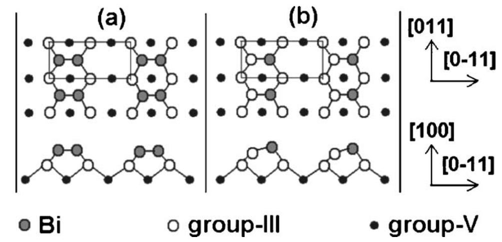

FIG. 8. Atomic models proposed for the Bi-stabilized (2×1) reconstructions. For details, see the text.

Several III–V(100) surfaces, e.g., P/InP(100)c(4×4),[24] obey the ECM and have dimer vacancies. Thus, an interesting question is why the Bi/InP and Bi/GaAs$_x$N$_{1-x}$(100)×(2×1) surfaces without dimer vacancies are stable. One reason may be that the surface stress, related to dimers,[25,26] is considerably reduced on these (2×1) surfaces. The longer bond lengths of the Bi dimers, as compared to the P and As dimers, can lead to a reduced surface stress, which is in a balance with the continuous dimer rows,[4] making the formation of the Bi-induced (2×1) reconstructions possible. However, the electronic energy cost of a metallic surface structure does not appear to be compensable for the Bi/InP(100)(2×1) system, in contrast to the Bi/GaAs$_x$N$_{1-x}$(100)(2×1) surface where the surface-stress relief seems to overcompensate the electronic energy cost. This may be related to the smaller lattice constant of the GaAs$_x$N$_{1-x}$(100) surface as compared to the InP(100) one; that is, the Bi-Bi dimers (≈3 Å in length) may accommodate better on the GaAs$_x$N$_{1-x}$(100) surface than on the InP(100) surface.

IV. CONCLUSIONS

With decreasing coverage, Bi is found to stabilize the (2×1), (2×8), and (2×4) reconstructions on the InP(100) and the (2×1) and (2×4) reconstructions on the GaAs$_x$N$_{1-x}$(100) surface. The α2-like structural model explains the STM observations of both the Bi/InP(100)(2×4) and Bi/GaAs$_x$N$_{1-x}$(100)(2×4) surfaces. The current-voltage properties measured by STS show the Bi/InP(100)×(2×1) and Bi/GaAs$_x$N$_{1-x}$(100)(2×1) surfaces to be semiconducting and metallic, respectively. On the basis of the experimental findings, atomic models are proposed for the (2×1) reconstructions, and the differences of these surfaces are tentatively discussed. Theoretical calculations and complementary measurements are needed to establish the models and to solve the question why Bi stabilizes the unusual (2×1) reconstructions.

ACKNOWLEDGMENTS

We thank W. G. Schmidt for valuable discussions and H. Ollila for technical assistance. This work has been supported in part by the Academy of Finland Grant No. 205766 (I.J.V.) and by TEKES within Project No. 40126/05.

[1] W. G. Schmidt, P. H. Hahn, F. Bechstedt, N. Esser, P. Vogt, A. Wange, and W. Richter, Phys. Rev. Lett. **90**, 126101 (2003).
[2] M. D. Pashley, Phys. Rev. B **40**, 10481 (1989).
[3] P. Moriarty, P. H. Beton, M. Henini, and D. A. Woolf, Surf. Sci. **365**, L663 (1996).
[4] L. J. Whitman, P. M. Thibado, S. C. Erwin, B. R. Bennett, and B. V. Shanabrook, Phys. Rev. Lett. **79**, 693 (1997).
[5] B. Z. Nosho, W. H. Weinberg, W. Barvosa-Carter, B. R. Bennett, B. V. Shanabrook, and L. J. Whitman, Appl. Phys. Lett. **74**, 1704 (1999).
[6] F. Maeda, Y. Watanabe, and M. Oshima, Phys. Rev. B **48**, R14733 (1993).
[7] P. Moriarty, P. H. Beton, Y.-R. Ma, M. Henini, and D. A. Woolf, Phys. Rev. B **53**, R16148 (1996).
[8] N. Esser, A. I. Shkrebtii, U. Resch-Esser, C. Springer, W. Richter, W. G. Schmidt, F. Bechstedt, and R. Del Sole, Phys. Rev. Lett. **77**, 4402 (1996).
[9] Q.-K. Xue, T. Hashizume, and T. Sakurai, Prog. Surf. Sci. **56**, 1 (1997).
[10] C. H. Li, L. Li, D. C. Law, S. B. Visbeck, and R. F. Hicks, Phys. Rev. B **65**, 205322 (2002).
[11] P. Laukkanen, M. Ahola, M. Kuzmin, R. E. Perälä, I. J. Väyrynen, and J. Sadowski, Surf. Sci. **598**, L361 (2005).
[12] M. Ahola-Tuomi, P. Laukkanen, R. E. Perälä, M. Kuzmin, J. Pakarinen, I. J. Väyrynen, and M. Adell, Surf. Sci. **600**, 2349 (2006).
[13] A. Ohtake, J. Nakamura, S. Tsukamoto, N. Koguchi, and A. Natori, Phys. Rev. Lett. **89**, 206102 (2002).
[14] L. Li, B.-K. Han, Q. Fu, and R. F. Hicks, Phys. Rev. Lett. **82**, 1879 (1999).
[15] G. Chen, S. F. Cheng, D. J. Tobin, L. Li, K. Raghavachari, and R. F. Hicks, Phys. Rev. B **68**, 121303(R) (2003).
[16] P. Laukkanen, J. Pakarinen, M. Ahola-Tuomi, M. Kuzmin, R. E. Perälä, I. J. Väyrynen, A. Tukiainen, V. Rimpiläinen, M. Pessa, M. Adell, and J. Sadowski, Surf. Sci. **600**, 3022 (2006).
[17] C. D. MacPherson, R. A. Wolkow, C. E. J. Mitchell, and A. B. McLean, Phys. Rev. Lett. **77**, 691 (1996).
[18] W. G. Schmidt, F. Bechstedt, N. Esser, M. Pristovsek, Ch. Schultz, and W. Richter, Phys. Rev. B **57**, 14596 (1998).
[19] S. Mirbt, N. Moll, K. Cho, and J. D. Joannopoulos, Phys. Rev. B **60**, 13283 (1999).
[20] N. Esser, W. G. Schmidt, J. Bernholc, A. M. Frisch, P. Vogt, M. Zorn, M. Pristovsek, W. Richter, F. Bechstedt, Th. Hannappel, and S. Visbeck, J. Vac. Sci. Technol. B **17**, 1691 (1999).
[21] L. Li, Q. Fu, C. H. Li, B.-K. Han, and R. F. Hicks, Phys. Rev. B **61**, 10223 (2000).
[22] R. M. Feenstra, Phys. Rev. B **50**, 4561 (1994).
[23] W. G. Schmidt, Appl. Phys. A **75**, 89 (2002).
[24] V. P. LaBella, Z. Ding, D. W. Bullock, C. Emery, and P. M. Thibado, J. Vac. Sci. Technol. A **18**, 1492 (2000).
[25] O. L. Alerhand, A. N. Berker, J. D. Joannopoulos, D. Vanderbilt, R. J. Hamers, and J. E. Demuth, Phys. Rev. Lett. **64**, 2406 (1990).
[26] J. Tersoff, Phys. Rev. B **45**, 8833 (1992).

Paper 3

J. Pakarinen, V. Polojärvi, P. Laukkanen, A. Tukiainen, A. Laakso, C.S. Peng, P. Tuomisto, V-M. Korpijärvi, J. Puustinen, M. Pessa, An effect of As flux on GaAs/AIAs quantum wells: A combined photoluminescence and reflection high-energy electron diffraction study, Applied Surface Science **255**, 2985 (2008).

Reprinted with permission from the publisher. Copyright 2008, Elsevier.

Applied Surface Science 255 (2008) 2985–2988

Contents lists available at ScienceDirect

Applied Surface Science

journal homepage: www.elsevier.com/locate/apsusc

An effect of As flux on GaAs/AlAs quantum wells: A combined photoluminescence and reflection high-energy electron diffraction study

J. Pakarinen *, V. Polojärvi, P. Laukkanen, A. Tukiainen, A. Laakso, C.S. Peng, P. Tuomisto, V.-M. Korpijärvi, J. Puustinen, M. Pessa

Optoelectronics Research Centre, Tampere University of Technology, FIN-33101 Tampere, Finland

A R T I C L E   I N F O

Article history:
Received 25 January 2008
Received in revised form 2 July 2008
Accepted 24 August 2008
Available online 29 August 2008

PACS:
71.35.-y
73.21.Fg

Keywords:
Crystal structure
Interfaces
Molecular beam epitaxy
Quantum wells
Semiconducting III–V materials

A B S T R A C T

Photoluminescence (PL) measurements and in situ reflection high-energy electron diffraction (RHEED) observations were used to optimize GaAs/AlAs multi-quantum-well (MQW) structures grown by molecular beam epitaxy (MBE) under different As fluxes. PL peaks were identified with computer simulations, intensity behavior as a function of temperature, and with previous results in literature. The room temperature PL intensity from our MQW samples first increases with the As flux and then decreases as the flux is increased. Combining our RHEED and PL observations, we propose that an optimum As flux for growth of GaAs/AlAs structures is close to the special As flux at which the GaAs(1 0 0) surface reconstruction changes from (2×4) to (4×2). The reasons for the findings are discussed.

© 2008 Elsevier B.V. All rights reserved.

1. Introduction

GaAs/AlAs multilayers are widely used in engineering III–V semiconductors. Nearly a perfect lattice match, efficient optical and electrical confinement, easy doping, and well-known physical properties make the GaAs/AlAs proper building block for many epitaxially grown GaAs-based devices [1–6]. It is well known that the quality of GaAs/AlAs interfaces plays a key role in GaAs-based devices. It has been shown, for example, that the electrically active defects of the GaAs/AlAs heterostructures accumulate on or very near the interfaces [7,8].

The electrical and the structural differences of the normal AlAs-on-GaAs and the inverted GaAs-on-AlAs interfaces are significant [9–12]. The interface defects are, in general, attributed to Ga segregation, reconstruction-induced phase shifts, and even to surface contamination [13–16]. However, with the current-state molecular-beam epitaxy (MBE), the contribution of surface contamination can be ignored.

Although the GaAs/AlAs interfaces have been studied several decades, it is still unclear what is an optimum As/group-III flux ratio for the growth of GaAs/AlAs multi-quantum-well (MQW) structures, and why. Difficulties originate from the structural and electrical dissimilarities of the normal AlAs-on-GaAs and the inverted GaAs-on-AlAs interfaces and from the different optimal growth parameters (e.g. growth temperature) of GaAs and AlAs [17–20]. The QW PL intensity is an important parameter from the device viewpoint since, as is well known, it often can be correlated with the semiconductor laser threshold. In this work, we address the above-mentioned unresolved issues and study an effect of the As flux on photoluminescence(PL) from GaAs/AlAs MQW structures. Using the surface-science technique, reflection high-energy electron diffraction (RHEED), we identify an optimum As flux to correspond to the (2×4)-reconstruction growth condition close to a phase transition from GaAs(1 0 0)(2×4) to GaAs(1 0 0)(4×2).

2. Experimental procedure

The samples were grown by using MBE with elemental high-purity Ga and Al effusion cells. We use the ratio of Bayard–Albert type ionization-gauge readings (in nA) to describe the As/group-III

* Corresponding author.
E-mail address: Janne.Pakarinen@tut.fi (J. Pakarinen).

0169-4332/$ – see front matter © 2008 Elsevier B.V. All rights reserved.
doi:10.1016/j.apsusc.2008.08.062

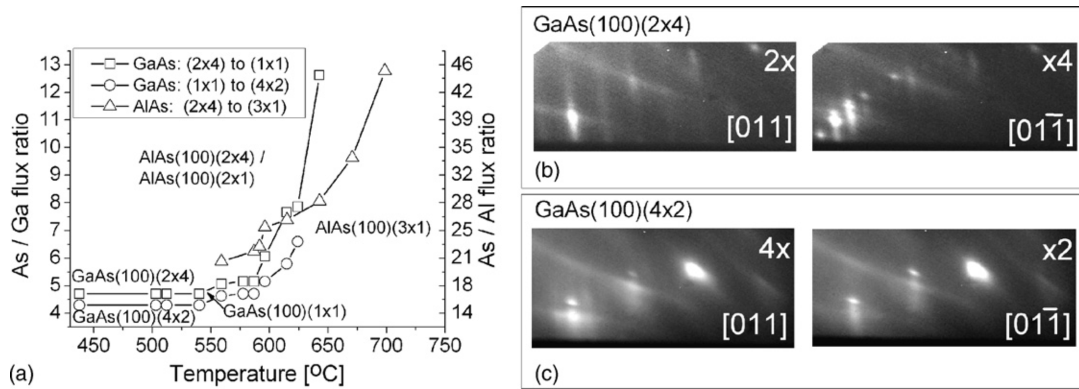

Fig. 1. (a) As/group-III flux ratio dependent surface phases of GaAs(1 0 0) and AlAs(1 0 0) surfaces as a function of temperature. RHEED patterns for (b) GaAs(1 0 0)(2×4) and (c) GaAs(1 0 0)(4×2). The patterns were taken during growth by using an As/Ga flux ratios close the GaAs(1 0 0)(2×4)–(4×2) transition.

flux ratio, although it depends on the geometry of the MBE reactor. The surface phases, shown in Fig. 1, are more conveniently related to the growth stoichiometry and comparable among different types of MBE reactors. The flux-meter readings for Ga and Al were 195 and 54.2 nA, respectively. The As_2 flux was produced from a valved cracker cell and was kept constant during the growth, but varied between different samples. Five samples were grown with various As fluxes (from 1.37 to 4.68 μA). Growth temperature was 580 °C, as measured by an optical pyrometer. By varying the As flux, the applied As/Ga(Al) flux ratio was from 7(25) to 24(86). Growth rates of GaAs and AlAs were 1 and 0.9 μm/h, respectively. After the deposition of 50 nm undoped GaAs-buffer layer on the Si-doped *n*-GaAs(1 0 0) substrate, nine GaAs (10 nm)/AlAs (50 nm) QWs were grown and capped with a 10-nm thick GaAs layer. We have intentionally kept the layers thick enough in order to eliminate the possibility of type-II transitions to occur [21].

RHEED was used to study the growing surface. The As/Ga flux ratio corresponding to the (2×4)–(4×2) transition on GaAs(1 0 0) was determined by varying the As flux on the growth front of separate substrates. A similar RHEED test was made for the AlAs(1 0 0) growth front. A difference in RHEED patterns was that Al-rich reconstruction was (3×1), not (4×2), and that the (2×4) pattern was not as clear as it was for GaAs. Sometimes the As-rich AlAs(1 0 0) surface exhibited (2×1) reconstruction only. The RHEED observations for the surface phases are summarized in Fig. 1(a) and RHEED patterns taken during growth for GaAs(1 0 0)(2×4) and (4×2) are shown in Fig. 1(b) and (c), respectively. As can be seen in Fig. 1(c), the $\times$ 2 order was not apparent in the RHEED from the (4×2) surface. This is most likely due to the fact that the patterns shown were taken during the growth in a narrow range of the growth conditions quickly just after the (2×4) pattern disappears. This was necessary since as well known, the quality of the growing film becomes quickly poor under the (4×2) growth conditions.

The PL measurements were performed in a closed-cycle helium cooled cryostat with an Ar^+ laser operating at 488 nm. The laser power was 5 mW and the approximated beam diameter on the sample was 0.25 mm. The PL spectra were recorded at substrate temperatures ranging from 9 K to room temperature (RT) and were detected by a monochromator and a photomultiplier tube. X-ray diffraction (XRD) (0 0 4) rocking curves, in $\omega - 2\theta$ geometry, were recorded using a double-crystal Bede QC200 diffractometer and Cu K α radiation. The layer thicknesses of MQWs were derived from the XRD rocking curves using a commercial dynamical simulation program RADS Mercury from Bede Scientific Instruments Ltd.

The simulations of electronic properties were carried out with a commercial LASTIP simulation software from Crosslight Software Inc. The QW model employed for calculating the material gain spectrum was the LASTIP MQW model, which assumed that valence and conduction subbands are parabolic. Furthermore, the potential-energy profile was assumed to be flat-band and step-wise. Coupling between the QWs were allowed in principal, but the barriers were so thick that the coupling was, in fact, negligible. The material parameters used in the simulations were taken from [22].

3. Results and discussion

Fig. 2 shows the XRD (0 0 4)-rocking curves and the simulated spectra (dotted lines). The rocking curves for the samples grown with As/Ga(Al) flux ratio from 12(42) to 24(86) have only small variations. The widths of the satellite and substrate peaks are nearly identical, which indicates equal crystal quality of these samples. The dynamical RADS simulations indicate uncertainties of 0.3 and 1.2 nm for the thicknesses of GaAs QWs (9.8 nm) and AlAs barriers (50.6 nm), respectively.

The rocking-curve measured from the sample grown with the As/Ga(Al) flux ratio 7(25) clearly differs from the other ones. We attribute the distorted spectral features to deterioration of the crystal quality. The poor crystal quality is most likely caused by an unsuitable (3×1) growth mode of AlAs with too small an As flux. The surface of this low As flux sample also looked foggy to a naked eye when comparing with the other samples confirming crystal deterioration.

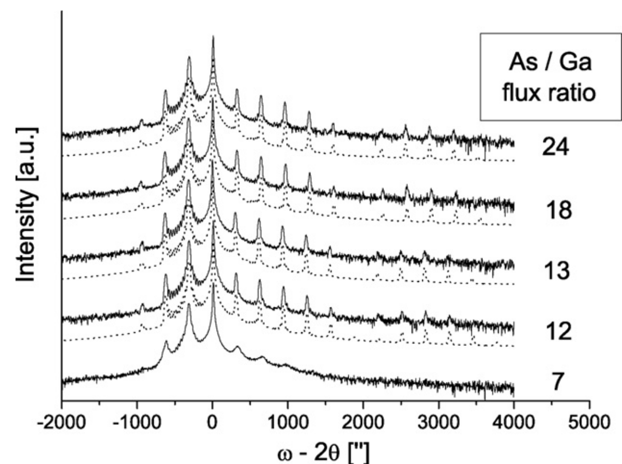

Fig. 2. Measured XRD (0 0 4) rocking-curves. Curves from the samples with As/Ga flux ratio from 12 to 24 are almost identical, while the sample with the lowest As/Ga flux ratio (7) is degraded. Simulated spectra are shown with the dotted lines. The curves are shifted in the vertical direction for clarity.

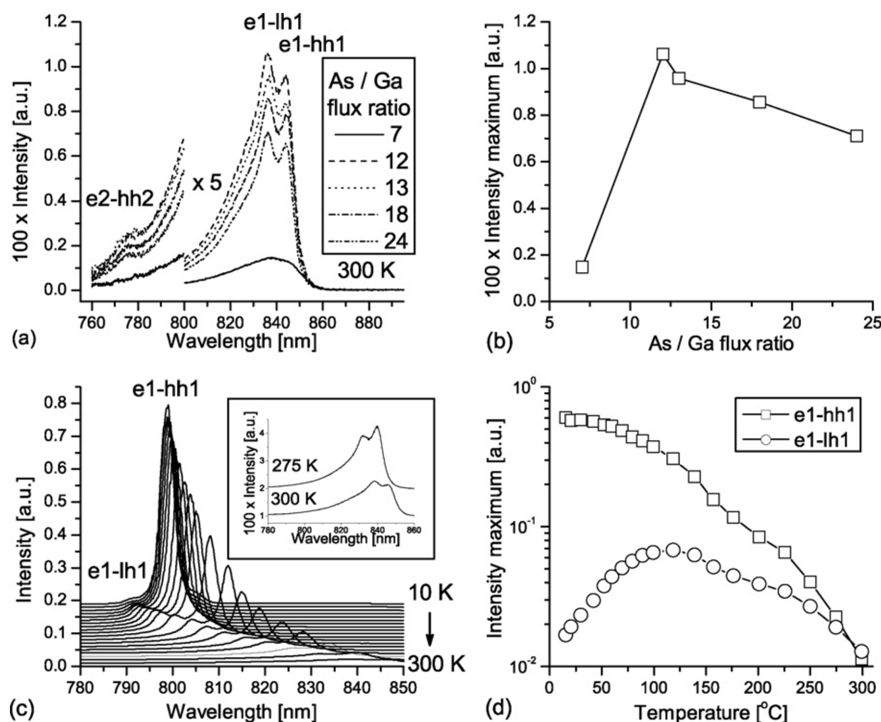

Fig. 3. (a) RT-PL spectra from the samples grown with varied As/Ga flux ratio. Transitions e1-hh, e1-lh, and e2-hh2 are labeled. (b) Maxima of the RT-PL intensities shown as a function of As/Ga flux ratio. (c) A temperature-dependent PL study of the sample grown with As/Ga flux ratio 12. The curves are shifted in the vertical direction for clarity. (d) Temperature behavior of the labeled e1-hh and e1-lh transitions.

In Fig. 3(a) RT-PL spectra are shown. The best PL intensity is obtained from the sample grown at the As/Ga flux ratio 12, while the lowest PL intensity is obtained from the sample grown at the As/Ga flux ratio 7. The intensity maxima are collected to Fig. 3(b) for a comparison. The spectra (As/Ga flux ratio from 12 to 24) in Fig. 3(a) clearly show three peaks at 775, 835, 845 nm, and a broad background. To identify these spectral features we measured the temperature dependence of the PL. As can be seen from Fig. 3(c) the intensity distribution between the two major peaks changes when the temperature decreases from RT to 10 K. The main mechanism between the intensity change is the formation of thermodynamical equilibrium of free carriers and excitons [23].

Based on the previous work of Kumar et al. [23] and the temperature-to-intensity behavior shown in Fig. 3(d), we can identify the RT-PL features as follows. The peak at 775 nm is due to transition e2-hh2, the peak at 835 nm originates from the e1-lh1, and the 845 nm emission comes from the e1-hh1 transition [23,24]. The background originates from free carrier recombination.

To further ensure the PL-peak identification, we simulated the material gain (Fig. 4) by using LASTIP. The material gain is calculated based on the parameterized quantum mechanical model. It shows the positions of the QW transitions, e.g. peaks at the calculated material gain correspond to the peaks at the ideal defect-free PL spectrum. Because the LASTIP simulation neglects interface roughness and Γ-X-intermixing, we can, indeed, conclude that the peaks in Fig. 3(a) really evolve from QW transitions. Furthermore, the observed double-peak structure agrees well with previous studies [25,26]. Interface roughness broadens the observed PL peaks, but we do not observe a splitting of the PL emission, which would originate from the terraces larger than the exciton diameter [27]. It is also worth noting that, using a logarithmic presentation of the 10 K PL spectra (not shown here), the e1-hh (≈ 799 nm) and e1-lh (≈ 791 nm) peaks can be distinguished from the emissions of GaAs (≈ 815 nm) and of the carbon-related defects located at the substrate (≈ 835 nm) [20,28].

Properties of the normal and the inverted GaAs/AlAs interfaces are known to be different. By applying a constant As/group-III flux ratio (which is reasonable for practical device growth) during the MQW growth, the optimized outcome is most likely a complex compromise between the different interfaces and the material quality. We shall discuss these issues next.

Krispin et al. found by deep-level transient spectroscopy (DLTS) and capacitance–voltage (C–V) measurements that electrically active defects in the GaAs/AlAs heterostructures are concentrated on the AlAs side [8,10]. Behrend et al. and Lüerßen et al. further confirmed the interpretation by their scanning-tunneling-microscopy (STM), RHEED, and Raman studies [11,12]. Defects were related to the presence of As vacancies on the inverted interface. On the other hand, Obata et al. noticed [20], that an excess of As in AlAs barriers reduced PL intensity. Our results are consistent with

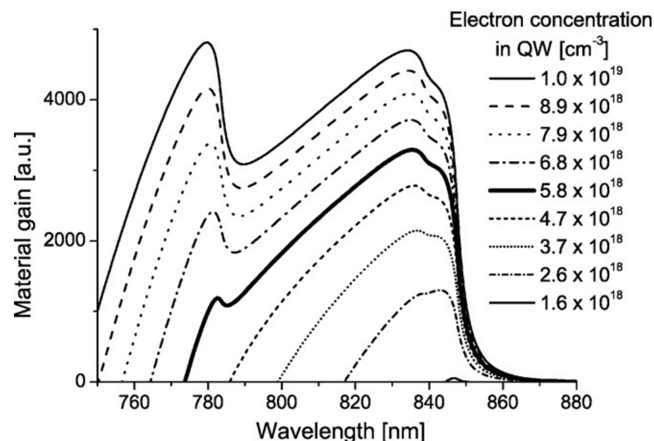

Fig. 4. Calculated material gain at 300 K with different electron concentrations in the QW. The thickest line at the electron concentration of 5.8×10^{18} cm^{-3} closely resembles the measured RT-PL spectra.

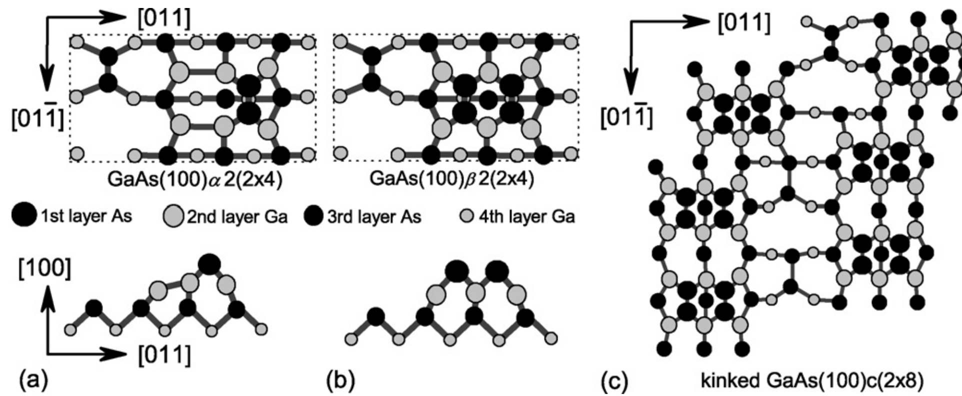

Fig. 5. Structure models ((a) $\alpha 2$ (b) $\beta 2$) for the GaAs(1 0 0) surface close to a phase transition from GaAs(1 0 0)(2×4) to GaAs(1 0 0)(4×2) [31]. (c) Kinked GaAs(1 0 0)c(2×8) surface [32].

those observations suggesting that there exist As-induced defects. Furthermore, our study shows that the amount of defects can be minimized by choosing appropriate As/Ga(Al) flux ratio. Fig. 3(b) indicates that the optimum As/Ga flux ratio is between 7 and 12.

The surface migration length and diffusivity of Ga and Al have been shown to be greatly reduced when increasing the As flux during layer growth [18,19,29]. A short migration of atoms leads to rough GaAs-on-AlAs interfaces and AlAs surfaces. Our results reveal that an optimal GaAs/AlAs growth by MBE is achieved by choosing the lowest possible As flux that produces the (2×4) reconstruction. In such conditions, the structure of the GaAs(1 0 0)(2×4) surface has been shown to be a mixture of the $\alpha 2$ and $\beta 2$ phases (shown in Fig. 5(a) and (b)) [30,31]. Then, the number of kink sites (Fig. 5(c)) caused by As atoms is reduced on this (2×4) surface, increasing the diffusion length of group-III atoms [29]. Indeed, our observations agree well with previous ab-initio calculations [29] and allow us to propose that the found PL-intensity behavior with the As flux arise from the diffusion properties of group-III atoms. Moreover, our results show that the Al-rich (3×1) growth mode of AlAs(1 0 0) should be avoided.

4. Conclusions

Our PL findings of GaAs/AlAs MQW structures show that the QW-related PL intensity does not increase linearly with the As flux used in MBE growth, but an optimum As flux can be found near the conditions where the GaAs(1 0 0)(2×4)–(4×2) transition occurs in RHEED. On the basis of previous results in literature, a reason for this finding is qualitatively related to the surface migration length of group-III atoms which depends on the amount of As on the growing surface.

Acknowledgements

J. Pakarinen acknowledges the financial support from the TUT Graduate School (Finland). The work is supported by the Academy of Finland within the NEONATE Project.

References

[1] J. Konttinen, A. Härkönen, P. Tuomisto, M. Guina, J. Rautiainen, M. Pessa, O. Okhotnikov, New J. Phys. 9 (2007) 140.
[2] A. Härkönen, J. Rautiainen, M. Guina, J. Konttinen, P. Tuomisto, L. Orsila, M. Pessa, O. Okhotnikov, Opt. Express 15 (2007) 3224.
[3] T. Jouhti, O. Okhotnikov, J. Konttinen, L.A. Gomes, C.S. Peng, S. Karirinne, E.-M. Pavelescu, M. Pessa, New J. Phys. 5 (2003) 84.
[4] N. Xiang, H.F. Liu, J. Kong, D.Y. Tang, M. Pessa, J. Cryst. Growth 301–302 (2007) 989.
[5] N. Lanzillotti-Kimura, A. Fainstein, A. Lemaître, B. Jusserand, Appl. Phys. Lett. 88 (2006) 083113.
[6] B. Zhang, G.S. Solomon, M. Pelton, J. Plant, C. Santori, J. Vuĉković, Y. Yamamotoe, J. Appl. Phys. 97 (2005) 073507.
[7] T.K. Woodward, T.C. McGill, R.D. Burnham, J. Vac. Sci. Technol. B 4 (1986) 1022.
[8] P. Krispin, R. Hey, H. Kostial, M. Höricke, J. Cryst. Growth 127 (1993) 1073.
[9] B. Deveaud, A. Chomette, N. Roy, S. Sermage, D.S. Katzer, Surf. Sci. 267 (1992) 199.
[10] P. Krispin, R. Hey, H. Kostial, J. Appl. Phys. 77 (1995) 5773.
[11] J. Behrend, M. Wessermeier, W. Braun, P. Krispin, K.H. Ploog, Phys. Rev. B 53 (1996) 9907.
[12] D. Lüerßen, A. Dinger, H. Kalt, W. Braun, R. Nötzel, K. Ploog, J. Tümmer, J. Geurts, Phys. Rev. B 57 (1998) 1631.
[13] M. Asom, M. Geva, R. Leibenguth, S. Chu, Appl. Phys. Lett. 59 (1991) 976.
[14] W. Braun, A. Trampert, L. Däweritz, K.H. Bloog, Phys. Rev. B 55 (1997) 1689.
[15] R. Hey, I. Gorbunova, M. Ramsteiner, M. Wassermeier, L. Däweritz, K.H. Ploog, J. Cryst. Growth 175/176 (1997) 1167.
[16] D. Wohlert, K. Chang, H. Lin, K. Hsieh, K. Cheng, J. Vac. Sci. Technol. B 18 (2000) 1590.
[17] P.K. Bhattacharya, J.W. Ku, S.J.T. Owen, V. Aebi, C.B. Cooper, R.L. Moon, Appl. Phys. Lett. 36 (1980) 304.
[18] T. Noda, M. Tanaka, H. Sakaki, Appl. Phys. Lett. 57 (1990) 1651.
[19] J.Y. Kim, D. Bassi, L. Jostad, Appl. Phys. Lett. 57 (1990) 2107.
[20] T. Obata, S. Fukushima, T. Araya, N. Otsuka, J. Crystal Growth 227–228 (2001) 112.
[21] B. Wilson, IEEE J. Quant. Elect. 24 (1988) 1763.
[22] I. Vurgaftman, J.R. Meyer, L.R. Ram-Mohan, J. Appl. Phys. 89 (2001) 5815.
[23] R. Kumar, S.S. Prabhu, A.S. Vengurlekar, Phys. Scripta 56 (1997) 308.
[24] S. Wu, W. Wang, L. Guo, Z. Li, X. Shang, F. Liu, Q. Huang, J. Zhou, J. Crystal Growth 278 (2005) 548.
[25] P. Dawson, G. Duggan, H.I. Ralph, K. Woodbridge, Phys. Rev. B 28 (1983) 7381.
[26] J. Martinez-Pastor, A. Vinattieri, L. Carraresi, M. Colocci, P. Roussignol, G. Weinmann, Phys. Rev. B 47 (1993) 10456.
[27] M.A. Herman, D. Bimberg, J. Christen, J. Appl. Phys. 70 (1991) R1.
[28] A.R. Adams, Properties of Gallium Arsenide, INSPEC, London and New York, 1986,
[29] K. Shiraishi, Appl. Phys. Lett. 60 (1992) 1363.
[30] A. Ohtake, Phys. Rev. B 74 (2006) 165322.
[31] M.P. Punkkinen, P. Laukkanen, K. Kokko, M. Ropo, M. Ahola-Tuomi, I.J. Väyrynen, H.-P. Komsa, T.T. Rantala, M. Pessa, M. Kuzmin, L. Vitos, J. Kollár, B. Johansson, Phys. Rev. B 76 (2007) 115334.
[32] T. Hashizume, Q.K. Xue, A. Ichimiya, T. Sakurai, Phys. Rev. B 51 (1995) 4200.

Paper 4

J. Pakarinen, C.S. Peng, V. Polojärvi, A. Tukiainen, V.-M. Korpijärvi, J. Puustinen, M. Pessa, P. Laukkanen, J. Likonen, E. Arola, Suppression of annealing-induced In diffusion in Be-doped GaInAsN/GaAs quantum well, Applied Physics Letters **93**, 052102 (2008).

Reprinted with permission from the publisher. Copyright 2008, American Institute of Physics.

Suppression of annealing-induced In diffusion in Be-doped GaInAsN/GaAs quantum well

J. Pakarinen,[1,a)] C. S. Peng,[1] V. Polojärvi,[1] A. Tukiainen,[1] V.-M. Korpijärvi,[1] J. Puustinen,[1] M. Pessa,[1] P. Laukkanen,[2] J. Likonen,[3] and E. Arola[4]

[1]*Optoelectronics Research Centre, Tampere University of Technology, FIN-33101 Tampere, Finland*
[2]*Department of Physics, University of Turku, FIN-20014 Turku, Finland*
[3]*VTT Technical Research Centre of Finland, P.O. Box 1000, 02044 VTT Espoo, Finland*
[4]*Department of Physics, Tampere University of Technology, FIN-33101 Tampere, Finland*

(Received 18 June 2008; accepted 10 July 2008; published online 6 August 2008)

The authors report on an interesting observation regarding thermal annealing of a beryllium-doped $Ga_{0.65}In_{0.35}As_{0.99}N_{0.01}$/GaAs quantum well (QW) grown by molecular beam epitaxy. A QW doped at 6×10^{19} cm^{-3} exhibited superior thermal properties and about six times larger photoluminescence than an undoped QW of the same structure. X-ray diffraction and secondary ion mass spectrometry provided evidence that beryllium suppressed indium diffusion and stabilized (metastable) dilute nitride heterostructure upon annealing. © *2008 American Institute of Physics*. [DOI: 10.1063/1.2966146]

The unique properties of dilute nitrides ($Ga_{1-x}In_xAs_{1-y}N_y$) have attracted significant scientific and commercial attention. It is well known that substitutional nitrogen atoms induce highly localized resonant energy levels near the GaInAs conduction band edge. These levels cause a decrease in the fundamental band gap of the alloy.[1] GaInAsN, closely lattice matched to GaAs, enables the growth of GaAs-based laser diodes for the 1.3–1.55 μm spectral band, which is currently dominated by InP diode lasers.[2] Other advantages of the GaAs technology over the InP include (1) the possibility to grow GaAs/(Al,Ga)As Bragg gratings with a high refractive index difference (Δn), (2) to use low-cost substrates, and (3) to improve thermal stability of the lasers. GaInAsN can also be tailored to any wavelength from 1.2 to 1.3 μm for potential nontelecom applications.[3]

Doping dilute nitrides is much less explored than doping more conventional GaN and (Al,Ga)As.[4] It was only recently that the first-principles calculations by Janotti *et al.*[5] could confirm experimental observations by Li *et al.*[6] and Yu *et al.*,[7] who suggested that silicon dopants in dilute nitrides form a stable split interstitial with nitrogen, giving rise to a "mutual passivation." Adding *p*-type Be dopants into the GaInAsN QWs is known to drastically change the effects of thermal annealing on photoluminescence (PL) and to improve lasing performance.[8]

We show in this letter that Be affects the microscopic diffusion of indium in GaInAsN/GaAs QWs. While the outdiffusion of indium from the undoped quantum well (QW) upon annealing at relatively high annealing temperature is clearly visible, it remains almost unnoticed for a Be-doped GaInAsN QW.

In our experiments, a 100 nm thick GaAs buffer was first grown at $T_{growth}=580$ °C by molecular beam epitaxy (MBE) on a Si-doped GaAs(100) substrate. Then, $Ga_{0.65}In_{0.35}As_{0.99}N_{0.01}$ QWs (6.50 nm in thickness) were deposited at $T_{growth}=460$ °C and capped with a 100 nm thick GaAs cap (T_{growth} was ramped back to 580 °C). In one sample, the QW was undoped; in another one, the QW was doped with Be to 6×10^{19} cm^{-3}, as calibrated by separate Hall samples. Postgrowth annealing of the samples was done at 800 °C in a closed GaAs box.[9] The PL was measured with a system equipped with a 532 nm Nd:YAG (yttrium aluminum garnet) laser and a GaInAs detector array. X-ray diffraction (XRD) rocking curves in ω-2θ geometry were recorded by using a double-crystal diffractometer and Cu $K\alpha$ radiation. Secondary-ion-mass spectrometry (SIMS) was used to study the depth profiles of ^{9}Be and ^{113}In. A primary ion source, O_2^+, was employed to sputter (150 nA, 3 keV) the QW sample areas of 320×460 μm^2 in size. The analyzed area was approximately 10% of the sputtered area.

Figure 1(a) shows the effects of annealing on integrated PL intensities for the undoped and Be-doped QW. PL from the undoped QW reached its maximum in a few seconds time of annealing at 800 °C. This improvement is likely due to the reduction in point defects, which are induced by introducing nitrogen and using low T_{growth}.[10] Further annealing reduced PL due to thermal energy induced lattice relaxation (via dislocation lines) and other annealing-induced defects.[11] Overall annealing effects on the Be-doped QW are similar to the undoped case at the beginning of the test, namely, PL was first improved and then decreased in prolonged annealing. However, when annealing was continued, PL for the Be-doped QW kept growing—in sharp contrast to the undoped QW. The wavelengths of the undoped and Be-doped QW samples behaved in much the same way, i.e., a blueshift took

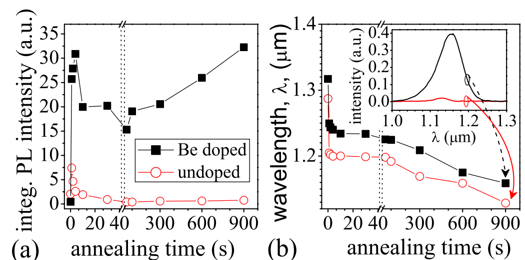

FIG. 1. (Color online) Integrated PL intensity (a) and the emission wavelength (b) as a function of the annealing time at 800 °C. The inset in (b) shows the measured PL spectra after 900 s annealing.

a)Electronic address: janne.pakarinen@tut.fi.

 © 2008 American Institute of Physics

Author complimentary copy. Redistribution subject to AIP license or copyright, see http://apl.aip.org/apl/copyright.jsp

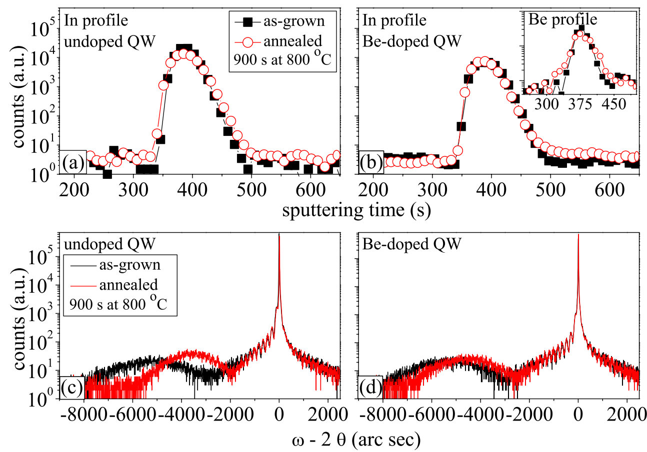

FIG. 2. (Color online) SIMS indium profiles from the undoped and the Be-doped GaInNAs QWs. Upon annealing, the In profile of the undoped sample becomes wider (a), whereas Be doping seems to suppress the In diffusion (b). XRD (004) rocking curves [(c) and (d)] are in good line with the SIMS results. The inset in (b) shows a beryllium SIMS profile in the as-grown case as well as in the annealed case.

place [Fig. 1(b)]. However, the wavelength of the Be-doped sample remained systematically longer (by about 40 nm) than that of the undoped sample at all annealing times.

Figure 2(a) shows SIMS data of indium concentration profiles for the undoped QW before and after 900 s annealing at 800 °C. This depth profile widens upon annealing, the effect that provides clear-cut evidence that indium diffused out of the QW. No widening of the depth profile is seen for the Be-doped QW [Fig. 2(b)] (a small "tale" of the In profile on the substrate side indicates that a small amount of In actually diffused from the QW). Consistent with the SIMS results, the XRD (004) rocking curves in Figs. 2(c) and 2(d) reveal that the QW peak moves closer to the GaAs substrate peak upon annealing. Annealing introduced large atomic structural and compositional changes in the undoped GaInAsN QW [Fig. 2(c)], but to a much lesser extent in the Be-doped QW [Fig. 2(d)], which further confirms that diffusion of In was suppressed in the latter case.[12] Due to the high strain inside the QW, we cannot exclude the possibility of annealing-induced relaxation present in the QW,[13] which in addition to In diffusion, would give an extra contribution to the observed shift in the QW XRD peak.

GaAsN and GaInAsN contain vacancies,[14,15] especially those related to the group III atoms. These vacancies are thought to be responsible for In diffusion in *n*-type GaAs,[16] GaInAs,[17] and GaInAsN.[18] We believe that Be and In atoms propagate in the lattice via the same vacancy-assisted diffusion path. As the diffusivity of Be is larger than that of In [inset in Fig. 2(b)], vacancies close to the GaInAsN QW will become occupied by Be. It is most likely that this is the mechanism that suppresses diffusion of indium, as judged from our SIMS and XRD data. This desired phenomenon of Be doping has already been observed in low-T_{growth} AlAs/GaAs:Be heterostructures.[19] It has also been found that diffusion of group III vacancies is limited to *p*-type semiconductors.[20] Indeed, the GaAs layers next to the GaInAsN QW of our sample may become *p*-doped by annealing-induced Be outdiffusion. Therefore, our interpretation is that beryllium passivates point defects left behind by annealing; they are most likely Ga vacancies which tend to enhance indium diffusion.

It has been reported that Be doping increases the sticking coefficient of nitrogen (increasing the mole fraction y) in MBE-grown $Ga_{1-x}In_xAs_{1-y}N_y$ QW.[21] We measured [see Fig. 1(b)] a 40 nm longer PL wavelength for the as-grown and annealed Be-doped GaInAsN QW compared to the corresponding undoped case. When the annealing time was increased [Fig. 1(b)], a similarly behaving blueshift occurred for both types of QWs. Based on previous studies,[22,23] the blueshifts observed for our QWs (annealed at 800 °C) can be attributed to two distinct phenomena, (i) indium diffusion and (ii) short-range ordering of the nearest-neighbor Ga and In atoms around the N atoms toward the In segregation configuration.

The postgrowth annealing strongly enhances PL (by a factor of 6) from the Be-doped GaInAsN/GaAs QW as compared to the PL from the undoped QW. There is a large compressive strain in the $Ga_{1-x}In_xAs_{1-y}N_y$/GaAs due to a large indium composition ($x > 0.30$). Annealing-induced thermal energy reduces this strain by forming dislocations,[11] which in turn act as nonradiative centers and cause a decrease in PL. Our interpretation is that beryllium in the QW reduces the local stress simply by becoming a substitutional atom in the group-III sublattice, thus suppressing the formation of strain-related crystal defects.

To recapitulate, adding Be into GaInAsN/GaAs single QW suppresses the diffusion of indium and remarkably improves optical properties upon prolonged annealing. It is suggested that Be prevents the formation of annealing-induced defects and suppresses the diffusion of indium by passivating point defects, most likely Ga vacancies.

The corresponding author (J.P.) acknowledges financial support from the Graduate School of TUT (Finland). This work was supported by the Academy of Finland within the NEONATE Project.

[1] K. Laaksonen, H.-P. Komsa, E. Arola, T. T. Rantala, and R. M. Nieminen, J. Phys.: Condens. Matter **18**, 10097 (2006).
[2] J. S. Harris, Semicond. Sci. Technol. **17**, 880 (2002).
[3] A. Härkönen, J. Rautiainen, M. Guina, J. Konttinen, P. Tuomisto, L. Orsila, M. Pessa, and O. Okhotnikov, Opt. Express **15**, 3224 (2007).
[4] H. J. Queisser and E. E. Haller, Science **281**, 945 (1998).
[5] A. Janotti, P. Reunchan, S. Limpijumnong, and C. G. V. de Walle, Phys. Rev. Lett. **100**, 045505 (2008).
[6] W. Li, M. Pessa, J. Toivonen, and H. Lipsanen, Phys. Rev. B **64**, 113308 (2001).
[7] K. M. Yu, W. Walukiewicz, J. Wu, D. E. Mars, D. R. Chamberlin, M. A. Scarpula, O. D. Dubon, and J. F. Geisz, Nat. Mater. **1**, 185 (2002).
[8] C. S. Peng, J. Konttinen, T. Jouhti, and M. Pessa, Proc. SPIE **6020**, 60200H (2005).
[9] J. Pakarinen, C. S. Peng, J. Puustinen, P. Laukkanen, V.-M. Korpijärvi, A. Tukiainen, and M. Pessa, Appl. Phys. Lett. **92**, 232105 (2008).
[10] C. S. Peng, E.-M. Pavelescu, T. Jouhti, S. Karirinne, J. Konttinen, and M. Pessa, Appl. Phys. Lett. **80**, 4720 (2002).
[11] H. F. Liu, S. J. Chua, and N. Xiang, J. Appl. Phys. **102**, 013504 (2007).
[12] G. Mussler, L. Däweritz, and K. H. Ploog, Appl. Phys. Lett. **87**, 081903 (2005).
[13] A. L. Gray, A. Stintz, K. J. Malloy, T. C. Newell, and L. F. Lester, J. Cryst. Growth **75**, 115337 (2001).
[14] J. Slotte, K. Saarinen, E.-M. Pavelescu, T. Hakkarainen, and M. Pessa, Appl. Phys. Lett. **89**, 061903 (2006).
[15] A. Janotti, S.-H. Wei, S. Zhang, S. Kurtz, and C. V. de Walle, Phys. Rev. B **67**, 161201 (2003).
[16] W. M. Li, R. M. Cohen, D. S. Simons, and P. H. Chi, Appl. Phys. Lett. **70**, 3392 (1997).
[17] H. S. Djie, O. Gunawan, D.-N. Wang, B. S. Ooi, and J. C. M. Hwang, Phys. Rev. B **73**, 155324 (2006).
[18] H. F. Liu, C. S. Peng, E.-M. Pavelescu, T. Jouhti, S. Karirinne, J. Kont-

Author complimentary copy. Redistribution subject to AIP license or copyright, see http://apl.aip.org/apl/copyright.jsp

tinen, and M. Pessa, Appl. Phys. Lett. **84**, 478 (2004).

[19]K. Tillmann, M. Luysberg, P. Sprecht, and E. R. Weber, Thin Solid Films **437**, 74 (2003).

[20]B. S. Ooi, K. McIlvaney, M. W. Street, A. S. Helmy, S. G. Ayling, A. C. Bryce, J. H. Marsh, and J. S. Roberts, IEEE J. Quantum Electron. **33**, 1784 (1997).

[21]S. Y. Xie, S. F. Yoon, S. Z. Wang, Z. Z. Sun, P. Chen, and S. J. Chua, J. Cryst. Growth **260**, 366 (2004).

[22]C. S. Peng, H. F. Liu, J. Konttinen, W. Li, and M. Pessa, J. Cryst. Growth **278**, 259 (2005).

[23]M. Hugues, B. Damilano, J.-M. Chauveau, J.-Y. Duboz, and J. Massies, Phys. Rev. B **75**, 045313 (2007).

Author complimentary copy. Redistribution subject to AIP license or copyright, see http://apl.aip.org/apl/copyright.jsp

Paper 5

J. Pakarinen, V. Polojärvi, A. Aho, P. Laukkanen, C.S. Peng, A. Schramm, A. Tukiainen, M. Pessa, Annealing of self-assembled InAs/GaAs quantum dots: a stabilizing effect of beryllium doping, Applied Physics Letters **94**, 072105 (2009).

Reprinted with permission from the publisher. Copyright 2009, American Institute of Physics.

Annealing of self-assembled InAs/GaAs quantum dots: A stabilizing effect of beryllium doping

J. Pakarinen,[1,a)] V. Polojärvi,[1] A. Aho,[1] P. Laukkanen,[2] C. S. Peng,[1] A. Schramm,[1] A. Tukiainen,[1] and M. Pessa[1]

[1]*Optoelectronics Research Centre, Tampere University of Technology, FIN-33101 Tampere, Finland*
[2]*Department of Physics and Astronomy, University of Turku, FIN-20014 Turku, Finland*

(Received 13 January 2009; accepted 31 January 2009; published online 19 February 2009)

We investigated the effects of postgrowth thermal annealing on optical properties of beryllium-doped InAs quantum dot (QD) heterostructures grown by molecular beam epitaxy. Thermal annealing induced a blueshift of up to 200 meV in light emission from an undoped sample, while a sample having GaAs layer heavily doped with beryllium on top of the QD region exhibited a much smaller blueshift. This phenomenon is interpreted as due to suppression of annealing-induced In/Ga interdiffusion. © *2009 American Institute of Physics*.
[DOI: 10.1063/1.3086298]

Indium arsenide quantum dots (QDs) on GaAs substrates are the building blocks of semiconductor devices.[1–4] Modulation doping of the QD structures with beryllium improves the temperature stability of lasers[5–7] but increases the lasing threshold. Growth conditions of GaAs cladding (barrier) layers play a significant role in the performance features of QD-based devices.[8] The QDs are grown at somewhat lower substrate temperature (T_{sub}) than what is usually applied to GaAs layers. In addition to ramping T_{sub} up and down during barrier growth (before and after QD deposition), the uppermost barrier layer suffers from crystal defects because it is deposited onto the dotted surface.[9] Postgrowth thermal annealing has been widely used to improve the material quality.[10–17] Recent photoluminescence (PL) studies[18] imply that the *p*-doping of the GaAs barriers improves the thermal stability of QD heterostructures. However, it has remained unresolved what the optimum position of *p*-doping is.

In this letter, effects of thermal annealing on optical properties of InAs QD samples are investigated. It was found that annealing an undoped (reference) QD sample at 800 °C for a few seconds quenched the intensity of PL and blueshifted the emission by about 200 meV relative to the as-grown sample. This undesired phenomenon was significantly suppressed by doping the sample with beryllium (1×10^{20} cm^{-3}). We found that the samples containing modulation-doped GaAs layers (GaAs:Be) of 3 nm in thickness exhibited a far less blueshift (BS) than did the reference sample upon annealing. It appeared that if the GaAs:Be layer was situated below the QD layer, no suppression in the BS occurred. The BS suppression only occurred when GaAs:Be was placed above and close to the QDs. Reasons for these observations are discussed below.

QD structures (Fig. 1) were grown by molecular beam epitaxy. After the deposition of a 100 nm thick GaAs buffer (at T_{sub}=580 °C) on an *n*-GaAs (100) substrate, a 50 nm $Al_{0.45}Ga_{0.55}As$ barrier layer was grown, followed by a 60 nm thick *i*-GaAs cladding (waveguide) layer. T_{sub} was ramped down to 505 °C during the growth of the cladding layer, and 2.2 monolayers of InAs (QD) were deposited by an interrupted growth process. T_{sub} was raised back to 580 °C while a 100 nm *i*-GaAs layer was grown on top of the QDs. Finally, a 100 nm $Al_{0.45}Ga_{0.55}As$ barrier layer was grown and the samples were capped with *i*-GaAs layers of 5 nm in thickness. By modifying the same growth recipe, six samples (samples 1–6) with different doping schema were prepared (Fig. 1). Sample 1 was unintentionally doped. Sample 2 was undoped except for the QDs which were doped with Be up to about 1×10^{20} cm^{-3}, as estimated from the *p*-GaAs calibration samples using Hall effect measurements. Sample 3 consisted of a 3 nm thick layer of (modulation) doped GaAs (again [Be]$\sim1\times10^{20}$ cm^{-3}), which was placed 15 nm above and below the undoped QDs. Sample 4 contained 3 nm thick GaAs:Be layers placed 40 nm above and below the undoped QDs. Sample 5 had a similarly doped layer 15 nm above the QDs. Sample 6 had a doped layer placed 15 nm below the QDs.

Annealing was performed inside a GaAs box under nitrogen flux.[11] Annealing temperature (T_{ann}) was controlled by an optical pyrometer. $T_{ann}\sim800$ °C was applied for all the samples. PL was measured at room temperature using a neodymium doped yttrium aluminum garnet laser for excitation and a GaInAs detector array. The spectra were simulated too by fitting the peak positions to the experimental data. We assumed that the spectra contained three Gaussian peaks, corresponding to the emission from the QD ground state (E_0), the first excited state (E_1), and the second excited state (E_2).

Figure 2 shows integrated PL intensities of E_0, as determined from the simulated spectra; the measured spectra of the as-grown samples are displayed in the insets in Fig. 2. PL intensity for sample 1 decreased drastically upon 1 s annealing and was hardly detectable when further annealed. In sharp contrast to sample 1, sample 2 with doped QDs exhibited low PL before thermal treatment, but showed improved PL (from E_0) after 50 s annealing. For sample 3, PL decreased upon 1s annealing, but increased after 10–50 s annealing (bearing a resemblance to a combined behavior of samples 1 and 2). For samples 4 and 6, PL intensities decreased upon 50 s annealing, resembling the behavior of undoped sample 1. Finally, sample 5 behaved much the same way as sample 3, exhibiting the smallest BS.

a)Electronic mail: janne.pakarinen@tut.fi.

 © 2009 American Institute of Physics

Author complimentary copy. Redistribution subject to AIP license or copyright, see http://apl.aip.org/apl/copyright.jsp

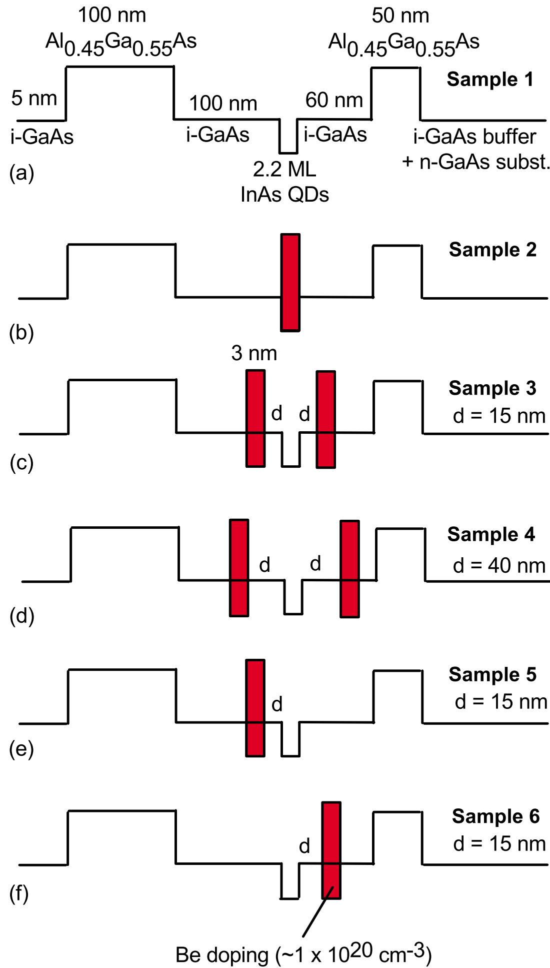

FIG. 1. (Color online) Schematic of the grown structures: (a) sample 1 without Be doping; (b) sample 2 with Be-doped QDs; (c) sample 3 with 3 nm thick Be-doped GaAs layers placed 15 nm away from the QDs; (d) sample 4 with 3 nm thick Be-doped layers placed 40 nm away from the QDs; (e) sample 5 with a 3 nm thick Be-doped GaAs layer placed 15 nm above the QDs; (f) sample 6 with a 3 nm thick Be-doped GaAs layer placed 15 nm below the QDs. Doping concentration was about 1×10^{20} cm^{-3}.

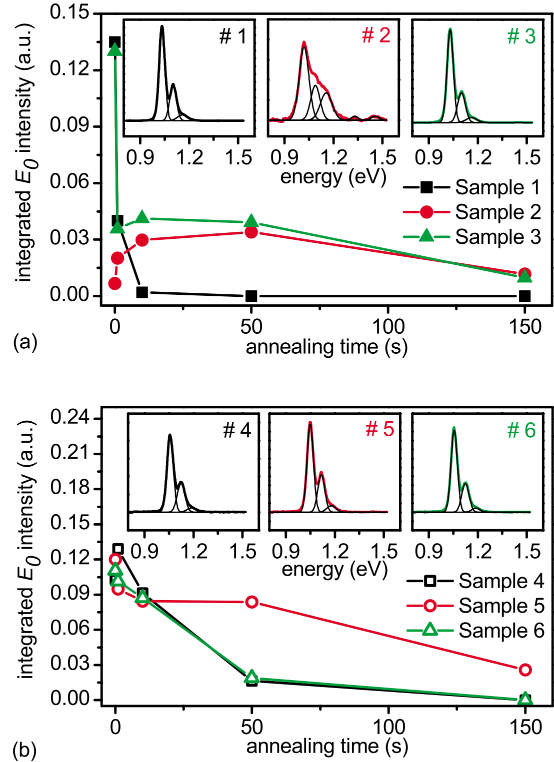

FIG. 2. (Color online) Integrated PL intensities for transitions from the ground states E_0 as annealing time was varied. Annealing temperature was at ~800 °C. The insets show experimental and fitted spectra for the as-grown samples.

Figure 3 shows the results for (a) BSs of emission from E_0, (b) energy difference $\Delta E = E_1 - E_0$, and (c) full width at half maximum (FWHM) of the E_0 line upon annealing. Similar trends of BS and ΔE are seen for all the samples. It is likely that the main mechanism governing the behavior of BS and ΔE is In/Ga interdiffusion through the QD interfaces.[16] Consistent with this interpretation is the fact that the FWHM for the undoped QDs was first increased, as E_0 was increased, and then it decreased. This effect is addressable to In/Ga interdiffusion in the growth direction, which lowers the quantum confinement energy of the active region and shifts E_0 upwards.[19,20] Figure 3 further shows that interdiffusion was strongly suppressed for samples 2, 3, and 5, where Be was incorporated into the QDs (sample 2) or into the 3 nm thick GaAs layers placed 15 nm around the undoped QDs (samples 3 and 5). Incorporating Be into the QDs tended to deteriorate the optical properties (sample 2) but postgrowth annealing improved the PL. The GaAs:Be layers which were situated away from the QDs did not affect the properties of the QDs, as determined from PL [Figs. 2 and 3(c)]. The fact that beryllium stabilized the structure is readily observable when comparing the spectra for samples 1, 2, and 3 with each other: upon 1 s annealing at 800 °C [Fig. 3(a)] the BS was 93 meV for sample 1 (and 200 meV after 10 s annealing), while much smaller BSs upon 1 s annealing appeared for sample 2 (26 meV) and sample 3 (12 meV). The barrier layer above the QDs contains more defects than the other layers because this layer is grown on a dotted sample surface.[9] Samples 4, 5, and 6 with the varying GaAs:Be locations clearly point out that the most detrimental defects do exist in the layer grown on top of the QDs. If the GaAs:Be layer is situated below the QDs (sample 6), or placed far away the QDs (sample 4), the doping effects were hardly discernable.

It should be noted that the effect of an increased hole concentration, due to the presence of Be, is opposite to the behavior of In/Ga intermixing-induced BS.[21] Since the difference in BSs among samples 1, 2, and 3 is very large, over 100 meV upon 10 s annealing [the left panel of Fig. 3(a)], suppression of the BS cannot be assigned to the high hole concentration since the "redshift" upon doping is less than 50 meV according to Ref. 21. Therefore, the BS suppression must be assigned to inhibition of In/Ga interdiffusion by insertion of a thin modulation-doped region in the GaAs overlayer close (15 nm in our experiments) to the QDs. Finally, our results indicate that by properly *p*-doping it is possible to improve both, the thermal stability and the PL intensity of QD structures, which could improve the QD-laser performance.

To recapitulate, annealing-induced In/Ga interdiffusion in InAs QD heterostructures, which were modulation-doped with beryllium in a certain way, was strongly suppressed. This phenomenon is attributable to the presence of beryllium which tends to passivate the crystal defects generated by

Author complimentary copy. Redistribution subject to AIP license or copyright, see http://apl.aip.org/apl/copyright.jsp

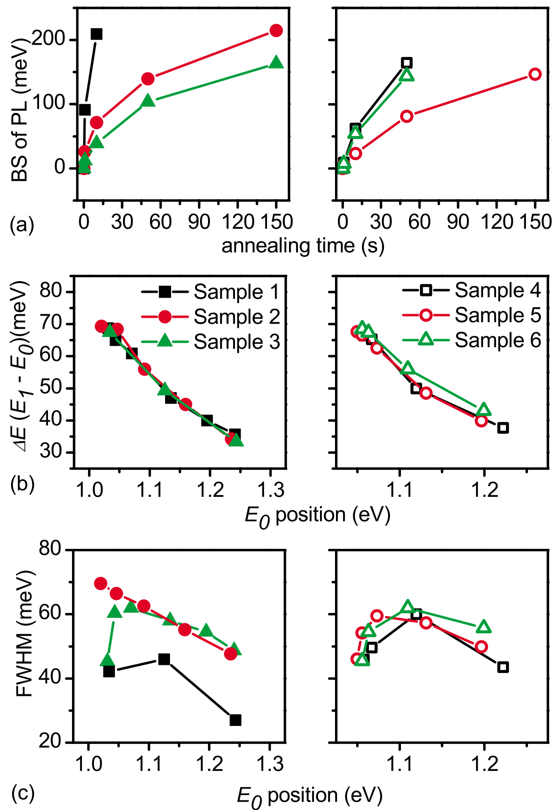

FIG. 3. (Color online) PL features determined from the fitted PL spectra: (a) BSs of PL, (b) energy separation $\Delta E = E_1 - E_0$ as a function of the ground state energy E_0, and (c) FWHM of E_0 as a function of its energy.

growth of a barrier layer on top of the QDs, improving thermal stability of the QDs.

The corresponding author (J.P.) acknowledges financial support from the Graduate School of Tampere University of Technology (Finland). This work was supported, in part, by the Academy of Finland within NEONATE and NANO-TOMO Projects.

[1] M. V. Maximov, V. M. Ustinov, A. E. Zhukov, N. V. Kryzhanovskaya, A. S. Payusov, I. I. Novikov, N. Y. Gordeev, Y. M. Shernyakov, I. Krestnikov, D. Livshits, S. Mikhrin, and A. Kovsh, Semicond. Sci. Technol. **23**, 105004 (2008).

[2] T. D. Germann, A. Strittmatter, J. Pohl, U. W. Pohl, D. Bimberg, J. Rautiainen, M. Guina, and O. G. Okhotnikov, Appl. Phys. Lett. **93**, 051104 (2008).

[3] C. Meuer, J. Kim, M. Laemmlin, S. Liebich, D. Bimberg, A. Capua, G. Eisenstein, R. Bonk, T. Vallaitis, J. Leuthold, A. R. Kovsh, and I. L. Krestnikov, Appl. Phys. Lett. **93**, 051110 (2008).

[4] L. Fu, Q. Li, P. Kuffner, G. Jolley, P. Gareso, H. H. Tan, and C. Jagadish, Appl. Phys. Lett. **93**, 013504 (2008).

[5] C. Y. Jin, H. Y. Liu, Q. Jiang, M. Hopkinson, and O. Wada, Appl. Phys. Lett. **93**, 161103 (2008).

[6] I. P. Marko, N. F. Massè, S. J. Sweeney, A. D. Andreev, A. R. Adams, N. Hatori, and M. Sugawara, Appl. Phys. Lett. **87**, 211114 (2005).

[7] T. J. Badcock, R. J. Joyce, D. J. Mowbray, M. S. Skolnick, H. Y. Liu, M. Hopkinson, K. M. Groom, and Q. Jiang, Appl. Phys. Lett. **90**, 111102 (2007).

[8] H. Y. Liu, I. R. Sellers, T. J. Badcock, D. J. Mowbray, M. S. Skolnick, K. M. Groom, M. Gutiérrez, M. Hopkinson, J. S. Ng, J. P. R. David, and R. Beanland, Appl. Phys. Lett. **85**, 704 (2004).

[9] X. Q. Meng, Z. Q. Chen, P. Jin, Z. G. Wang, and L. Wei, Appl. Phys. Lett. **91**, 093510 (2007).

[10] H. S. Djie, O. Gunawan, D.-N. Wang, B. S. Ooi, and J. C. M. Hwang, Phys. Rev. B **73**, 155324 (2006).

[11] J. Pakarinen, C. S. Peng, J. Puustinen, P. Laukkanen, V.-M. Korpijärvi, A. Tukiainen, and M. Pessa, Appl. Phys. Lett. **92**, 232105 (2008).

[12] B. S. Ooi, K. McIlvaney, M. W. Street, A. S. Helmy, S. G. Ayling, A. C. Bryce, J. H. Marsh, and J. S. Roberts, IEEE J. Quantum Electron. **33**, 1784 (1997).

[13] J. Pakarinen, C. S. Peng, V. Polojärvi, A. Tukiainen, V.-M. Korpijärvi, J. Puustinen, M. Pessa, P. Laukkanen, J. Likonen, and E. Arola, Appl. Phys. Lett. **93**, 052102 (2008).

[14] J. Tatebayashi, N. Hatori, M. Ishida, H. Ebe, M. Sugawara, Y. Arakawa, H. Sudo, and A. Kuramata, Appl. Phys. Lett. **86**, 053107 (2005).

[15] T. Yang, J. Tatebayashi, M. Nishioka, and Y. Arakawa, Appl. Phys. Lett. **89**, 081902 (2006).

[16] R. Leon, S. Fafard, P. G. Piva, S. Ruvimov, and Z. Liliental-Weber, Phys. Rev. B **58**, R4262 (1998).

[17] S. Malik, C. Roberts, R. Murray, and M. Pate, Appl. Phys. Lett. **71**, 1987 (1997).

[18] Q. Cao, S. F. Yoon, C. Y. Liu, and C. Z. Tong, J. Appl. Phys. **104**, 033522 (2008).

[19] N. Perret, D. Morris, L. Francomme-Fossè, R. Côtè, S. Fafard, V. Aimez, and J. Beauvais, Phys. Rev. B **62**, 5092 (2000).

[20] A. Rastelli, S. M. Ulrich, E.-M. Pavelescu, T. Leinonen, M. Pessa, P. Michler, and O. G. Schmidt, Superlattices Microstruct. **36**, 181 (2004).

[21] M. Ilegems, J. Appl. Phys. **48**, 1278 (1977).

Author complimentary copy. Redistribution subject to AIP license or copyright, see http://apl.aip.org/apl/copyright.jsp